Calcium/Calmodulin-Dependent Protein Kinase II Serves as a Biochemical Integrator of

Calcium Signals for the Induction of Synaptic Plasticity

by

Jui-Yun Chang

Department of Biochemistry
Duke University

Date:_____
Approved:

_____
Ryohei Yasuda, Co-Supervisor

_____
G. Vann Bennett, Co-Supervisor

_____
Richard G. Brennan

_____
Kenichi Yokoyama

Dissertation submitted in partial fulfillment of
the requirements for the degree of Doctor of Philosophy
in the Department of Biochemistry in the Graduate School of
Duke University

2016

ABSTRACT

Calcium/Calmodulin-Dependent Protein Kinase II Serves as a Biochemical Integrator of

Calcium Signals for the Induction of Synaptic Plasticity

by

Jui-Yun Chang

Department of Biochemistry
Duke University

Date:_____
Approved:

_____

Ryohei Yasuda, Co-Supervisor

_____

G. Vann Bennett, Co-Supervisor

_____

Richard G. Brennan

_____

Kenichi Yokoyama

An abstract of a dissertation submitted in partial fulfillment of
the requirements for the degree of Doctor of Philosophy
in the Department of Biochemistry in the Graduate School of
Duke University

2016

Abstract

Repetitive Ca^{2+} transients in dendritic spines induce various forms of synaptic plasticity by transmitting information encoded in their frequency and amplitude. CaMKII plays a critical role in decoding these Ca^{2+} signals to initiate long-lasting synaptic plasticity. However, the properties of CaMKII that mediate Ca^{2+} decoding in spines remain elusive. Here, I measured CaMKII activity in spines using fast-framing two-photon fluorescence lifetime imaging with millisecond temporal resolution. Following each repetitive Ca^{2+} elevations, CaMKII activity increased in a stepwise manner. This signal integration, at the time scale of seconds, critically depended on Thr286 phosphorylation. In the absence of Thr286 phosphorylation, only by increasing the frequency of repetitive Ca^{2+} elevations could high peak CaMKII activity or plasticity be induced. In addition, I measured the association between CaMKII and Ca^{2+}/CaM during spine plasticity induction. Unlike CaMKII activity, association of Ca^{2+}/CaM to CaMKII plateaued at the first Ca^{2+} elevation event. This result indicated that integration of Ca^{2+} signals was initiated by the binding of Ca^{2+}/CaM and amplified by the subsequent increases in Thr286-phosphorylated form of CaMKII. Together, these findings demonstrate that CaMKII functions as a leaky integrator of repetitive Ca^{2+} signals during the induction of synaptic plasticity, and that Thr286 phosphorylation is critical for defining the frequencies of such integration.

Dedication

This dissertation is dedicated to my Mom, my Dad, and Chien-Pin, for whose continued support I am extremely grateful.

Contents

List of Tables

List of Figures

xiv

List of Reaction Schemes

List of Abbreviations

2pFLIM	two-photon fluorescence lifetime imaging microscopy
2pLSM	two-photon laser-scanning microscopy
AC-3	autocamide - 3
ACSF	artificial cerebrospinal fluid
AIP2	autocamtide - 2 - related inhibitory peptide
Ala	alanine
AMPA	2-amino-3-(5-methyl-3-oxo-1,2-oxazol-4-yl) propanoic acid
AMPAR	AMPA-type glutamate receptor
ANOVA	analysis of variance
AP	action potential
APV	2-amino-5-phosphonopentanoate
Ca^{2+}	calcium ion
CA1	cornu ammonis 1
CA3	cornu ammonis 3
CaM	calmodulin
CaMKII	Ca^{2+}/CaM-dependent protein kinase II
cAMP	cyclic adenosine monophosphate
CaN	calcineurin

CNS	central nervous system
DIV	days *in vitro*
EPSC	excitatory postsynaptic current
EPSP	excitatory postsynaptic potential
ERK	extracellular signal-regulated kinases
FLIM	fluorescence lifetime imaging microscopy
FRAP	fluorescence recovery after photobleaching
FRET	fluorescence resonance energy transfer
Glu	glutamate
HEPES	4-(2-hydroxyethyl)-1-piperazineethanesulfonic acid
HFS	high frequency stimulation
I-1	protein phosphatase 1 inhibitor
LTD	long-term depression
LTP	long-term potentiation
mCherry	monomeric Cherry fluorescent protein
mEGFP	monomeric enhanced green fluorescent protein
MEM	minimum essential medium eagle
Mg^{2+}	magnesium ion
MNI-glutamate	4-Methoxy-7-nitroindolinyl-caged-L-glutamate

Na$^+$	sodium ion
NMDA	N-Methyl-D-aspartate
NMDAR	N-Methyl-D-aspartate-type glutamate receptor
NR2B	N-Methyl-D-aspartate receptor subunit 2B
PMT	photoelectron multiplier tubes
PP1	protein phosphatase 1
PP2A	protein phosphatase 2A
PSD	postsynaptic density
PTFE	polytetrafluoroethylene
Q-dot	quantum dots
SAXS	small-angle X-ray scattering
Ser	serine
sem	standard error mean
sLTP	structural basis long-term potentiation
tdTM	tandem dimer tomato fluorescent protein
Thr	threonine
Trolox	6-hydroxy-2,5,7,8-tetramethylchroman-2-carboxylic acid
TTX	tetrodotoxin
uEPSC	uncaging-evoked excitatory postsynaptic current

VSCC	voltage sensitive calcium channel

Acknowledgements

I would like to thank my Ph.D. advisor, Ryohei Yasuda, for your valuable guidance, critical thinking and support. My academic growth was truly assisted by this valuable scientific training. I would also like to thank my Ph.D. co-advisor, Vann Bennett, and my committees, Richard Brennan and Kenichi Yokoyama, for your valuable input and feedback.

I would also like to thank Paula Parra-Bueno for the beautiful electrophysiology experiments, Jaime Richards and Mo Hu for the beautiful hippocampal slice cultures, Lesley Colgan for the critical reading of the manuscript, Long Yen for the help in optics, and David Kloetzer for the help of lab stuff. I would also like to thank all the members of Yasuda lab for the critical discussion, support and help: Helena Decker, Nathan Hedrick, Tal Laviv, Takayasu Mikuni, Jun Nishiyama, Mikihiro Shibata, Myung Shin, Michael Smirnov, Erzsebet Szatamari, Ada Tang, Rohit Ramnath, Jie Wang, Ye Sun, Kathy Liu and Boram You.

Chapter 1.   Introduction

1.1 Long-term potentiation

1.1.1 History

The hippocampus has long been known to be a brain region that is essential for learning and memory, mainly through the study of the famous H.M. patient. In the early 1970s, Lomo showed that repetitive activation of excitatory synapses in the hippocampus caused an increase in synaptic strength that can last for hours or even days (Lomo, 1971). It was not until the discovery of long-term potentiation (LTP) that the "memory" mechanism has cellular support to be attributed to the long-lasting, activity-dependent changes in the efficacy of synaptic transmission. During the past 45 years, emerging studies have been focusing on LTP, and LTP is now still one of the interesting topics in neuroscience.

1.1.2 LTP and memory

Around 1973, the discovery of places cells in the hippocampus (O'Keefe and Dostrovsky, 1971) and detailed description of long-term potentiation (Bliss and Lomo, 1973) together changed the perspective that we have of memory system. In 1981, Morris *et al* published the first paper about "place navigation" based on the first water maze spatial learning experiment paradigm. They later showed that this type of spatial learning is severely impaired when the hippocampus is damaged (Morris et al., 1982). In

1986, Morris *et al* further infused D,L-AP5 (an NMDA receptor antagonist) to the free moving rat and test their spatial memory in water maze they constructed. LTP and spatial learning is completely blocked *in vivo* (while no change in the saline group). Baseline synaptic transmission is intact in these mice, and they can learn other non-hippocampus dependent task. These were the first findings demonstrating that hippocampal LTP is NMDA-receptor dependent (Morris et al., 1986).

1.1.3 Basic properties of LTP

I will mainly focus on the LTP at CA1 synapses since it is used as my experimental model. In the CA1 region, (i) LTP is input-specific. This means that only the synapses receive the repetitive activation will increase its synaptic strength; other synapses on the same neuron will not be modified. (ii) LTP is associative. This means that LTP can be induced at synapses by low-frequency, sub-threshold stimuli if this stimulation is temporally concurrent with a normal LTP stimulation at another set of synapses on the same cell. This property is attractive for the reason that two pieces of information being conveyed by different afferents can be associated on the same postsynaptic cell. (iii) LTP is cooperative. This property is explained by the fact that, to trigger LTP, the postsynaptic cell must be sufficiently depolarized to remove Mg^{2+} block and allow Ca^{2+} to enter through NMDA-receptors (Figure 1.1) (Malenka, 2003).

2
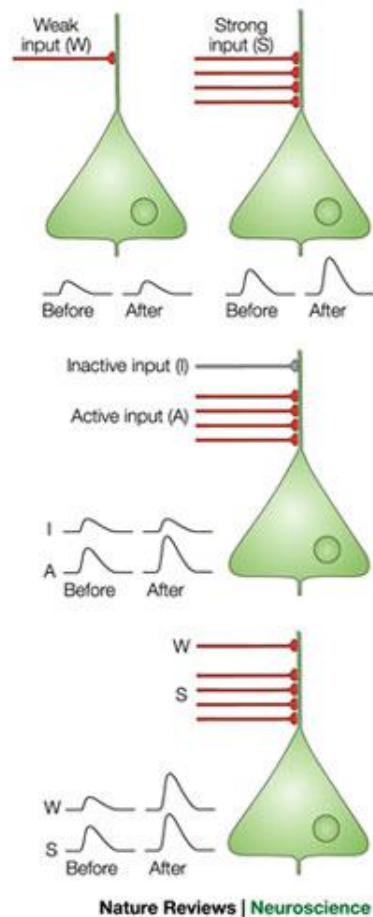
Figure 1.1: Basic properties of long-term potentiation
Three key properties of LTP: cooperativity, input specificity and associativity (from the top to the bottom). Adapted from (Malenka, 2003).

1.1.4 LTP induction mechanism

Induction of LTP requires synaptic activation of NMDA-receptors and

depolarization of the postsynaptic cells occurring simultaneously. There are two major

subtypes of glutamate receptors: AMPA-receptors and NMDA-receptors. AMPA-

receptor is permeable to monovalent cations (Na$^+$ and K$^+$) and is responsible for the

major inward current when the cell is in the resting state. NMDA-receptor has voltage-dependence property because of the extracellular Mg^{2+} block on the resting potential. Removal of Mg^{2+} block during depolarization allows Ca^{2+} and Na^+ influx through NMDA-receptor. Entry of Ca^{2+} triggers the downstream signaling responsible for LTP. If the NMDAR-mediated Ca^{2+} influx does not reach the threshold for LTP, the Ca^{2+} influx may instead trigger short-term potentiation (STP) or long-term depression (LTD) (Bear and Malenka, 1994; Malenka and Nicoll, 1993).

1.2 Ca^{2+}/calmodulin-dependent protein kinase II (CaMKII)

1.2.1 CaMKII in LTP, learning and memory

The role of CaMKII and its kinase activity and individual phosphorylation sites (mainly residing on the regulatory segment) has been extensively studied in synaptic plasticity and memory. Below, I list the effects of different manipulations of CaMKII on hippocampal LTP and learning by far reported on the literatures.

1.2.1.1 Pharmacology inhibition of CaMKII activity

CaMKII biochemical activity can be inhibited by various inhibitors targeted to different domains of CaMKII. One group of inhibitors interferes with CaM binding (KN62, KN93) (Anderson et al., 1998; Hidaka and Yokokura, 1996), one mimics CaMKII substrates (autocamide-3 (AC-3), AIP2) (Ishida and Fujisawa, 1995; Ji et al., 2003), and one mimics the peptide domain around the T-site of the regulatory segment of CaMKII

(CN21) (Buard et al., 2010; Vest et al., 2007). Below, I summarize the effects of the different CaMKII inhibitors on hippocampal LTP and memory.

KN62: Electrical stimulated LTP is prevented (Bortolotto and Collingridge, 1998). Sustained phase of structural plasticity is partially impaired while transient phase of structural plasticity is preserved (10μM, KN62) (Harvey et al., 2008; Lee et al., 2009). However, KN-compounds suffer from low specificity towards Ca^{2+}/CaM-kinase protein family and have off-site targets to voltage-gated K^+ channels (Rezazadeh et al., 2006).

AC-3/AIP2: Autocamide-3 (AC-3) and autocamide-2-related inhibitory peptide (AIP2) are pseudo-substrates of CaMKII, and thus function as competitive inhibitors (Ishida and Fujisawa, 1995; Ji et al., 2003). LTP induction is blocked by the bath application of AC-3 and AIP2. On the other hand, bath application of inhibitors after LTP induction did not interfere with the maintenance of LTP (Otmakhov et al., 1997).

CN21: CN21 is derived from CaM-KIIN (a.a. 43-63), which is a specific and natural CaMKII inhibitor (Vest et al., 2007). CN21 blocks Ca^{2+}-stimulated and autonomous substrate phosphorylation, but T286 phosphorylation remains. In rat hippocampal slices, tatCN21 inhibited (5μM) LTP induction but not LTP maintenance. In a mouse *in vivo* model, tatCN21 inhibited learning, but not memory storage or retrieval (Buard et al., 2010).

1.2.1.2 Genetics manipulation of CaMKII activity

Knock-out mice of *camk2a* and *camk2b* have been generated to study the role and function of CaMKIIα and CaMKIIβ in LTP and learning. Transgenic knock-in mice at several different phosphorylation sites (T286, T305/T306) and at central kinase domain (K42) have also been generated and investigated.

$\Delta camk2a^{-/-}$: CaMKIIα knock-out mice exhibited completely blocked LTP (Silva et al., 1992b)(or significantly impaired LTP, see (Elgersma et al., 2002)) and impaired spatial learning and memory (Elgersma et al., 2002; Silva et al., 1992a; Silva et al., 1992b).

$\Delta camk2a^{+/-}$: These mice have normal hippocampal LTP and spatial learning (Elgersma et al., 2002).

$\Delta camk2b^{-/-}$: CaMKIIβ knock-out mice exhibited impaired LTP when induced at 100 Hz (Schaffer-collateral pathway), but retained normal LTP when induced at 200 Hz. Contextual fear conditioning is impaired (Borgesius et al., 2011).

camk2a[T286A]: *camk2a*[T286A] knock-in mice exhibited impaired hippocampal LTP and spatial learning (Giese et al., 1998). Hippocampal place field in *camk2a*[T286A] knock-in mice is also unstable (Cho et al., 1998).

Over expression of CaMKIIα-T286D: In this study, *camk2a*[T286D] transgene is driven by CaMKIIα promoter. In these transgenic mice, LTP induced by 10 Hz stimulation (theta frequency) is blocked, and spatial learning is impaired (Mayford et al., 1996).

These mice also suffer from the lack of stable hippocampal place cells (Rotenberg et al.,

1996). However, LTP induced at normal frequency range (~100 Hz) is not affected in

these transgenic mice.

$camk2a^{K42R}$: $camk2a^{K42R}$ knock-in mice (kinase dead mutation) exhibited impaired

hippocampal LTP, impaired spatial learning and inhibitory avoidance learning.

Structural plasticity in CA1 neurons is also blocked (Yamagata et al., 2009).

$camk2a^{T305VT306A}$: $camk2a^{T305VT306A}$ knock-in mice have lower threshold for

hippocampal LTP induction (Elgersma et al., 2002).

$camk2a^{T305D}$: $camk2a^{T305D}$ knock-in mice have completely blocked hippocampal LTP

and severely impaired spatial learning (Elgersma et al., 2002).

1.2.2 Temporal and spatial expression of CaMKIIα in mice brain

Regional distribution of CaMKIIα in mice brain has been mapped by

immunochemical and immunohistochemical methods (Erondu and Kennedy, 1985). Its

high abundance accounts for about 2% of the total protein in hippocampus. Expression

of CaMKIIα is also abundant in cortex (about 1.3% of the total cortical protein) and

striatum (about 0.7% of total striatal protein). CaMKIIα is exclusively found in

glutamatergic pyramidal neurons in hippocampus and cortex; whereas, in striatum, it is

localized to GABAergic medium-spiny neurons (Benson et al., 1992; Sik et al., 1998;

Takeuchi et al., 2002). CaMKIIα is less concentrated in brain stem structures (about 0.3%

of hypothalamic protein and about 0.1% of protein in the pons/medulla) (Figure 1.2).

Concentration of endogenous CaMKIIα in neuronal compartments has also been semi-

quantitatively measured. Concentration of CaMKIIα subunits in cell bodies, proximal

dendrites and dendritic spines are 71, 46 and 103 μM, respectively (Otmakhov and

Lisman, 2012). CaMKIIα promoter is active postnatally. CaMKIIα mRNA is barely

detected at birth but becomes abundant during the third postnatal week (Burgin et al.,

1990).
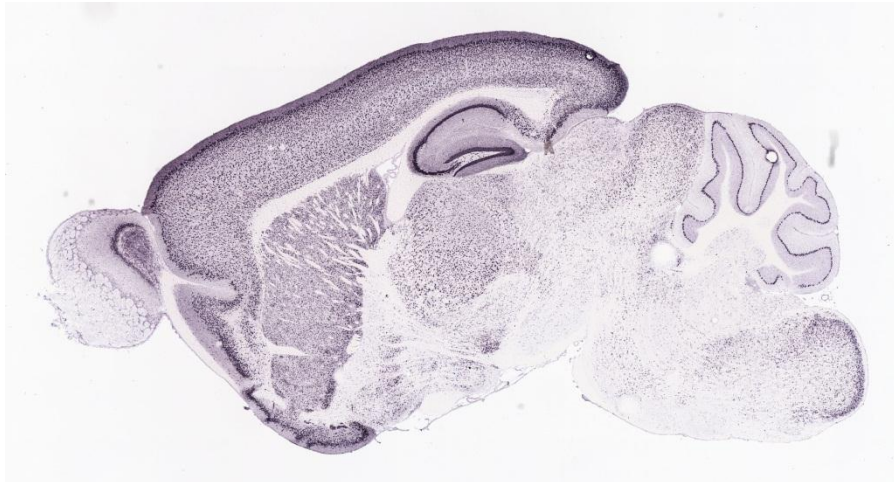
Figure 1.2: Regional distribution of CaMKIIα mRNA in adult mice
sagittal view, from P56 adult mice. Adapted from Allen Brain atlas.

1.2.3 Molecular architecture of CaMKII

CaMKII is a Ser/Thr protein kinase (~54 kDa) and unlike most of other protein

kinase, it adopts a dodecamer assembly (Chao et al., 2011; Rellos et al., 2010). Individual

CaMKII subunit is composed of three domains: an N-terminal kinase domain, a

regulatory segment and an association domain (Hudmon and Schulman, 2002) (Figure 1.3). Historically, CaMKII holoenzyme assembly has been documented in electron microscopy (EM) and small-angle X-ray scattering (SAXS), but with different views of holoenzyme assembly. The two sets of views agree that CaMKII holoenzyme adopts a six-fold symmetry with the association domain contacting individual subunits in two hexameric ring structure (central hub). However, in one set of EM reconstructions, individual kinase domains are arranged above and below the midplane of the central hub (Kolodziej et al., 2000; Woodgett et al., 1984); while in another set of EM reconstructions and SAXS analysis, individual kinase domains are arranged outside the central hub and are in proximity to each other (Morris and Torok, 2001; Rosenberg et al., 2005). It was not until the full-length human CaMKIIα holoenzyme structure solved by Chao *et al*. in 2011 that the two viewpoints reconciled. Chao *et al* showed that CaMKIIα dodecameric holoenzyme structure (Figure 1.4) (Chao et al., 2011) has a compact arrangement of kinase domains around the central hub. Each kinase domain has extensive contacts with the two adjacent association domains. There are two distinct autoinhibited (basal) conformations of the CaMKII holoenzyme. The compact conformation of CaMKII holoenzyme has limited access to Ca^{2+}/CaM; while Ca^{2+}/CaM can easily bind to CaMKII in the extended conformation (Figure 1.4). This compact and extended autoinhibited arrangements might account for the frequency response of

CaMKII (De Koninck and Schulman, 1998; Dupont et al., 2003) and the interaction

between kinase and association domain is affected by the length of linker connecting

these two regions.
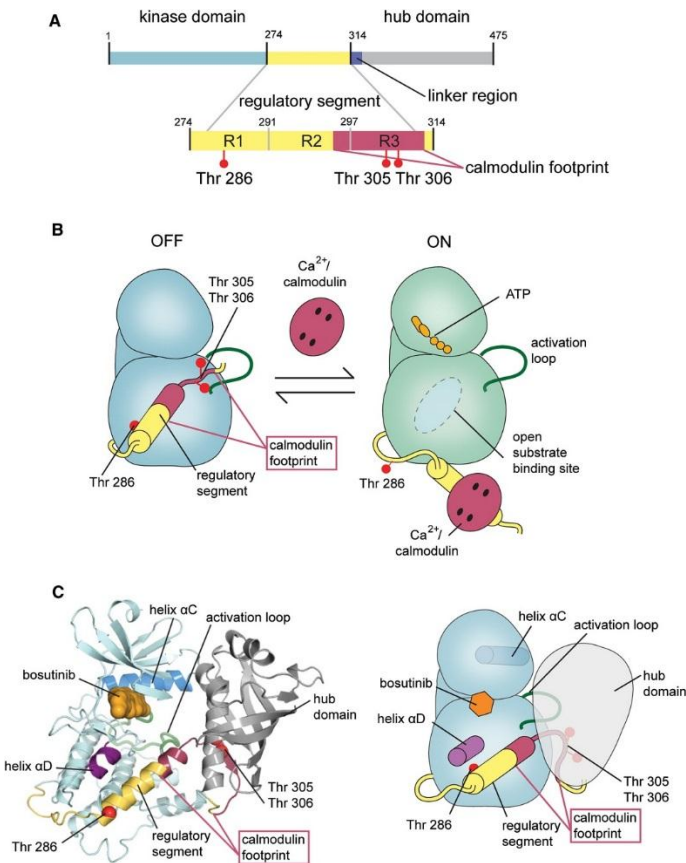
Figure 1.3: CaMKII domain organization and illustration of CaMKII subunit activation
(A) CaMKII domain organization. N-terminus kinase domain is followed by the regulatory segment, a linker region and the association domain. The regulatory segment is comprised of R1, R2 and R3 regions. The CaM footprint region lies in R3 and a partial R2 region.
(B) Mechanism of CaMKII subunit activation induced by Ca^{2+}/CaM binding.
(C) CaMKII subunit structure. In an inactivated state, the α helix domain has strong hydrophobic interaction with the kinase domain and blocks the substrate entry.
Adapted from (Chao et al., 2011).
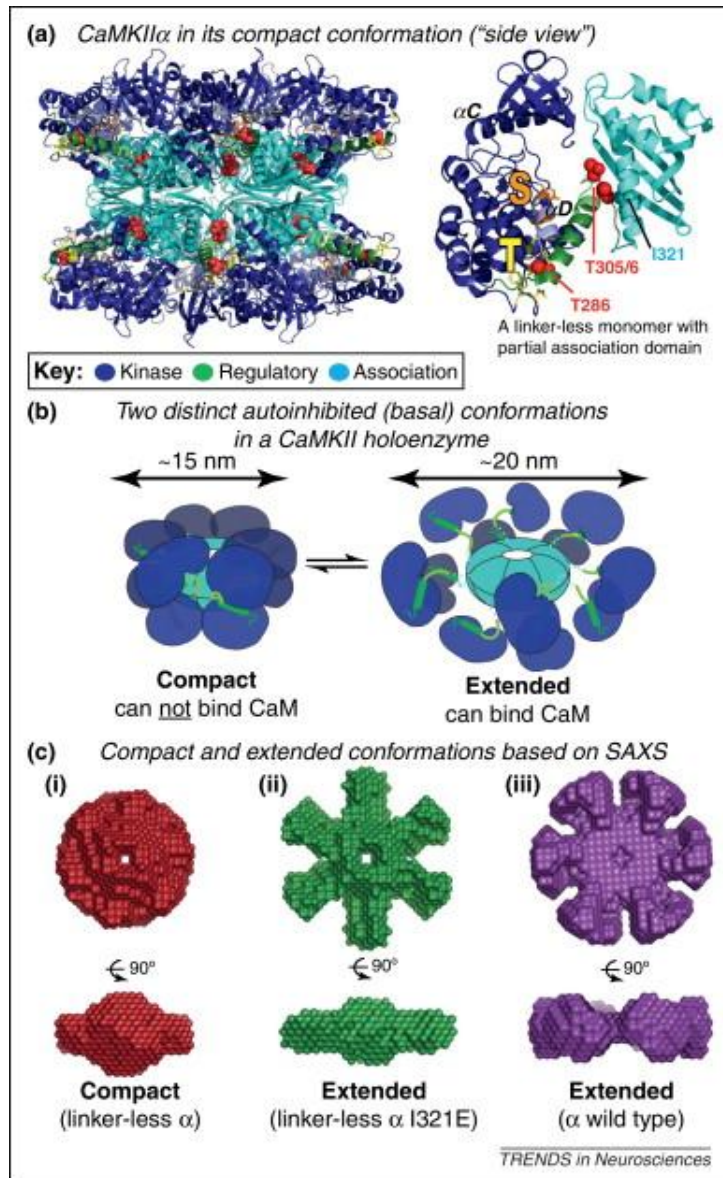
Figure 1.4: CaMKII holoenzyme structure
The holoenzyme assembly is comprised of two hexameric rings with the kinase domain
tightly arranged around the central hub domain.
Adapted from (Chao et al., 2011).

1.2.4 CaMKII activation mechanism

There are three critical phosphorylation sites in the regulatory segment of CaMKII (T286, T305 and T306). T286 phosphorylation site locates in the R1 regulatory segment and is at the base of an α helix formed by the regulatory segment (Figure 1.3). The α helix blocks the entry of the substrate binding site, and CaMKII is locked in the inactive state in the absence of Ca^{2+}/CaM. Binding of Ca^{2+}/CaM to CaMKII forces the release of the regulatory segment, thus opening the substrate binding site and presents T286 to adjacent activated CaMKII subunits. The exposed T286 then undergoes a transphosphorylation reaction (Hanson et al., 1989; Hanson et al., 1994; Lisman et al., 2002; Miller and Kennedy, 1986). Phosphorylation at T286 interrupts the docking of regulatory segment against the kinase domain and switches CaMKII to a Ca^{2+}/CaM-independent state (autonomous activity) (Figure 1.5). The autonomous activity retains partial CaMKII activity even when the Ca^{2+} returns to the basal level (~nM range).

T305/T306 phosphorylation sites reside in the CaM-binding site in the R3 regulatory segment of CaMKII (Figure 1.3). This part of regulatory segment is buried in the central hub and is difficult to access in its autoinhibited state (Chao et al., 2011). Phosphorylation at T305 and/or T306 follows T286 phosphorylation and prevents binding of Ca^{2+}/CaM (Colbran, 1993; Hanson and Schulman, 1992).
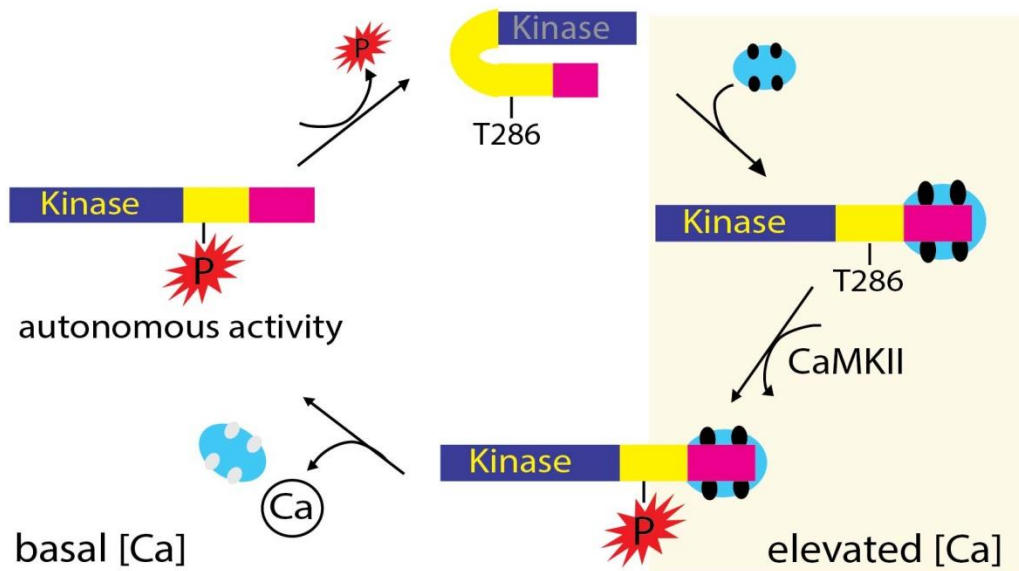
Figure 1.5: CaMKII regulatory mechanism
Ca²⁺ influx during LTP induction triggers CaMKII activation. Phosphorylation at T286 retains partial CaMKII activity (autonomous activity) even when [Ca²⁺] returns to the basal level.

1.2.5 Phosphorylation at Thr286 induces calmodulin trapping

Phosphorylation at T286 not only generates autonomous activity that bypasses the requirement of Ca²⁺, but also enhances the binding affinity between Ca²⁺/CaM and CaMKII for >10,000 fold, a phenomena termed 'CaM trapping' (Meyer et al., 1992). From the *in vitro* biochemical measurements (fluorescence emission anisotropy measurements from densylated-CaM), the dissociation time constant ($1/k_{off}$) of Ca²⁺/CaM from T286 phosphorylated CaMKII is > 1000 s; while for non-phosphorylated CaMKII (in the absence of ATP) is 0.46 s in the presence of ~1 μM Ca²⁺. The dissociation time constant of Ca²⁺/CaM from CaMKII strongly depends on [Ca²⁺], and the *in vitro* measurements

suggest that it requires $[Ca^{2+}]$ lower than 100 nM for > 10 s to have Ca^{2+}/CaM dissociate from CaMKII. Site-directed mutagenesis study further shows that interaction between CaMKII F293 and CaM E120 and CaM M124 specifically stabilize CaMKII-CaM trapped complex but only when CaMKII T286 is phosphorylated (Singla et al., 2001).

1.2.6 CaMKII: a frequency decoder of Ca^{2+} oscillation *in vitro*

Ca^{2+} frequency decoding behavior of CaMKII was first shown *in vitro* by Schulman *et al* (De Koninck and Schulman, 1998). They immobilized CaMKII (through HA tag) in PVC tubing that was connected to a pulse-flow device. After the stimulus, tubing was removed for the subsequent kinase activity assay. The amount of CaMKII autonomous activity depends on CaM concentration, indicating the requirement of two CaM binding events for T286 phosphorylation. Also, the amount of CaMKII autonomous activity depends on the frequency and duration of Ca^{2+} pulses. An earlier simulation study suggested that limiting the amount of Ca^{2+}/CaM is a prerequisite for CaMKII being a Ca^{2+} frequency decoder (Hanson et al., 1994).

Schulman *et al* further showed that CaMKII isoforms bear different Ca^{2+}-frequency dependent responses (Bayer et al., 2002). The alternative splice variants of CaMKIIβ have highly conserved kinase domain and regulatory segment, but with significantly different amounts of autonomous activity generated by Ca^{2+} spikes. Isoforms with longer linkers (regions that connecting kinase and the hub domain) have a

14

higher affinity for Ca^{2+}/CaM and acquire autonomous activity at lower frequencies.

Based on the holoenzyme structure, SAXS analysis and the stochastic simulation,

Kuriyan *et al* provides a molecular architecture explanation that the length of linker

affects the equilibrium between the compact and extended autoinhibited conformations

of CaMKII holoenzyme (Chao et al., 2011). CaMKII holoenzyme with a longer linker

length favors the extended autoinhibited conformation and has easier access for

Ca^{2+}/CaM, therefore has lower frequency threshold for acquiring autonomous activity.

1.2.7 CaMKII translocation and binding to NMDA-receptors

1.2.7.1 CaMKII translocation to PSD

Translocation of CaMKII from the cytoplasm to the PSD was first shown in

hippocampal cultured neurons after bath application of glutamate stimulation (Shen and

Meyer, 1999). Electron microscopy immunolabelling was further used to measure

CaMKII levels in PSD after chemical LTP (cLTP) stimulation in hippocampal slice

cultures (Otmakhov et al., 2004). cLTP stimulation results in a persistent accumulation of

CaMKIIα in PSD (Figure 1.6). Phosphorylation at T286 prolongs CaMKII localization to

PSD through the enhancing binding affinity of Ca^{2+}/CaM to CaMKII which is required

for PSD translocation of CaMKII (Shen and Meyer, 1999). CaMKII translocation to

synapse is activity-dependent and spine specific (Lee et al., 2009). Translocation of

CaMKII is mainly fulfilled by simple diffusion and binding of activated CaMKII to

synaptic proteins (mainly to NMDARs), and is also driven by spine enlargements. The

increase of F-actin in spines after enlargements of spine results in higher numbers of

CaMKIIα-CaMKIIβ heteromers that are bound to F-actin (Ahmed et al., 2006; Shen et al.,

1998).
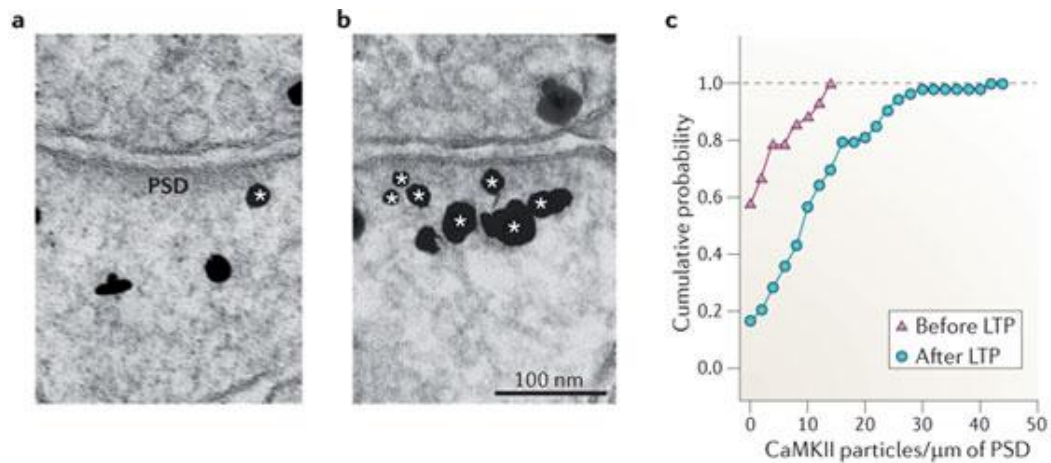
Figure 1.6: Translocation of CaMKII to PSD after LTP induction
Immunolabelling of CaMKII imaged by electron microscopy shows that CaMKIIα
accumulates in PSD after cLTP induction. (a: before stimulation; b: 1 hour after cLTP
stimulation; c: cumulative distribution of CaMKIIα per unit length of PSD)
Adapted from (Otmakhov et al., 2004).

1.2.7.2 Discovery of CaMKII/NR2B complex

Association of CaMKII to NMDA-receptors (mainly to NR2B) was first

demonstrated in cortical slices by immunoprecipitation after NMDA treatment (Leonard

et al., 1999). *In vitro* studies showed that binding of CaMKII to NR2B is independent of

T286-phosphorylated state and suppresses inhibitory phosphorylation at T305/T306

(Bayer et al., 2001). There are two regions in NR2B that were identified for CaMKII

binding: regions around S1303 (no requirement for but is enhanced by CaMKII T286 phosphorylation), and another upstream region between amino acids 839 to amino acids 1120 (requires CaMKII T286 phosphorylation). I205 in CaMKII (located in the T-site of regulatory segment) is a key residue in facilitating the CaMKII/NR2B interaction since I205K mutation in CaMKII blocks CaMKII/NR2B complex formation and significantly impairs CaMKII translocation in HEK293 cells that co-express CaMKII and NMDARs (Bayer et al., 2001; Bayer et al., 2006).

The functional importance of CaMKII/NR2B complex might be that it targets CaMKII to the proximity of Ca^{2+} influx and recruit activated CaMKII to modulate AMPA-receptors mediated transmission (Derkach et al., 1999; Hayashi et al., 2000; Rongo and Kaplan, 1999). CaMKII/NR2B complex also generates another form of 'autonomous activity' of CaMKII without the requirement of T286 phosphorylation or CaM trapping, and the form of 'autonomy' can not be reversed by phosphatase. However, some conflicting results showed that binding to NR2B subunits inhibits CaMKII activity have been reported (Robison et al., 2005).

1.2.7.3 CaMKII/NR2B complex in LTP

The role of CaMKII/NR2B complex was examined in LTP in hippocampal slice cultures with overexpression of a mutant form of NR2B (NR2B RS/QD, which has a reduced affinity towards CaMKII). Overexpression of NR2B RS/QD prevents LTP and

overexpression of NR2A (which has a low affinity towards CaMKII) reduces LTP (~50%

reduction). Expression of NR2A with mutations that have high affinity towards CaMKII

recovers LTP (Barria and Malinow, 2005). Further, in a transgenic mice model carrying

tamoxifen (TAM)-activated expression of NR2B-C terminal segment (cNR2B),

expression of cNR2B disrupts the binding of endogenous CaMKII to endogenous NR2B

subunits and decreases the level of CaMKII T286 phosphorylation. Expression of cNR2B

results in LTP reduction (~ 50%) and impaired spatial learning, demonstrating the

requirement of CaMKII/NR2B complex in LTP and spatial learning (Zhou et al., 2007).

To complement the above studies, another RNA interference (RNAi) NR2B knockdown

experiment (carried out in hippocampal slice cultures) demonstrated that only NR2B-C

terminus segment is important for LTP (possibly for recruiting CAMKII and other

synaptic proteins to PSD). NR2A-C terminus segment, in contrast, is not essential for

LTP and its C terminus segment seems to carry inhibitory elements for LTP (Foster et al.,

2010).

CaMKII/NR2B complex seems to be an important form in pulling CaMKII to PSD

and in maintaining LTP. However, the rough estimate of NMDAR per synapse is

around 20-25 (compared to CaMKII in PSD: ~ 80 CaMKII holoenzyme) (Lisman et al.,

2012). Other CaMKII binding proteins might also play a role in targeting CaMKII to

PSD.

1.2.8 Other CaMKII binding proteins in PSD

Other PSD proteins that were identified as binding partners of CaMKII are as follows: densin180 (leucine-rich repeat-containing protein 7, LRRC7 (Walikonis et al., 2001), α-actinin (Walikonis et al., 2001), SAP97 (DLG1) (Nikandrova et al., 2010), and mPDZ (multiple PDZ domain protein) (Krapivinsky et al., 2004). CaMKII has also been reported to associate with L- and P/Q-type voltage-gated calcium channels (Hudmon et al., 2005b; Jiang et al., 2008) and dopamine receptors (Liu et al., 2009). Many of these channels and receptors are localized in PSD and might contribute to targeting CaMKII to PSD. CaMKII can also self-associate to other CaMKII holoenzyme to boost its concentration in PSD (Hudmon et al., 2005a). Localized CaMKII in PSD seems to be important in LTP maintenance; however, we have to keep in mind that the fraction of CaMKII in PSD (~80 molecules) is relatively small compared to CaMKII in the rest of the areas in dendritic spines (~ 1,000 molecules).

1.2.9 Potentiation of AMPA-receptors by CaMKII

During LTP, AMPA-receptor mediated transmission is enhanced through increases of single channel conductance and through increases of AMPA-receptors at synapse (Luthi et al., 2004; Opazo and Choquet, 2011; Poncer et al., 2002; Shi et al., 1999). There are many phosphorylation sites in AMPARs (S831, S845, S567 and S818) that have been linked to property of AMPA-receptor conductance and insertion of AMPA-

receptors to synapse (Banke et al., 2000; Barria et al., 1997a; Boehm et al., 2006; Lee et al., 2000; Roche et al., 1996). Among which, phosphorylation at S831 is carried out by CaMKII and PKC. Therefore, S831 phosphorylation will be discussed in the following section.

1.2.9.1 AMPA-receptors phosphorylation by CaMKII

Phosphorylation at S831 increases during LTP (Barria et al., 1997b; Lee et al., 2000), and enhances the probability that high conductance states of AMPARs that would be activated by intermediate concentration of glutamate (Kristensen et al., 2011). This property of AMPARs is eliminated in S831A knock-in mice. In contrast, in S831D knock-in mice, AMPAR conductance is enhanced and precludes further enhancement by CaMKII (Kristensen et al., 2011). However, S831A knock-in mice have normal LTP (as one would not expect). Only when S845A mutation exists along with S831A (double knock-in mice), LTP is reduced (Lee et al., 2010).

1.2.9.2 Insertion of AMPA-receptors to synapse

Exocytosis of AMPAR-containing vehicles into plasma membrane has been imaged by SEP-GluR1 (super ecliptic pHluorin, a pH-sensitive form of EGFP) combined with FRAP technique (fluorescence recovery after photobleaching) at the single spine level after glutamate uncaging induced LTP (Makino and Malinow, 2009; Patterson et al., 2010). Exocytosis of AMPARs occurs on the stimulated spines and the nearby

dendritic region (< 3 μm), and depends on the RAS-ERK signaling pathway, Rab-GTPase, syntaxin 4 and 13, and myosin Vb (Kennedy et al., 2010; Lledo et al., 1998; Park et al., 2004; Wang et al., 2008; Zhu et al., 2002). However, inhibition of the upstream signaling molecules on AMPAR exocytosis does not affect LTP in the first 20 min, but LTP in the later phase is reduced (Yang et al., 2008). This result suggests that the enhanced AMPAR-mediated transmission during LTP in the first 20 min is mediated through capture of extrasynaptic AMPARs to the synapse (Makino and Malinow, 2009).

AMPAR immobilization to synapse through lateral diffusion has been directly imaged by single-particle tracking with Q-dot tagged to extracellular region of AMPAR (Opazo et al., 2010). Immobilization of AMPAR to the synapse is blocked by CaMKII inhibitor (KN93 and CN21), and blocked by overexpression of CaMKII I205K (which is unable to translocate to synapse where it binds to NR2B). The relationship between CaMKII (especially the fraction targets to the synapse) and AMPAR trapping is that localization of AMPAR to synapse depends on the binding of stargazing to PSD, and stargazing S9 phosphorylation by CaMKII is required for AMPAR translocation from extrasynaptic sites to synapse (Bats et al., 2007; Opazo et al., 2010; Schnell et al., 2002). Figure 1.7 illustrates the role of CaMKII in regulating AMPAR-mediated transmission during early LTP.
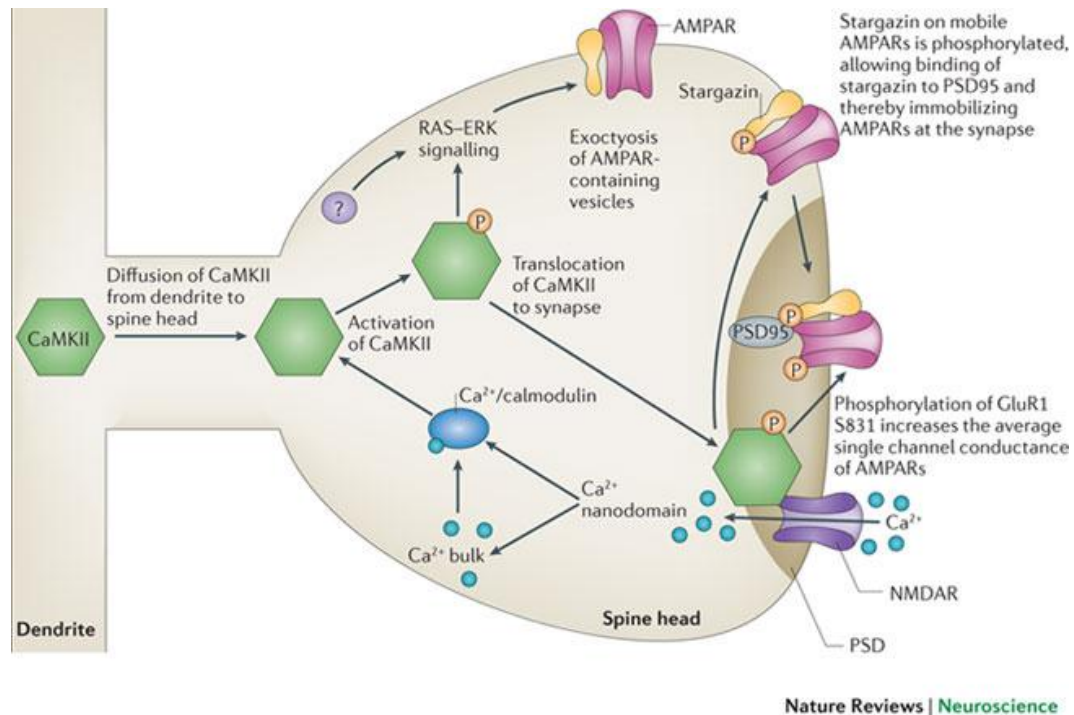
Figure 1.7: Role of CaMKII in AMPAR-mediated transmission during early LTP
CaMKII enhances AMPAR-mediated transmission by phosphorylation at GluR1 S831 and by phosphorylation at stargazing S9 to immobilize AMPARs at the synapse. Adapted from (Lisman et al., 2012).

1.2.10 Gating of CaMKII activity by protein phosphatase activity

CaMKII and cAMP pathways both play important roles in transmitting and regulating postsynaptic signaling required for LTP (Abel et al., 1997; Lisman et al., 2012; Otmakhova et al., 2000). Studies have shown that cAMP pathway gates CaMKII activity by inhibiting protein phosphatase 1 (PP1) activity through activation of protein phosphatase inhibitor (I-1) during LTP (Blitzer et al., 1998; Blitzer et al., 1995). However, we should note that in these studies, LTP is established by the 'well-separated HFS' protocol which consists of three trains of 100 pulses delivered at 100 Hz, separated by 10

min duration. Blitzer *et al* showed that PP1 activity is attenuated and I-1 activity is

enhanced after high-frequency stimulation in rat hippocampal slices (Blitzer et al., 1998).

cAMP produced during LTP induction activates protein kinase A (PKA). Active PKA

then phosphorylate and activate I-1 (Blitzer et al., 1995; Ingebritsen and Cohen, 1983).

Dephosphorylation of I-1 is fulfilled by calcinurin (Mulkey et al., 1994).

LTP can be induced by various stimulation protocols (Brown et al., 2000;

Coussens and Teyler, 1996; Dudek and Bear, 1992; Katsuki et al., 1997; Thomas et al.,

1996). Among which, LTP induced by theta frequency stimulation (5-12 Hz) depends on

cAMP pathway and is gated by PP1 (Brown et al., 2000). However, activation of cAMP

pathway alone is not sufficient to induce LTP. Thus, the postsynaptic cAMP pathway

does not transmit the signals for LTP but rather gates the transmittal pathway by

prohibiting inhibition of CaMKII activity through PP1 inhibition (Blitzer et al., 1995;

Brown et al., 2000).

1.3 Synaptic structural plasticity

1.3.1 Structural basis of LTP

Dendritic spines are tiny compartments (~0.1 fL) locate along the dendrites of

most of the principal neurons in the CNS. Structural remodeling of dendritic spines has

been proposed to be a cellular basis of learning and memory. Such a model has been

investigated through the assist of two-photon LASER scanning microscopy and the

development of two-photon photolysis of caged compounds (MNI-caged-glutamate) (Hayashi-Takagi et al., 2015; Matsuzaki et al., 2001). The structural basis of LTP was first demonstrated by Kasai *et al* in 2004 (Matsuzaki et al., 2004). They showed that electrical stimulation at the Schaffer collateral pathway either at high frequency (100 Hz, 1 s) or low frequency (2 Hz, 1 min) in the presence of Mg^{2+} induced spine enlargements similarly to that induced by directly applying repetitive glutamate uncaging pulses (1 Hz, 1 min) in the absence of Mg^{2+} (Figure 1.8). Spine volume enlargements were long-lasting (> 100 min) and input specific. There's no spine volume change in the nearby spines (within 3 μm). Enlargement of spine volume is NMDA-receptor and CaMKII dependent, similar to the electrical-stimulated LTP (Malenka et al., 1989; Malinow et al., 1989). AMPA-receptor mediated EPSC was also potentiated after repetitive glutamate uncaging pulses, demonstrating that both structural and functional plasticity of dendritic spines were modified. Interestingly, sustained phase spine volume change depended largely on the original spine volume size. Long-lasting spine enlargement (> 50% change) was observed in 50% of small spine (< 0.1 fL) but only 5% in large spines (> 0.1 fL). This result suggested that small spines are the plastic sites for subsequent LTP induction, while large spines might represent physical traces of cellular memory.
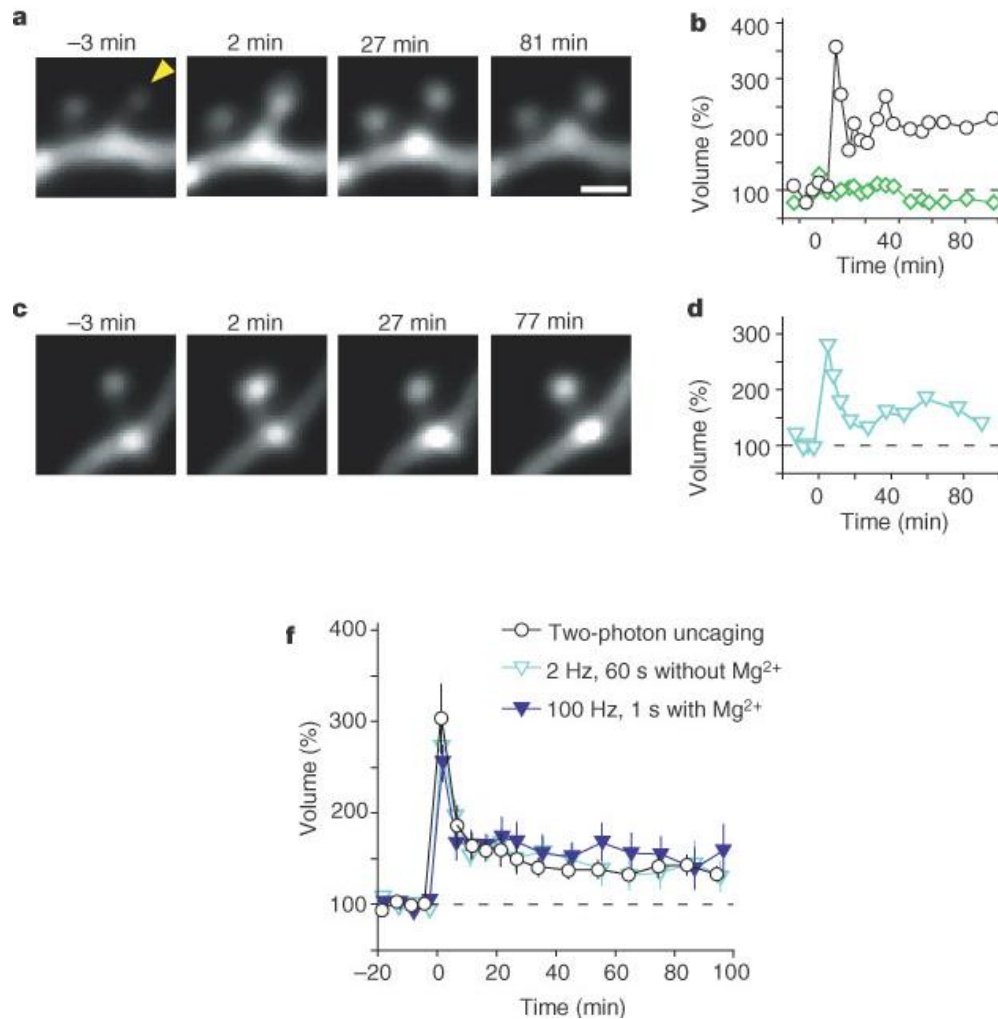
Figure 1.8: Spine volume change induced by repetitive glutamate uncaging
(A) Fluorescence images of CA1 hippocampal neurons (transfected with EGFP) before and after glutamate uncaging at 1 Hz. Quantitative spine volume change is shown in (B).
(C) Electrical stimulation at the Scaffer-collateral pathway (2 Hz) in the presence of Mg^{2+}. Quantitative spine volume change is shown in (D).
(F) Averaged spine volume change in response to different stimulation protocols.
Adapted from (Matsuzaki et al., 2004).

1.3.2 Biophysical basis of the synapse-specific signaling

Spines are tiny compartments (~ 0.1 fL) connected to dendritic shaft via a thin

spine neck (d ~ 0.1 μm) (Harris and Kater, 1994). This special geometry structure limits

diffusional exchange of signaling molecules, including Ca^{2+}, between spine heads, their

parent dendrites and neighboring spines. Therefore, dendritic spines serve as

biochemical compartmentalization necessary for synapse-specific signaling (Holmes,

1990; Koch and Zador, 1993). To achieve synapse-specific signaling, generally, the

activity of signaling molecules decays faster than the spine-neck diffusion coupling time.

Spine-neck diffusion coupling time can be estimated as (Svoboda et al., 1996):

$$\tau = \frac{Vl}{Ds}$$

where V is the spine volume (~ 0.2 μm³), l is the spine neck length (~ 1 μm), s is the cross

sectional area of spine neck (~ $0.05^2\pi$) and D is the diffusion constant (Lee and Yasuda,

2009; Yasuda and Murakoshi, 2011). Assuming for small molecules (such as Ca^{2+} ions), D

~ 100 μm²/s, τ is around 0.1 s. Thus, for small molecules, its activity will be localized if

the lifetime of the active state is < 0.1 s.

1.3.3 Ca²⁺ signaling during synaptic plasticity

Ca^{2+} signaling is the most common second messenger that triggers the signaling

network that underlies LTP. Through the direct Ca^{2+} imaging techniques, Svoboda *et al*

revealed the key biological factors that handling Ca^{2+} in dendritic spines under

physiological conditions. Endogenous Ca^{2+} buffer capacity in dendritic spines is low,

which allows large and rapid $[Ca^{2+}]$ changes. Ca^{2+} diffusion across the spine neck is

negligible, which allows $[Ca^{2+}]$ to accumulate during repetitive synaptic stimulations. In

addition, the kinetics of Ca^{2+} sources (such as kinetics of NMDA-receptors) primarily

governs the time course of Ca^{2+} signaling (Sabatini et al., 2002).

In pyramidal neurons, weak synaptic stimulation leads to Ca^{2+} influx mainly

through NMDA-receptors (Koester and Sakmann, 1998; Kovalchuk et al., 2000).

Suprathreshold stimulation leads to additional Ca^{2+} influx through VSCCs activated by

backpropagating action potentials (Majewska et al., 2000; Rusakov et al., 1996; Sabatini

and Svoboda, 2000). Ca^{2+}-induced Ca^{2+} release (CICR) might also be involved under

some conditions (Emptage et al., 1999). During glutamate uncaging evoked structural

plasticity, NMDA-receptor mediated Ca^{2+} change is ~ 1 to 2 uM, with the clearance rate

~100 ms (Lee et al., 2009).

1.3.4 Signaling molecules underlying LTP

Hundreds of signaling molecules are involved in LTP and have been extensively

studied. Signaling molecules that support the long-lasting modification of synaptic

strength are temporally and spatially regulated (Nishiyama and Yasuda, 2015; Patterson

and Yasuda, 2011). The advancement in FRET-FLIM technique enables us to probe

activity of individual signaling molecules during LTP with high temporal (~ s) and

spatial resolution (~ 1 μm) (Murakoshi et al., 2008). Ca^{2+} is the most common second messenger that influxes through NMDARs to trigger the downstream signaling cascades. Ca^{2+} signaling triggers the signaling pathway by changing the affinity of Ca^{2+}-binding proteins. CaMKII is activated by the binding of Ca^{2+}/CaM, and activation of CaMKII lasts for ~ 1 min during LTP (Lee et al., 2009). CaMKII activity is spine specific and occurs in the nanodomain near the channels. Small GTPases such as Cdc42, RhoA and H-Ras which are involved in remodeling of actin filaments are all activated during LTP and activate within ~ 1 min (Harvey et al., 2008; Murakoshi et al., 2011). Interesting, in contrast to transient CaMKII activation, the activity of Cdc42 and RhoA lasts for > 30 min. The activity of Cdc42 is spine-specific; while active RhoA and H-Ras spread along the dendrite (~ 5-10 μm) and invade nearby spines. Inhibition of CaMKII activity by KN62 also inhibits activity of Cdc42, RhoA and H-Ras, demonstrating they are downstream of CaMKII signaling. Further, recently it has been shown that signaling originated in spines can be transduced into the nucleus demonstrated by imaging ERK activity after LTP induction. In this study, Yasuda *et al* showed that LTP induction at only a few spines (3 to 7) is sufficient to activate ERK in the nucleus (Zhai et al., 2013) (Figure 1.9).
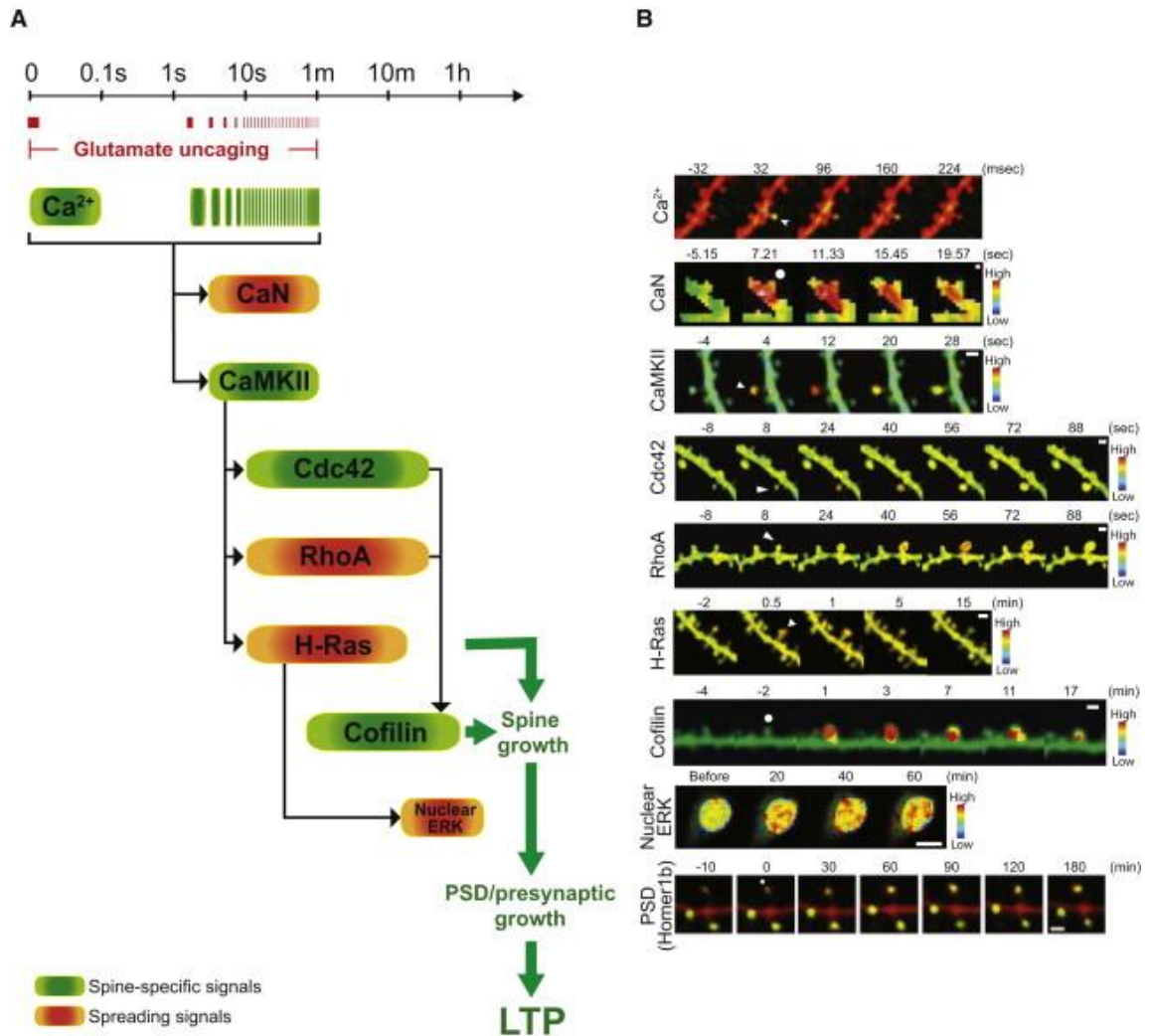
Figure 1.9: Spatiotemporal dynamics of signaling activities during sLTP
(A) Schematic timescale of signaling activity during sLTP. Spine-specific signaling is shown in green while spreading signaling is shown in orange.
(B) Images showing activity of different signaling activated at different timescale during sLTP. Ca^{2+} transients, CaN, CaMKII, Cdc42, RhoA, H-Ras, coffilin, ERK and accumulation of Homer1b are shown. Adapted from (Nishiyama and Yasuda, 2015).

1.4 Experimental rationale and specific aims

Experimental rationale

Structural plasticity of dendritic spines is thought to underlie synaptic plasticity and memory formation (Hayashi-Takagi et al., 2015; Matsuzaki et al., 2004). Various forms of spine plasticity are induced by a common signal: intracellular Ca^{2+} elevations (Hayama et al., 2013; Kwon and Sabatini, 2011; Matsuzaki et al., 2004; Oh et al., 2015; Zhou et al., 2004; Zucker, 1999). Therefore, dendritic spines must have intracellular machinery to interpret information encoded in the frequency, amplitude, and number of Ca^{2+} elevations (Berridge, 1997; Smedler and Uhlen, 2014). Furthermore, these transient Ca^{2+} signals (~100 ms) must be transduced into signals that can modify synaptic strength in a long-lasting manner (> hours) (Kennedy et al., 2005; Nishiyama and Yasuda, 2015).

Activation of CaMKII is considered to be one of the first biochemical steps in translating the information encoded in Ca^{2+} elevations (~100 ms) into long-lasting modifications of synaptic strength (> hours) (De Koninck and Schulman, 1998). CaMKII links Ca^{2+} elevations to downstream cellular targets responsible for spine plasticity through phosphorylation of its diverse substrates (Barria et al., 1997b; Murakoshi et al., 2011; Opazo et al., 2010; Walkup et al., 2015; Yang et al., 2013). Basally, CaMKII is locked in an inactive state through the binding of a regulatory segment to its substrate binding site. Upon the influx of Ca^{2+}, Ca^{2+}/calmodulin binds to CaMKII and induces its

activation. The subsequent autophosphorylation at Thr286 (for CaMKIIα or Thr287 for CaMKIIβ), which is located in the mouth of the regulatory segment, prevents the rebinding of the regulatory segment to the kinase domain. This permits an autonomous activity of CaMKII that is independent of Ca^{2+}/calmodulin binding (Chao et al., 2011; Hanson et al., 1989; Hanson et al., 1994; Lisman et al., 2002). Using knock-in mice in which Thr286 of CaMKIIα is mutated to Alanine (*Camk2a*[T286A]), phosphorylation at CaMKIIα Thr286 has been found to be essential for LTP, learning and memory (Giese et al., 1998).

Previously, CaMKII activation was measured during spine plasticity by using two-photon fluorescence lifetime imaging microscopy (2pFLIM) or ratiometric FRET imaging microscopy in combination with CaMKII activity sensors, Camuiα or its variants (Fujii et al., 2013; Lee et al., 2009; Yagishita et al., 2014). These sensors measured the conformation change of CaMKII by FRET between fluorophores attached to the two ends of CaMKIIα subunit, and their FRET efficiency was correlated with CaMKII activity (Lee et al., 2009; Takao et al., 2005). The imaging results showed that CaMKII is transiently activated during spine plasticity. CaMKII activity returned to basal levels within ~1 min (Lee et al., 2009; Yagishita et al., 2014). However, due to the limited temporal resolution (~seconds), the mechanisms of signal integration remained elusive.

Here, I plan to achieve our goal by pursuing the following three specific aims:

Specific aims:

Aim 1: Characterize CaMKII activation with high temporal resolution during the induction of spine plasticity

In order to directly probe the Ca^{2+} frequency-dependent activation of CaMKII, we will use fast framing imaging of 2pFLIM (~ 128 ms/frame) to measure CaMKII activity in accord with each of repetitive Ca^{2+} elevations (~ 100 ms)during the induction of spine plasticity.

Aim 2: Characterize the role of CaMKII Thr286 phosphorylation during spine plasticity

Autophosphorylation at Thr286 is critical in LTP, learning and memory. To characterize its role in regulating the frequency-dependent activation of CaMKII, we will use non-phosphorylated and phospho-mimetic mutants of Thr286 to characterize its role during spine plasticity.

Aim 3: Characterize the molecular mechanism that underlies Ca^{2+} signal integration by CaMKII

Ca^{2+} signal integration by CaMKII substantially prolongs the transient Ca^{2+} signaling. This signaling amplification could be mediated by the enhanced binding affinity towards Ca^{2+}/CaM or/and by the partial activity retained by the phosphorylation at Thr286. To investigate the molecular mechanism responsible for this integration, we

32

will develop a FRET-based sensor and measure CaMKII-CaM association during the induction of spine plasticity.

We expect that the three specific aims will collectively elucidate the role of CaMKII during spine plasticity and regulation of phospho-Thr286 on CaMKII activation during the induction of spine plasticity.

Chapter 2.   Materials and methods

2.1 Experimental animals

Mice from BL6/C57 strain (purchased from Charles River Laboratories) were used as wild-type group in 2pFLIM measurements. $Camk2a^{T286A}$ knock-in mice (gift from Dr. Giese) were used in the specified experiments. CaMKIIα conditional knock-out mice ($Camk2a^{fl/fl}$, strain name: C57BL/6-$Camk2a^{tm1Vyb}$; deposited by Dr. Tonegawa) carry a floxed exon 2 allele and were from the Jackson Laboratory (Hinds et al., 2003). All experimental animals were bred in-house under the animal care and guidelines of Duke University Medical Center and Max Planck Florida Institute for Neuroscience.

2.2 Preparation

Organotypic cultured hippocampal slices were prepared from postnatal 4-7 day mice (see a detailed protocol at (Stoppini et al., 1991)), tissue slices were plated on cell culture inserts (hydrophilic PTFE, 0.4 μm, Millipore) and maintained in tissue medium (minimum essential medium eagle (MEM) 8.4 mg/ml, horse serum 20%, L-glutamine 1 mM, $CaCl_2$ 1 mM, $MgSO_4$ 2 mM, D-glucose 12.9 mM, $NaHCO_3$ 5.2 mM, HEPES 30 mM, insulin 1 μg/ml, ascorbic acid 0.075%) at 37°C supplemented with 5% CO2 until experiments (DIV 12-19). Hippocampal slices were biolistically transfected with plasmids at DIV 5-10 (12 mg gold particle, size: 1 μm, 30 μg plasmid). Acute slices were prepared from postnatal 30-40 day $Camk2a^{T286A}$ mice and litter-mate control mice.

Preparation of slice cultures was in accordance with the animal care and guidelines of

Duke University Medical Center and Max Planck Florida Institute for Neuroscience.

2.3 Plasmids

Molecular cloning and mutations were carried out using QuikChange site-

directed mutagenesis kit (Agilent Technologies) and InFusion cloning kit (Clontech).

Expression of Camuiα was under pCAG promoter. Camuiα (dimVenus-CaMKII-mEGFP

or Green-Camuiα) was described previously (Lee et al., 2009).

2.3 Two-photon fluorescence lifetime imaging

Recent advances in two-photon fluorescence lifetime imaging microscopy

(2pFLIM) coupled with two-photon photochemistry technique have greatly facilitated

the study on the activity of signaling molecules at single synapse level (Svoboda and

Yasuda, 2006; Yasuda, 2006). Fluorescence resonance energy transfer (FRET) is a non-

radiative energy transfer process. The efficiency of FRET depends on the distance

between the donor and acceptor fluorophores and has a sensitive region around the

nanometer range (Yasuda, 2006). Thus, FRET is suitable in measuring the dynamics of

protein-protein interaction and protein conformation change. FRET efficiency measured

by FLIM is independent of the concentration of acceptor fluorophores and insensitive to

length-dependent light scattering. FLIM is also characterized of a high sensitivity

because each collected photon contributes to the signal. Therefore, 2pFLIM is suitable for

imaging FRET sensors in light-scattering tissues. Besides, because of the high resolution

of 2pLSM, 2pFLIM is suitable in imaging in small neuronal compartments such as single

synapses (Figure 2.1).
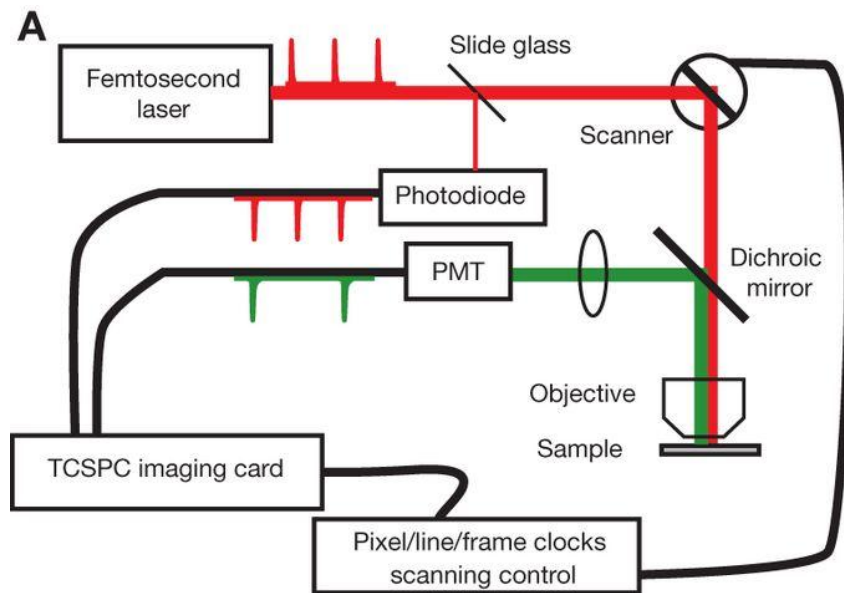
Figure 2.1: Schematic of a 2pFLIM setup
TCSPC: time-correlated single-photon counting, PMT: photomultiplier tube. Adapted
from (Yasuda, 2012).

2.3.1 CaMKII activity imaging

Hippocampal slices were bathed in artificial cerebrospinal fluid (ACSF) bubbled

with carbogen (95% O2/ 5% CO2) during the image recordings. Final ion concentrations

(in mM) in imaging solution: NaCl 127, $NaHCO_3$ 25, D-glucose 25, KCl 2.5, NaH_2PO_4

1.25, supplemented with $CaCl_2$ 4, MNI-caged L-glutamate (Tocris) 4, TTX 0.001, Trolox

(Sigma) 1. Between DIV 12-19, we imaged individual transfected CA1 pyramidal

neurons. Dendritic spines on the secondary and tertiary apical dendrites were used for

imaging. Images were acquired by a home-built 2pFLIM microscope controlled by custom software (MatLab). Experiments were performed at $25 \pm 0.5°C$ or 34-35 °C as indicated. The temperature was controlled with a control syringe heater and an inline solution heater (TC344C, SW-10/6 and SH-27B, Warner Instruments). Recordings were performed with 32x32 pixels (pixel size: 12.3 ± 1.72 pixel/μm) at 128 ms/frame (7.8 Hz).

2.3.1.1 Characterize CaMKII activation in HeLa cells

Fluorescence lifetime of Camuiα sensor and its different mutant forms in HeLa cells were characterized to validate the sensor sensitivity. Camuiα was activated by the bath application of ionomycin. Fluorescence lifetime change of the different mutant forms relative to its basal lifetime was also quantified (Figure 2.2). T286A- Camuiα exhibited a similar basal lifetime as wild-type but had limited conformation change. T286D- Camuiα exhibited much higher basal lifetime (which reflects the open conformation) and could be further activated. T305A/T306A- Camuiα also exhibited a higher basal lifetime and could be further activated. Interestingly, K42R- Camuiα (kinase dead mutation) exhibited similar basal lifetime as wild-type but could not be activated (no conformation change), suggesting that conformation change of CaMKII might require ATP hydrolysis. Monomeric Camuiα adopted an open conformation and did not response to the bath application of ionomycin (Figure 2.2).
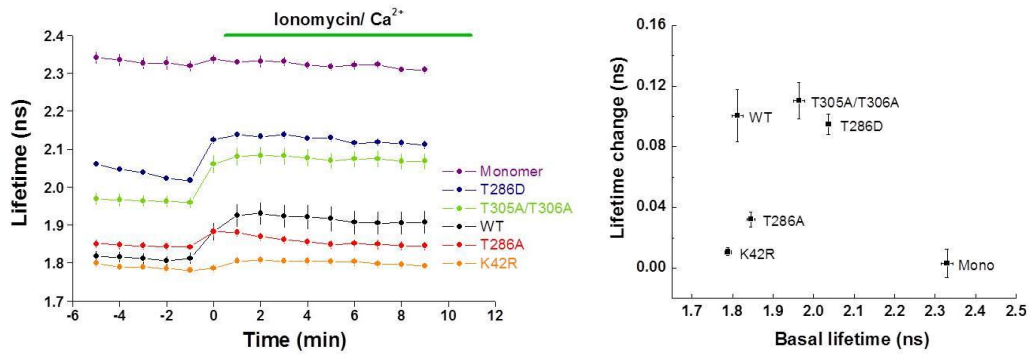
Figure 2.2: Characterization of CaMKII activation in HeLa cells
Wild-type, T286A, T286D, T305A/T306A, K42R-Camuiα and monomeric Camuiα activation in response to ionomycin measured in HeLa cells.

2.3.2 Binding of Ca^{2+}/CaM to CaMKII

Binding kinetics between CaM and CaMKII was directly probed by CaM/CaMKII FRET sensor: mEGFP-CaMKII and mCherry-CaM. We inserted cDNA sequence of calmodulin 1 (calm1) from *Mus musculus* into the C-terminus of mCherry containing pCAG plasmid. All fusion proteins are expressed under pCAG promoter. For CaMKII[T286A]/CaM FRET sensor, we used hippocampal slices from *Camk2a*[T286A] knock-in mice to eliminate the unwanted inter-subunit FRET between mEGFP-CaMKII[T286A] and mCherry-CaM bound to the nearby endogenous wild-type CaMKII. Plasmids were biolistically transfected into the slices (12mg gold particle, size: 1 μm, mEGFP-CaMKII 20μg, mCh-CaM 40μg, Cre recombinase 12 μg) between DIV 5-7. For other mutant forms of mEGFP-CaMKII, we used hippocampal slices from *Camk2a*^{fl/fl} mice. mEGFP-

CaMKII (T305A/T306A or T305DT306D, 20μg), mCh-CaM (40μg) and Cre recombinase

(12 μg) were simultaneously biolistically transfected into the slices.

2.4 2pFLIM data analysis

2.4.1 Camuiα

Fluorescence lifetime of mEGFP in Camuiα is affected by the FRET efficiency.

Fluorescence lifetime of mEGFP in Camuiα has at least 3 populations: closed

conformation (basal), open conformation (active), and mEGFP (donor) with unfolded

dimVenus (acceptor). The third population can be regarded as a constant component

throughout the measurement. Since Camuiα is a monomeric FRET pair sensor (1:1 ratio

of mEGFP: dimVenus), the change of mean fluorescence lifetime of Camuiα (τ_m) reflects

the change of FRET efficiency and thus the conformation change of Camuiα. The mean

fluorescence lifetime of Camuiα (τ_m) was derived from the mean photon arrival time $\langle t \rangle$

as follows:

$$\tau_m = \langle t \rangle - t_0 = \frac{\int dt \cdot t F(t)}{\int dt \cdot F(t)} - t_0$$

where $F(t)$ is the fluorescence lifetime decay curve, t_0 is offset. t_0 is estimated by fitting

to the fluorescence decay curve summing all pixels in all frames over a whole image

session (typically 1024 frames) with a double exponential function convolved with the

Gaussian pulse response function:

$$F(t) = F_0[P_D H(t, t_0, \tau_D \tau_G) + P_{AD} H(t, t_0, \tau_{AD} \tau_G)]$$

39

where τ_{AD} is the fluorescence lifetime of donor bound with acceptor, P_D and P_{AD} are the fraction of free donor and donor bound with acceptor, respectively, and $H(t)$ is a fluorescence lifetime curve with a single exponential function convolved with the Gaussian pulse response function:

$$H(t, t_0, \tau_D, \tau_G) = \frac{1}{2} exp \left(\frac{\tau_G^2}{2\tau_D^2} - \frac{t - t_0}{\tau_D} \right) erfc \left(\frac{\tau_G^2 - \tau_D(t - t_0)}{\sqrt{2}\tau_D\tau_G} \right)$$

in which τ_D is the fluorescence lifetime of the free donor, τ_G is the width of the Guassian pulse response function, F_0 is the peak fluorescence before convolution and t_0 is the time offset, and erfc is the error function.

2.4.2 CaM/CaMKII FRET biosensor

The binding fraction change of mEGFP-CaMKII bound to mCherry-CaM was used to report CaM-stimulated CaMKII activity. To measure the fraction of mEGFP-CaMKII (donor) bound to mCherry-CaM (acceptor), the fluorescence lifetime in all pixels within a field-of-view is summed and fitted with a double exponential decay function convolved with a Gaussian pulse response function:

$$F(t) = F_0[P_D H(t, t_0, \tau_D, \tau_G) + P_{AD} H(t, t_0, \tau_{AD}, \tau_G)]$$

where F_0 is constant, and

$$H(t, t_0, \tau_D, \tau_G) = \frac{1}{2} exp \left(\frac{\tau_G^2}{2\tau_D} - \frac{t - t_0}{\tau_D} \right) erfc \left(\frac{\tau_G^2 - \tau_D(t - t_0)}{\sqrt{2}\tau_D\tau_G} \right)$$

in which P_D, P_{AD} are the fractions of free donor (mEGFP-CaMKII) and donor bound with acceptor (mCherry-CaM), respectively. τ_D is the fluorescence lifetime of the donor without any bound acceptor ($\tau_D = 2.6\ ns$), τ_{AD} is the fluorescence lifetime of the donor bound with acceptor ($\tau_{AD} = 1.09\ ns$), τ_G is the width of the Gaussian pulse response function, F_0 is the peak fluorescence before convolution, t_0 is time offset, and erfc is error function. τ_D and τ_{AD} are fixed during the curve fitting to obtain P_D, P_{AD}. For regions of interests (ROI) within a field-of-view (such as spine and dendrite), the binding fraction P_{AD} is derived as follows:

$$P_{AD} = \frac{\tau_D(\tau_D - \tau_m)}{(\tau_D - \tau_{AD})(\tau_D + \tau_{AD} - \tau_m)}$$

2.5 Two-photon glutamate uncaging

Hippocampal slices were bathed in artificial cerebrospinal fluid (ACSF) bubbled with carbogen (95% O_2/5% CO_2) during the imaging. Final ion concentrations in imaging solution: NaCl 127 mM, $NaHCO_3$ 25 mM, D-glucose 25 mM, KCl 2.5 mM, NaH_2PO_4 1.25 mM, supplemented with $CaCl_2$ 4 mM, MNI-caged L-glutamate (Tocris) 4 mM, TTX 1 µM, Trolox (Sigma) 1 mM. A second Ti:Sapphire laser at 720 nm (laser power measured under the objective: 2.5-3 mW), pulse duration of 4-6 ms was used to photolysis MNI-caged L-glutamate (see detailed information at (Matsuzaki et al., 2004)) (Figure 2.3).

Figure 2.3: Structure of two-photon sensitive caged MNI-glutamate
Red: caging group, black: glutamate. Adapted from (Matsuzaki and Kasai, 2011).

2.6 Measurements of structural plasticity

Two-photon laser scanning microscopy (2pLSM) was used to quantify the spine volume change during glutamate uncaging of sLTP (Matsuzaki et al., 2004). When the experiments were performed in Camk2aT286A knock-in mice, hippocampal slices were cultured from Camk2aT286A/T286A (homozygous), Camk2aT286A/WT (heterozygous), and wild-type littermates. Hippocampal slices were biolistically transfected with mEGFP (12 mg gold particle, size: 1 μm, 30 μg plasmid) at DIV 7-10. Transfected CA1 neurons were imaged between DIV 12-17. For the experiments performed in Camk2afl/fl mice, the transfected plasmids are as follows: 1) conditional knock-out group: co-transfected with tdTomato labeled Cre recombinase (pCAG-tdTM-cre, 25 μg) and mEGFP (pCAG-mEGFP, 20 μg); 2) control group: co-transfected with tdTomato (pCAG-tdTM, 25 μg) and pCAG-mEGFP (20 μg). Transfected CA1 neurons with Cre positive cells were excited with Ti:Sapphire laser at 920 nm (Coherent, Chameleon) with laser power measured under the objective (Olympus, NA = 0.9, 60x) in the range of 1-1.5 mW.

Green-channel fluorescence collected from PMT (photoelectron multiplier tubes) placed after the 510 nm/70 nm (bandwidth) wavelength filters were used for spine volume change analysis.

2.7 Functionality of Camuiα sensor

To test the functionality of Camuiα, we exogenously expressed Camuiα in CA1 neurons from C$amk2a^{fl/fl}$ hippocampal slices along with tdTomato-Cre. Biolistic transfected plasmids were as follows: 1) control group: mEGFP (12 μg) and mCherry-mCherry (2mCh, 12 μg). 2) CaMKIIα conditional knock-out group: mEGFP (12 μg), tdTomato-Cre (25 μg) and 2mCh (12 μg). 3) CaMKIIα conditional knock-out + Camuiα (rescue group): Camuiα (20 μg), tdTomato-Cre (25 μg), 2mCh (12 μg). Transfected CA1 neurons were excited with Ti:Sapphire laser at 1100 nm (Spectra-Physics, InSight DeepSee) with laser power measured under the objective (Olympus, NA = 0.9, 60x) in the range of 1.5-2.5 mW. Fluorescence from 2mCherry is used to quantify the spine volume change.

2.8 Calcium imaging

We performed whole-cell patch clamp to hippocampal cultured neurons from C$amk2a^{T286A}$ mice and wild-type littermates with the pipette containing Fluo-4FF (Ca^{2+} indicator) and Alexa-594 in Potassium D Gluconate internal solution (in mM: K gluconate 130, Na phosphocreatine 10, MgCl$_2$ 4, Na$_2$ATP 4, MgGTP 0.3, L- Ascorbic acid

3, HEPES 10, pH 7.4, 310 mosm). 2pLSM and Ti:Sapphire laser at 920 nm (Coherent, Chameleon) was used to simultaneously excite the two fluorescent dyes and thus the fluorescence from each dye can be used to quantify the Ca^{2+} transients during glutamate uncaging of sLTP. Images were acquired every 64 ms. Quantification of Ca^{2+} transients can be found at (Noguchi et al., 2005).

2.9 Electrophysiology

Slice preparation: animals were sedated by isoflurane inhalation, and perfused intracardially with a chilled choline chloride solution. Brain was removed and placed in the same choline chloride solution composed of 124 mM Choline Chloride, 2.5 mM KCl, 26 mM $NaHCO_3$, 3.3 mM $MgCl_2$, 1.2 mM NaH_2PO_4, 10 mM glucose and 0.5 mM $CaCl_2$, pH 7.4 equilibrated with 95% O2/5% CO2. Coronal slices (250 μm) were prepared from $Camk2a^{T286A}$ mice and wild-type littermates age between P30-P40. Slices were maintained in a submerged chamber at 32°C for 1h and then at room temperature in oxygenated ACSF. Whole cell recordings and LTP protocol: CA1 pyramidal neurons were visualized using oblique illumination. Whole cell recordings were performed using a patch-clamp amplifier (Multiclamp 700B, Molecular Devices). Patch pipettes (3-6 ΩM) were filled with a K Gluconate solution (130 mM K gluconate, 10 mM Na phosphocreatine, 4 mM $MgCl_2$, 4 mM Na_2ATP, 0.3 mM MgGTP, 3 mM L- Ascorbic acid, 10 mM HEPES, pH 7.4, 310 mosm). Series resistances (10 to 40 MΩ) and input

resistances (100 to 300 MΩ) were monitored throughout the experiment using negative

voltage steps (−5 mV, 50 ms). The membrane potential was held at −70 mV. Experiments

were performed at room temperature and slices were perfused with oxygenated ACSF

(127 mM NaCl, 2.5 mM KCl, 10 mM glucose, 10 mM $NaHCO_3$, 1.25 mM NaH_2PO_4, 2 mM

$MgCl_2$, 2 mM $CaCl_2$, 0.1 mM Picrotoxin). Excitatory postsynaptic currents (EPSCs) were

evoked by extracellular stimulation of the Schaffer collateral fibers using a concentric

bipolar stimulating electrode (World Precision Instruments) at 0.03 Hz. LTP was

induced by pairing synaptic stimulation (2 Hz for 120 pulses, or 40 Hz for 600 pulses at

the end of the depolarization) with a postsynaptic depolarization to 0 mV (60 s). EPSP

potentiation was assessed for 50-60 min after LTP condition stimulation. All data was

analyzed with an in-house program written in MatLab.

2.10 Simulation of CaMKII kinetics scheme

We constructed a set of rate equations (elementary reaction) to describe CaMKII

biochemical reactions based on our proposed CaMKII kinetics model. The law of mass

action is applied to obtain non-linear ordinary differential equations (ODEs) and to solve

the concentration of each species (Ullah et al., 2006). We implemented the algorithm

written in Matlab. To simplify the simulation, influx of NMDA-receptor mediated Ca^{2+}

during repetitive glutamate uncaging is modelling as:

$$[Ca]_i = [Ca]_0 e^{-d(i-1)/\tau_2}$$

$$[Ca]_t = [Ca]_i e^{-[t-d(i-1)]/\tau_1}$$

Where i = number of uncaging pulses (integers, 1 to 30),

$d = 1/uncaging\ frequency$, $\tau_1 = 0.05\ s$ (Ca²⁺ clearance time constant) (Lee et al., 2009),

$\tau_2 = 30.0\ s$ (reflects glutamate uncaging evoked NMDA-receptor desensitization) (Lee et al., 2009). There are four Ca^{2+} binding sites on calmodulin (two on N-lobe and two on C-lobe CaM, respectively). Dissociation of N-lobe Ca^{2+} is much faster than C-lobe Ca^{2+} (~100 fold). It's been showed that Ca_2CaM(C-lobe) is the major calmodulin species during Ca^{2+} transients, and the binding of Ca^{2+} on each lobe is cooperative (Pepke et al., 2010). Therefore, we assumed that active calmodulin (CaM) only requires binding of one Ca^{2+}, and Ca^{2+} dissociation follows the slow phase dissociation step (Martin et al., 1985). Based on our study here, rebinding of CaM to T286 phosphorylated-CaMKII is assumed to be not preferable because of inhibitory phosphorylation on T305/T306.

Table 1: List of parameters used for simulation of the model

	Rate equation	Rate constant	Reference
R1:	$Ca^{2+} + CaM_d \rightarrow CaM$	$k_1: 1.4 \times 10^6 \ M^{-1}s^{-1}$	(Stefan et al., 2008)
R2:	$CaM \rightarrow Ca^{2+} + CaM_d$	$k_2: 30.0 \ s^{-1}$	(Martin et al., 1985; Stefan et al., 2008)
R3:	$CaM + CaMKII \rightarrow KCaM$	$k_3: 1.0 \times 10^6 \ M^{-1}s^{-1}$	(Tzortzopoulos et al., 2004)
R4:	$KCaM \rightarrow CaM + CaMKII$	$k_4: 5.0 \ s^{-1}$	this study and further refined during simulation
R5:	$KCaM \rightarrow PCaM$	$k_5: 6.3 \ s^{-1}$	(Lucic et al., 2008)
R6:	$PCaM \rightarrow KCaM$	$k_6: 0.1 \ s^{-1}$	estimated and refined during simulation
R7:	$PCaM \rightarrow P + CaM$	$k_7: 0.67 \ s^{-1}$	this study and further refined during simulation
R8:	$P + CaM \rightarrow PCaM$	$k_8: 0.01 \ s^{-1}$	estimated and refined during simulation
R9:	$P \rightarrow P2$	$k_9: 6.67 \times 10^{-3} \ s^{-1}$	estimated and refined during simulation
R10:	$P2 \rightarrow P$	$k_{10}: 1.67 \times 10^{-3} \ s^{-1}$	estimated and refined during simulation

R11:	$P \rightarrow CaMKII + P_i$	$k_{11}: 0.22\ s^{-1}$	this study
R12:	$P2 \rightarrow CaMKII + P_i$	$k_{12}: 1.67 \times 10^{-2}\ s^{-1}$	this study
	Concentrations:		
[Ca]$_0$	8 μM		(Higley and Sabatini, 2012; Lee et al., 2009)
[CaM$_d$]$_0$	30 μM		(Kakiuchi et al., 1982)
[CaMKII]$_0$	70 μM		(Petersen et al., 2003)

Table 2: List of rate equations used for simulation of the model

$$d[CaM_d]/dt = -k_1[Ca^{2+}][CaM_d] + k_2[CaM]$$

$$d[CaM]/dt = k_1[Ca^{2+}][CaM_d] - k_2[CaM] - k_3[CaM][CaMKII] + k_4[KCaM] + k_7[PCaM]$$
$$- k_8[P][CaM]$$

$$d[CaMKII]/dt = -k_3[CaM][CaMKII] + k_4[KCaM] + k_{11}[P] + k_{12}[P2]$$

$$d[KCaM]/dt = k_3[CaM][CaMKII] - k_4[KCaM] - k_5[KCaM] + k_6[PCaM]$$

$$d[PCaM]/dt = k_5[KCaM] - k_6[PCaM] - k_7[PCaM] + k_8[P][CaM]$$

$$d[P]/dt = k_7[PCaM] - k_8[P][CaM] - k_9[P] + k_{10}[P2] - k_{11}[P]$$

$$d[P2]/dt = k_9[P] - k_{10}[P2] - k_{12}[P2]$$

2.11 Statistical analysis

Error bars shown in the figures represent standard error of the mean (sem). One-way ANOVA analysis with post hoc Bonferroni test are used to compare different conditions ($\alpha = 0.05$). Asterisks denote statistical significance (*$p < 0.05$). sem of time constants is obtained by bootstrapping.

Chapter 3.   Kinetics of CaMKII activation during spine plasticity measured with millisecond temporal resolution

3.1 Introduction

To investigate the millisecond temporal profile of CaMKII activation in accord with Ca^{2+} transients induced by two-photon glutamate uncaging, we optimized our setup to improve the temporal resolution of 2pFLIM up to 128 ms/frame (32 × 32 pixels) (Figure 3.1A, 3.2).

3.2 Results

3.2.1 CaMKII activation during glutamate uncaging evoked sLTP

In response to repetitive pulses of two-photon glutamate uncaging in the absence of Mg^{2+}, Ca^{2+} was elevated to the micromolar level and decayed over ~100 ms (Figure 3.3). During a typical structural LTP (sLTP) induction protocol consisting of 30 pulses of glutamate uncaging at 0.49 Hz (Lee et al., 2009; Matsuzaki et al., 2004), we observed a rapid and robust activation of CaMKII in the stimulated spines. CaMKII activity decayed over tens of seconds (Figure 3.1A, 3.1B). The averaged time course of CaMKII activation during sLTP (Figure 3.1C) showed stepwise increases following each glutamate uncaging pulse until it reached a plateau within ~10 s. After the cessation of glutamate uncaging, CaMKII activity decayed with time constants of $\tau_{fast} = 6.4 \pm 0.7$ s (74%) and $\tau_{slow} = 92.6 \pm 50.7$ s (26%) (Figure 3.1C).
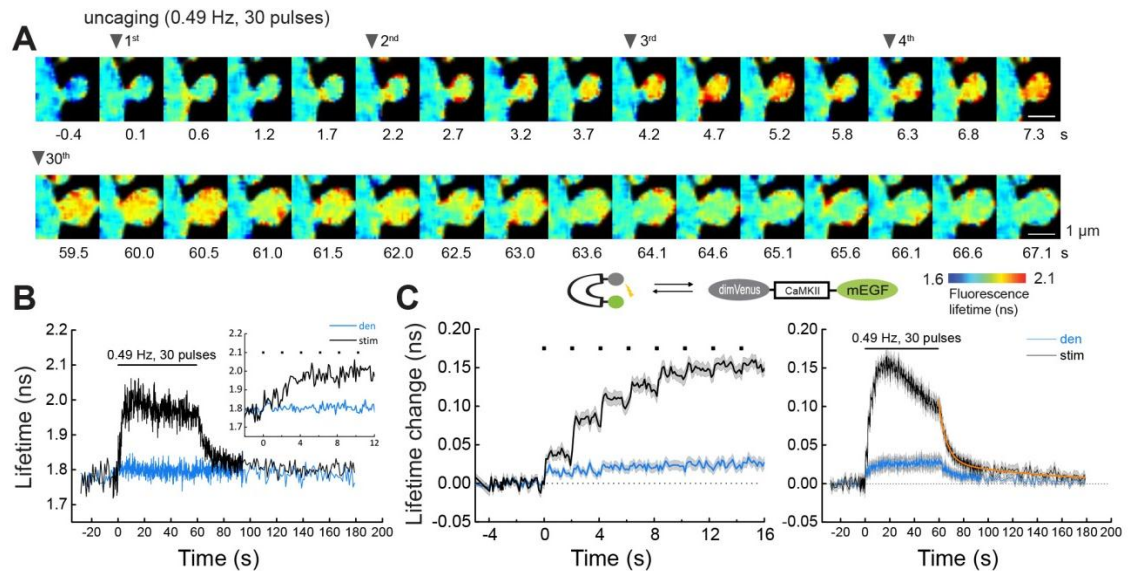
Figure 3.1: CaMKII activation measured at millisecond temporal resolution
(A) Representative fluorescence lifetime images of Camuiα during glutamate uncaging at 0.49 Hz. Warmer colors indicate higher fluorescence lifetime of Camuiα, corresponding to the active, open conformation of Camuiα.
(B) Time course of fluorescence lifetime of Camuiα in (A) of the stimulated spine (black) and dendritic region (blue). Inset is expanded view of the rising phase of Camuiα activation. Black dots represent uncaging pulses.
(C) Averaged change in fluorescence lifetime of Camuiα (n = 36 spines/14 neurons). Left panel is expanded view of the rising phase of right panel. The orange curve indicates the decay kinetics of fluorescence lifetime signal obtained by curve fitting of a double-exponential function: $F(t) = F_0 \cdot [P_{fast} \cdot e^{-t/\tau_{fast}} + P_{slow} \cdot e^{-t/\tau_{slow}}]$, where F_0 is the initial fluorescence lifetime, τ_{fast} and τ_{slow} are the fast and slow decay time constants and P_{fast} and P_{slow} are the respective populations. The time constants were obtained as $\tau_{fast} = 6.4 \pm 0.7$ s ($P_{fast} = 74\%$) and $\tau_{slow} = 92.6 \pm 50.7$ s ($P_{slow} = 26\%$). All data are shown in mean ± sem, and sem of time constants is obtained by bootstrapping. Scale bar, 1 μm.
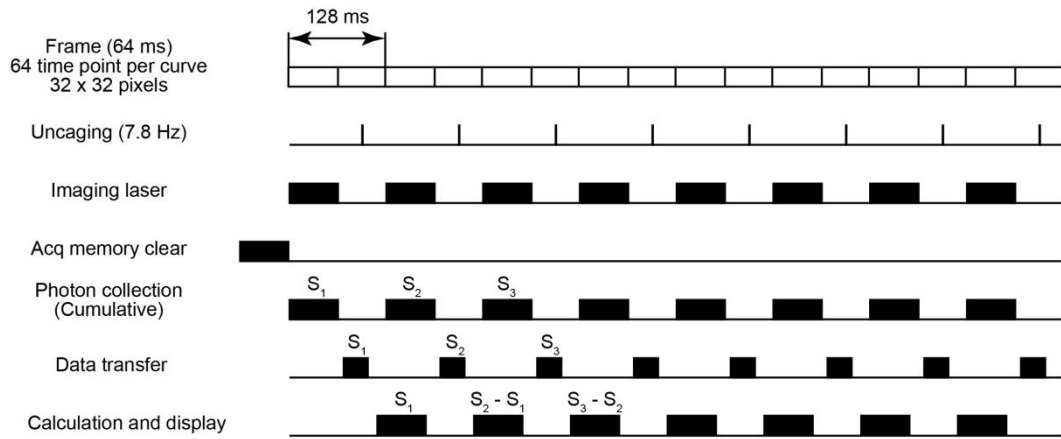
Figure 3.2: Schematic timing of fast-frame FLIM data acquisition and uncaging
We collected photons cumulatively throughout an imaging session (typically 768-1536 frames), since the memory clearance is relatively time consuming. The photon collection and data transfer were done alternatively in every other frame. Following the data transfer, the image was processed and displayed. The number of photons acquired in the previous frame was calculated as the data transferred in the current frame subtracted by that done two frames ago. When we performed uncaging, uncaging pulses were applied in the frame in which photons were not collected. The imaging laser was turned off when photons were not collected. The acquisition software was written in MatLab. Since the number of photons per pixel per lifetime channel never exceeded 10 photons, the signal did not saturate the memory (16 bits) during data acquisition.
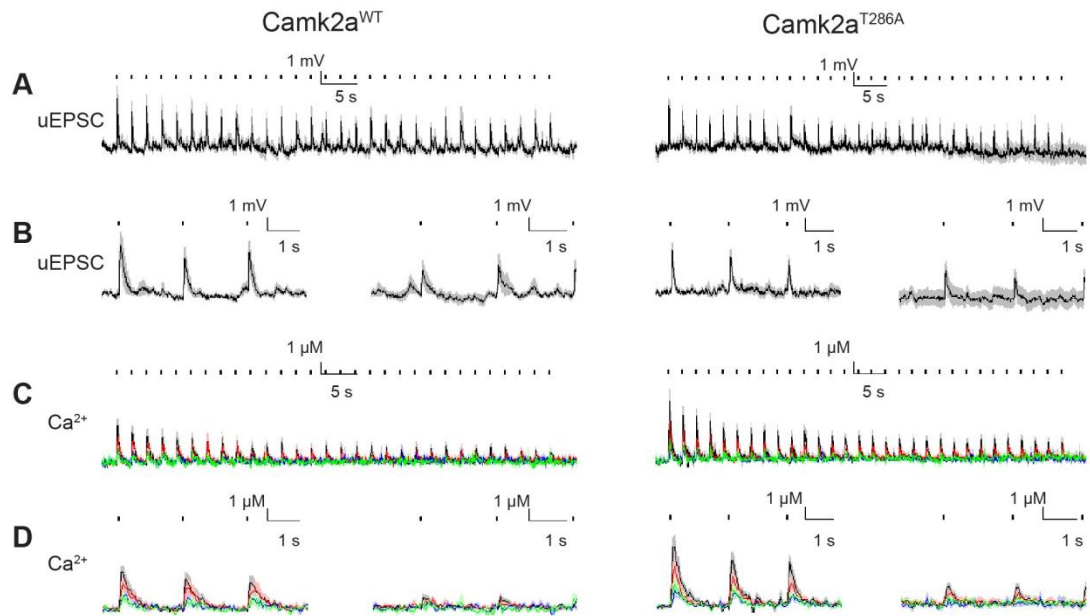
Figure 3.3: Measurements of uncaging-evoked EPSCs (uEPSCs) and Ca²⁺ transients during glutamate uncaging

(A) Uncaging-evoked EPSCs in CA1 neurons from *Camk2a*[T286A] (right; n = 62 spines/14 neurons) and litter-mate control (left; n = 43 spines/9 neurons) mice.

(B) Expanded view of the first and last three uEPSCs shown in (A).

(C) Ca²⁺ transients measured in the stimulated spine (black), adjacent spine (< 3μm, green), dendritic shaft (red), and distal dendritic region (>1 μm, blue) during glutamate uncaging. The decreases in the magnitude of Ca²⁺ transients was reported before (Lee et al., 2009) and may be due to the desensitization of NMDA-receptors (Sobczyk and Svoboda, 2007).

(D) Expanded view of the first and last three Ca²⁺ transients shown in (C). All data are shown in mean ± sem.

3.2.3 CaMKII activation in response to a single glutamate uncaging pulse

To clarify how CaMKII integrates Ca^{2+} signals, we measured CaMKII activation in response to a single pulse of glutamate uncaging (Figure 3.4A, 3.4B). The time course showed a rapid activation that reached its peak within 1 s and then decayed over tens of seconds. On average, the time constant of the CaMKII activation was 0.3 ± 0.1 s, and that of the fast component of the decay was $\tau_{fast} = 8.2 \pm 1.7$ s (Figure 3.4C). Comparing this curve with CaMKII activation during sLTP induction (Figure 3.1C, 3.5), CaMKII appears to linearly summate its activity in response to repetitive pulses of glutamate uncaging until reaching its plateau, suggesting that CaMKII activity is modulated by Ca^{2+} elevations and acts as a leaky integrator with time constants of ~6 s and ~1 min (Figure 3.5).
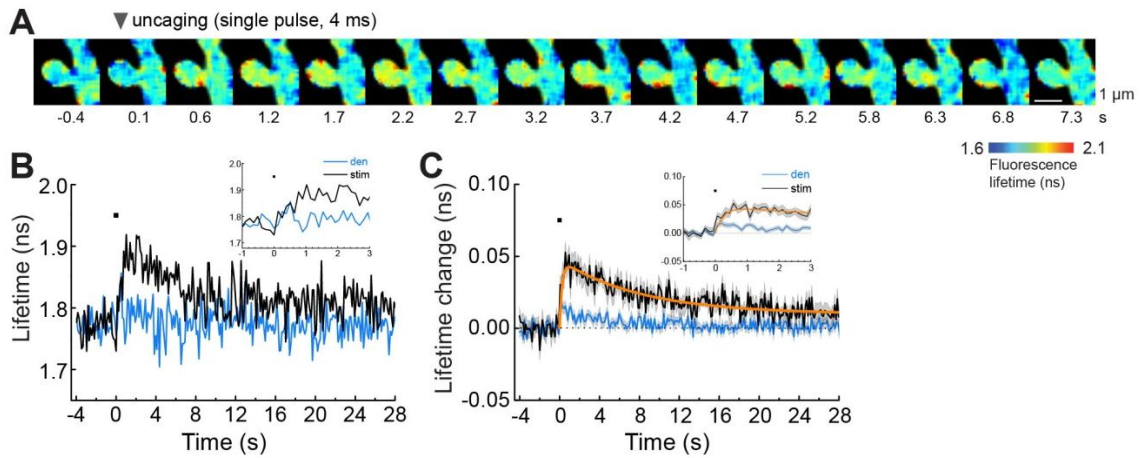
Figure 3.4: CaMKII activation in response to a single glutamate uncaging pulse

(A) Representative fluorescence lifetime images of Camuiα in response to a single glutamate uncaging pulse.

(B) Time course of fluorescence lifetime of Camuiα in (A) of the stimulated spine (black) and dendritic region (blue). Inset is expanded view of the rising phase of Camuiα activation. Black dots represent uncaging pulses.

(C) Averaged change in fluorescence lifetime of Camuiα (n = 35 spines/8 neurons) in response to a single glutamate uncaging pulse. The orange curve indicates the kinetics of fluorescence lifetime signal obtained by curve fitting of a function: $F(t) = [a \cdot e^{-t/\tau_{fast}} + c] \cdot [1 - e^{-t/\tau_{rise}}]$, where c is the constant which representing the slow decay component as described in (Figure 3.1C). The time constants were obtained as: τ_{rise} = 0.3 ± 0.1 s and τ_{fast} = 8.2 ± 1.7 s. All data are shown in mean ± sem, and sem of time constants is obtained by bootstrapping. Scale bar, 1 μm.

A
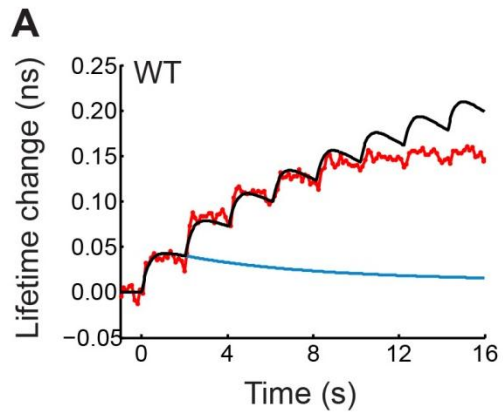
Figure 3.5: Model of integration property of CaMKII^WT

Black: simulated curves of linear summation of fluorescence lifetime change of Camuiα^WT in response to 8 pulses of glutamate uncaging at 0.49 Hz. Blue: simulated curves in response to a single glutamate uncaging pulse. Red: fluorescence lifetime change of Camuiα^WT during glutamate uncaging at 0.49 Hz. Simulated curve is based on a function: $F(t) = \left[a \cdot e^{-t/\tau_{fast}} + b \cdot e^{-t/\tau_{slow}}\right] \cdot \left[1 - e^{-t/\tau_{rise}}\right]$, where $a = 0.03, \tau_{fast} = 5.5, \; b = 0.02, \tau_{slow} = 62.5, \tau_{rise} = 0.3$. The parameters are adapted from curve fitting to fluorescence lifetime change of Camuiα^WT in response to a single glutamate uncaging pulse to the same function.

3.2.4 CaMKII activation at a near physiological temperature

The above experiments were performed at room temperature (25 ± 0.5°C). At a near physiological temperature (34-35°C), CaMKII activity decays faster (τ_{fast} = 1.8 ± 1.6 s (45%) and τ_{slow} = 11.0 ± 19.0 s (55%); Figure 3.6). From these results, the temperature dependency of the decay kinetics in spines was determined to be: Q10 = 3.6 (τ_{fast}) and 8.4 (τ_{slow}).
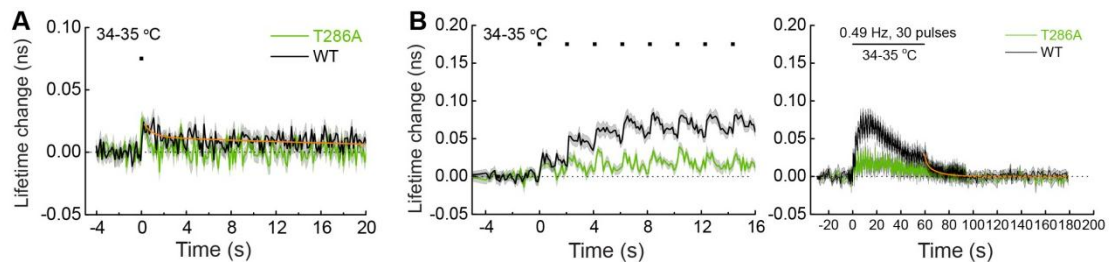
Figure 3.6: Camuiα activation at a near physiological temperature (34-35 °C)
(A) Time course of activation of Camuiα^{WT} (black, n =26 spines/7 neurons) and Camuiα^{T286A} (green, n = 23 spines/6 neurons) in stimulated spines in response to a single glutamate uncaging pulse. The orange curve on Camuiα^{WT} is obtained by curve fitting of a double-exponential function: $F(t) = F_0 \cdot \left[P_{fast} \cdot e^{-t/\tau_{fast}} + P_{slow} \cdot e^{-t/\tau_{slow}} \right]$. The decay time constants were obtained as τ_{fast} = 0.4 s (57%) and τ_{slow} = 28.1 s (43%).
(B) Glutamate uncaging at 0.49 Hz. The orange curve on Camuiα^{WT} (black) is obtained by curve fitting of a double-exponential function, τ_{fast} = 1.8 ± 1.6 s (45%) and τ_{slow} = 11.0 ± 19.0 s (55%) (n = 28 spines/9 neurons). Time course of Camuiα^{T286A} is shown in green (n =19 spines/6 neurons). All data are shown in mean ± sem, and sem of time constants is obtained by bootstrapping.

3.2.5 Functionality of Camuiα sensor

To test the functionality of Camuiα sensor, we used hippocampal slices from

Camk2a^{fl/fl} mice and performed the rescue experiments via the exogenous expression of

Camuiα. In the Cre recombinase positive cells, overexpression of Camuiα rescued the

impaired sLTP and Camuiα was activated during the induction of spine plasticity

(Figure 3.7).
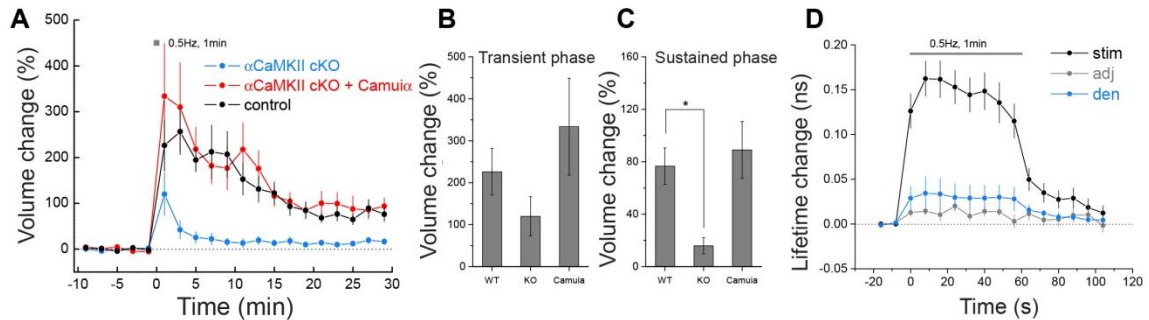
Figure 3.7: Functionality of Camuiα sensor
(A) Averaged change of spine volume induced by glutamate uncaging at 0.5 Hz.
Exogenous expression of Camuiα rescued the impaired structural plasticity in CaMKIIα
conditional knock-out CA1 neurons, demonstrating that Camuiα retains the
functionality. n: control = 9/4, CaMKIIα cKO = 13/6, Camuiα rescue = 10/5
(spines/neurons).
(B) Quantification of transient phase spine volume change (peak value recorded at 1
min).
(C) Quantification of sustained phase spine volume change (averaged over 25-30 min).
control: 76.8 ± 13.8 %; CaMKIIα cKO: 15.9 ± 6.1 %; Camuiα rescue: 89.0 ± 21.7 %.
(D) Averaged fluorescence lifetime change of Camuiα during glutamate uncaging
measured in Camuiα rescue group. Asterisks denote statistical difference (p < 0.05). All
data are shown in mean ± sem.

Chapter 4.   The role of Thr286 phosphorylation in the sensitivity of calcium signals integration

4.1 Introduction

CaMKII activation is known to be regulated by auto-phosphorylation at Thr286 (Lisman et al., 2002). Thus, to examine the role of Thr286 phosphorylation, we used Camuiα mutants in which the phosphorylation site is mutated to alanine (Camuiα^{T286A}) or aspartate (Camuiα^{T286D}), which mimic non-phosphorylated and pseudo-phosphorylated threonine, respectively. Consistent with constitutively active nature of Camuiα^{T286D} mutant, the fluorescence lifetime of Camuiα^{T286D} (2.06 ± 0.01 ns) was higher than that of the maximum activation of Camuiα^{WT} (1.75 ± 0.02 ns; Figure 4.1). Pseudo-phosphorylation at Thr286 appears to be sufficient to force CaMKII to adopt an open conformation in the absence of Ca^{2+} influx. There are no statistically significant differences of the basal fluorescence lifetime between Camuiα^{T286A} (1.69 ± 0.03 ns) and Camuiα^{WT} (Figure 4.1).
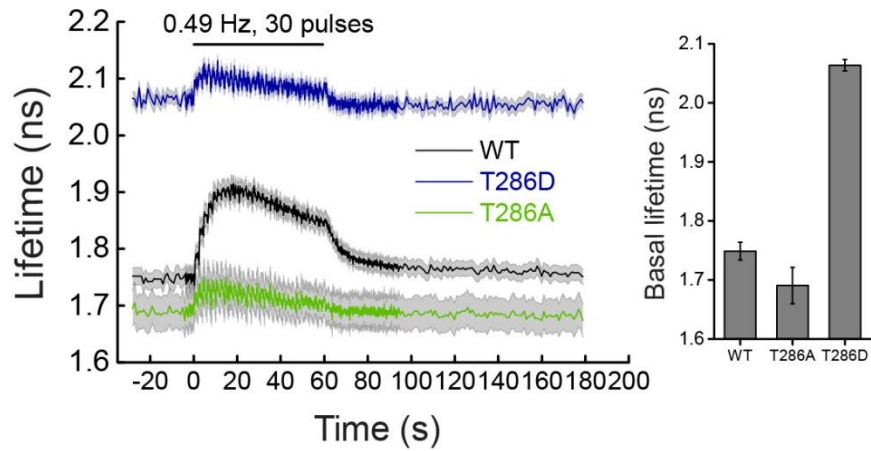
Figure 4.1: Fluorescence lifetime of Camuiα^WT, Camuiα^T286D and Camuiα^T286A
Averaged fluorescence lifetime of Camuiα^WT, Camuiα^T286D, Camuiα^T286A during sLTP induction. Fluorescence lifetime averaged over -4-0 s: Camuiα^WT: 1.75 ± 0.02 ns; Camuiα^T286D: 2.06 ± 0.01 ns; Camuiα^T286A: 1.69 ± 0.03 ns.

4.2 Results

4.2.1 Activation of CaMKIIα^{T286A} in response to a single glutamate uncaging pulse

We first compared the activation of the T286A mutant to that of Camuiα^{WT} in response to a single glutamate uncaging pulse (Figure 4.2). The activity of CaMKIIα^{T286A} exhibited a rapid increase to a level similar to CaMKIIα^{WT}, but decayed with a single fast component that was much faster than CaMKIIα^{WT} ($\tau_{decay} = 1.9 \pm 0.3$ s). These results indicate that Thr286 phosphorylation substantially slows the decay of CaMKII activity.
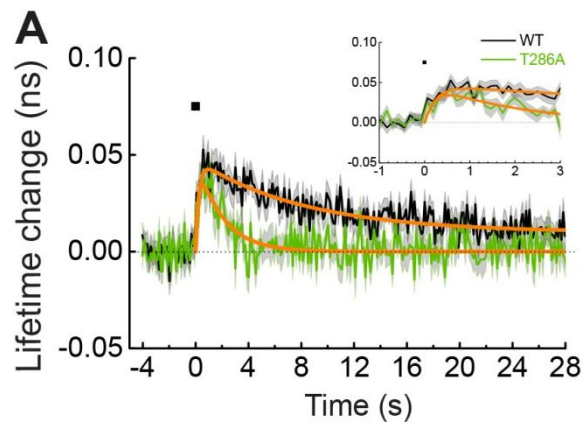
Figure 4.2: Camuiα^{T286A} activation in response to a single glutamate uncaging pulse
Activation of Camuiα^{T286A} (green) and Camuiα^{WT} (black) in response to a single glutamate uncaging pulse (black dot). The data and fitted curve for Camuiα^{WT} are from (Figure 3.4C) for comparison. The orange curve on Camuiα^{T286A} indicates the decay kinetics obtained by curve fitting of a function: $F(t) = C \cdot \left[1 - e^{-t/\tau_{rise}}\right] \cdot e^{-t/\tau_{decay}}$, where τ_{rise} is adapted from (Figure 3.4C) and is fixed during curve fitting ($\tau_{rise} = 0.3$ s). The decay time constant for Camuiα^{T286A} is 1.9 ± 0.3 s (n = 30 spines/9 neurons). Inset is expanded view of the rising phase of Camuiα^{T286A} activation. All data are shown in mean ± sem.

4.2.2 Activation of CaMKIIα[T286A] during spine plasticity induction

Next, we measured the activity of CaMKIIα[T286A] during sLTP induction

(glutamate uncaging at 0.49 Hz). In contrast to the activation of Camuiα[WT], Camuiα[T286A]

failed to accumulate its activity due to its rapid decay. Its activity remained attenuated,

activating and decaying in accord with each uncaging pulse (τ_{decay} = 1.9 ± 1.2 s; Figure

4.3A, 4.5). To determine whether activation of Camuiα[T286A] might be affected by its

incorporation into endogenous CaMKII holoenzyme with wild-type CaMKII subunits,

we measured Camuiα[T286A] activation in hippocampal slices from *Camk2a*[T286A] knock-in

mice. In this scheme, Thr286 residues of all subunits in the holoenzyme are mutated.

The activity of Camuiα[T286A] rapidly increased and decayed with a time constant of τ_{decay} =

1.9 ± 0.2 s in response to a single glutamate uncaging pulse (Figure 4.4). This decay time

is similar to the measurements of Camuiα[T286A] in wild-type hippocampal slices,

suggesting that the assembly with wild-type CaMKII subunits does not affect the

kinetics of Camuiα[T286A].
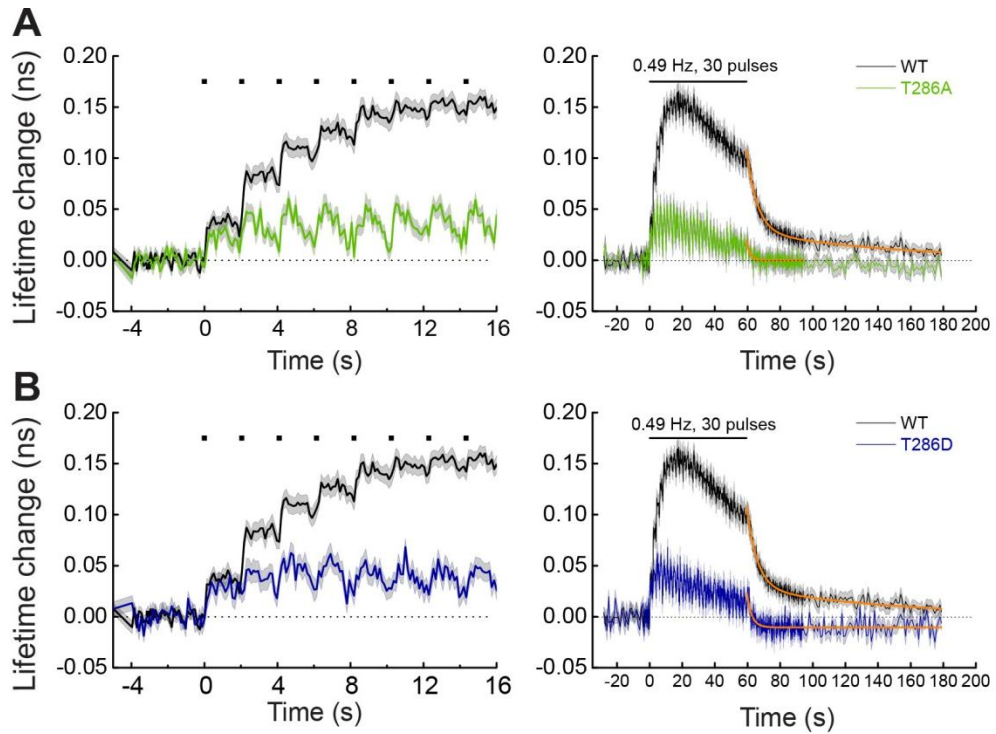
Figure 4.3: Activation of Camuiα^T286A and Camuiα^T286D during glutamate uncaging
Averaged change in fluorescence lifetime of Camuiα^T286A (A; green), Camuiα^T286D (B; indigo) and Camuiα^WT (black) in the stimulated spine during glutamate uncaging. The data and fitted curve for Camuiα^WT are from (Figure 3.1C) for the comparison. Left panel is expanded view of the right panel. The orange curve on Camuiα^T286A is obtained by curve fitting of a function: $F(t) = C \cdot e^{-t/\tau_{decay}}$. The decay time constant is obtained as 1.9 ± 1.2 s (26 spines/12 neurons). The orange curve on Camuiα^T286D is obtained by curve fitting of a function: $F(t) = C \cdot e^{-t/\tau_{decay}} + d_0$, where d_0 is a constant. The decay time constant is obtained as 3.0 ± 0.6 s for Camuiα^T286D (33 spines/10 neurons). All data are shown in mean ± sem, and sem of time constants is obtained by bootstrapping.
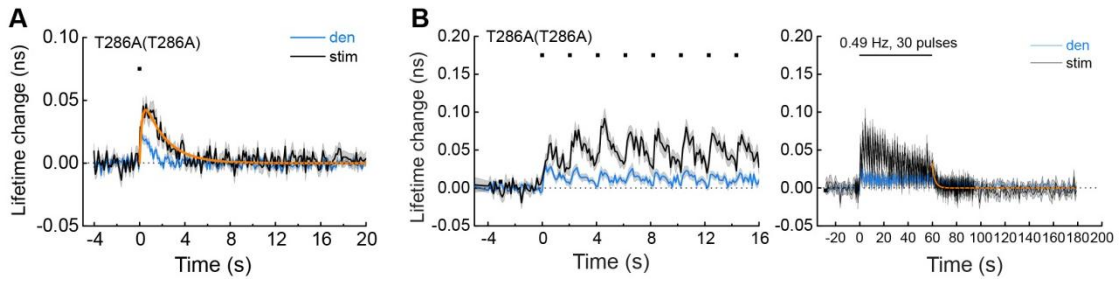
Figure 4.4: Activation of Camuiα^T286A measured in hippocampal slices from *Camk2a*^T286A knock-in mice

(A) Camuiα^T286A activation in response to a single glutamate uncaging pulse. The orange curve is obtained by curve fitting of a function: $F(t) = C \cdot \left[1 - e^{-t/\tau_{rise}}\right] \cdot e^{-t/\tau_{decay}}$ where τ_{rise} is fixed during curve fitting ($\tau_{rise} = 0.3$ s). The decay time constant is $\tau_{decay} = 1.9 \pm 0.2$ s (n = 37 spines/9 neurons).

(B) Glutamate uncaging at 0.49 Hz. Left panel is expanded view of the right panel. The orange curve is obtained by curve fitting of a function: $F(t) = C \cdot e^{-t/\tau_{decay}}$. The time constant is $\tau_{decay} = 2.4 \pm 1.4$ s (n = 17 spines/9 neurons). All data are shown in mean ± sem, and sem of time constants is obtained by bootstrapping.
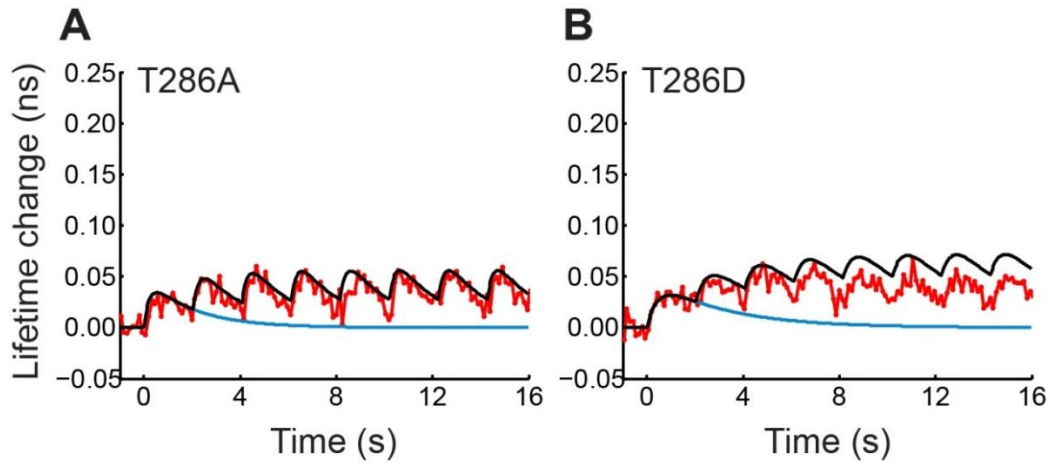
Figure 4.5: Model of integration property of CaMKII[T286A] and CaMKII[T286D]
Black: simulated curves of linear summation of fluorescence lifetime change of
Camuiα[T286A] (left) or Camuiα[T286D] (right) in response to 8 pulses of glutamate uncaging at
0.49 Hz. Blue: simulated curves in response to a single glutamate uncaging pulse. Red:
fluorescence lifetime change of Camuiα[T286A] or Camuiα[T286D] during glutamate uncaging
at 0.49 Hz.
(A) A simulated curve is based on a function: $F(t) = C \cdot \left[1 - e^{-t/\tau_{rise}}\right] \cdot e^{-t/\tau_{decay}}$, where
$C = 0.05, \tau_{rise} = 0.3, \tau_{decay} = 1.9$. Parameters are adapted from curve fitting to
fluorescence lifetime change of Camuiα[T286A] in response to a single glutamate uncaging
pulse.
(B) A simulated curve based on a function: $F(t) = C \cdot \left[1 - e^{-t/\tau_{rise}}\right] \cdot e^{-t/\tau_{decay}}$, where
$C = 0.05, \tau_{rise} = 0.3, \tau_{decay} = 3.0$. τ_{decay} is adapted from curve fitting to fluorescence
lifetime change of Camuiα[T286D] in response to 0.49 Hz glutamate uncaging pulse and C
and τ_{rise} are adapted from Camuiα[T286A] in response to a single glutamate uncaging.

4.2.3 Activation of CaMKIIα^{T286D} during spine plasticity induction

To further investigate the role of Thr286 phosphorylation, we also imaged the activity of Camuiα^{T286D}, a phospho-mimetic mutation. Camuiα^{T286D} showed a small, but significant activation by glutamate uncaging, presumably due to the binding of Ca^{2+}/calmodulin to the subunit (Figure 4.3B). While activation in response to the first pulse is similar to that of Camuiα^{WT}, there was no further accumulation of the activity. The decay time constant, which likely reflects Ca^{2+}/calmodulin dissociation from phosphorylated form of CaMKII, is 3.0 ± 0.6 s. Camuiα^{T286D} activity decays slightly slower than Camuiα^{T286A} (~1.9 s) and faster than that of Camuiα^{WT} (~6 s and ~1 min). To test whether the fast decay observed in Camuiα^{T286D} activity might be originated from the inhibitory phosphorylation on Thr305/Thr306, we measured Camuiα$^{T286D/T305A/T306A}$ activity during spine plasticity induction (Figure 4.6, 4.7). Similar to Camuiα^{T286D}, Camuiα$^{T286D/T305A/T306A}$ showed a limited accumulation in its activity with a decay time constant of 5.7 ± 0.5 s.

Our results indicate that, similar to Camuiα^{T286A}, phospho-mimetic Camuiα^{T286D} cannot integrate Ca^{2+} signals because of its fast decay (Figure 4.5). The fast decay of Camuiα^{T286D} is not because of the inhibitory phosphorylation on Thr305/Thr306. Together, our results suggest that active Thr286 phosphorylation is a prerequisite for CaMKII to integrate Ca^{2+} signals during the induction of spine plasticity.
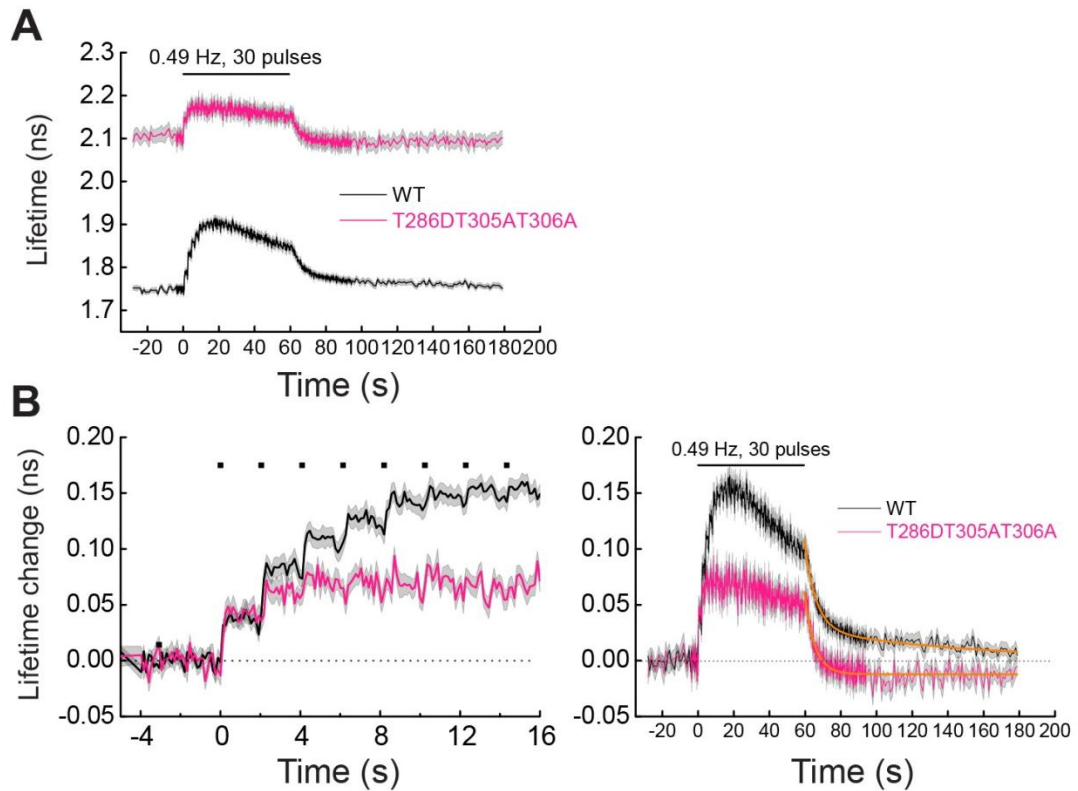
Figure 4.6: Activation of Camuiα^{T286D/T305A/T306A} during glutamate uncaging

(A) Averaged fluorescence lifetime of Camuiα^{T286D/T305A/T306A} and Camuiα^{WT} during sLTP induction. The data for Camuiα^{WT} are from (Figure 4.1).

(B) Averaged change in fluorescence lifetime of Camuiα^{T286D/T305A/T306A} (magenta) and Camuiα^{WT} (black) in the stimulated spine during glutamate uncaging. The data and fitted curve for Camuiα^{WT} are from (Figure 3.1C) for the comparison. Left panel is expanded view of the right panel. The orange curve on Camuiα^{T286D/T305A/T306A} is obtained by curve fitting of a function: $F(t) = C \cdot e^{-t/\tau_{decay}} + d_0$. The decay time constant is obtained as 5.7 ± 0.5 s (32 spines/7 neurons). All data are shown in mean ± sem, and sem of time constants is obtained by bootstrapping.
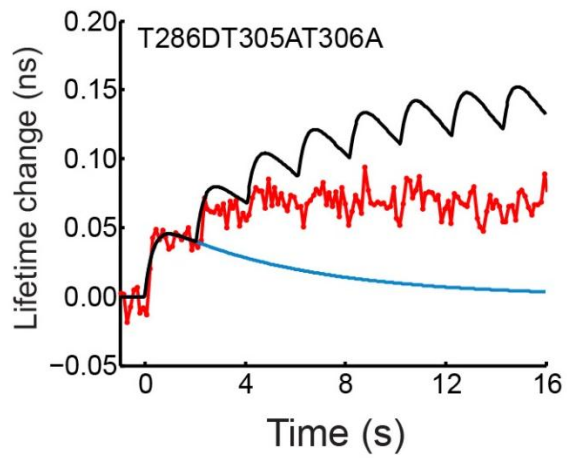
Figure 4.7: Model of integration property of CaMKII[T286D/T305A/T306A]

Black: simulated curves of linear summation of fluorescence lifetime change of Camuiα[T286D/T305A/T306A] in response to 8 pulses of glutamate uncaging at 0.49 Hz. Blue: simulated curves in response to a single glutamate uncaging pulse. Red: fluorescence lifetime change of Camuiα[T286D/T305A/T306A] during glutamate uncaging at 0.49 Hz. Simulated curve is based on a function: $F(t) = C \cdot \left[1 - e^{-t/\tau_{rise}}\right] \cdot e^{-t/\tau_{decay}}$, where $C = 0.057, \tau_{rise} = 0.3, \tau_{decay} = 5.7$.

Chapter 5. Frequency dependent activation of CaMKII

5.1 Introduction

The above results suggest that the impaired CaMKIIα^{T286A} activation during sLTP induction results from the fast decay of Camuiα^{T286A} activity (τ ~1.9 s), which is comparable to the interval of glutamate uncaging (~2 s). If this is the case, uncaging intervals shorter than the decay time should result in a higher degree of accumulation of CaMKII activity.

5.2 Results

5.2.1 Activation of Camuiα^{T286A} in response to high frequency stimulation

As expected, when we applied high frequency glutamate uncaging stimulations (1.9 Hz and 7.8 Hz), we found that CaMKIIα^{T286A} activity increased and plateaued at a significantly higher level (Figure 5.1A-5.1C). The decay time of Camuiα^{T286A} depended slightly on the frequency of stimulation: τ_{decay} measured from different glutamate uncaging stimulations are: τ_{decay} = 1.9 ± 0.7 s (1.9 Hz for 30 pulses, Figure 5.1A), τ_{decay} = 1.5 ± 1.0 s (1.9 Hz for 120 pulses, Figure 5.1B), and τ_{decay} = 3.1 ± 1.0 s (7.8 Hz for 120 pulses, Figure 5.1C).
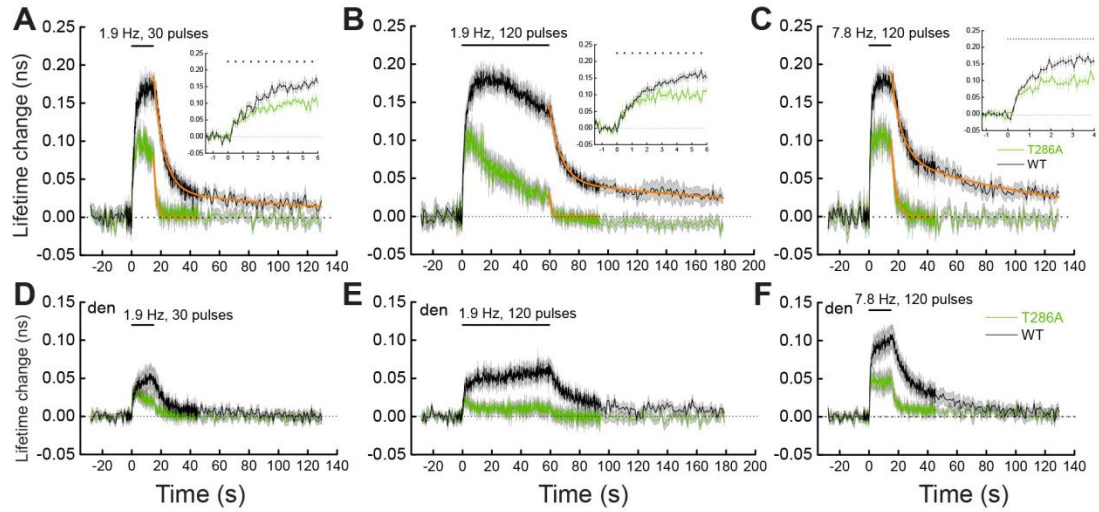
Figure 5.1: Activation of Camuiα^WT and Camuiα^T286A in response to high-frequency glutamate uncaging

(A-C) Averaged change in fluorescence lifetime of Camuiα^WT (black) and Camuiα^T286A (green) in response to high frequency glutamate uncaging at 1.9 Hz (A, B) or 7.8 Hz (C) for 30 pulses (A) or 120 pulses (B, C) in the dendritic spines. Insets are expanded view. The orange curves indicate the decay kinetics obtained by a double-exponential fitting for Camuiα^WT (see details in Figure 1C) and mono-exponential fitting for Camuiα^T286A (see details in Figure 2C). The obtained decay time constants are as follows (number of samples: spines/neurons): (A) Camuiα^WT: τ_{fast} = 6.9 ± 0.5 s (81%) and τ_{slow} = 127 ± 84 s (19%) (21/14). Camuiα^T286A: τ_{decay} = 1.9 ± 0.7 s (22/16). (B) Camuiα^WT: τ_{fast} = 7.8 ± 0.9 s (69%) and τ_{slow} = 192 ± 132 s (31%) (18/11). Camuiα^T286A: τ_{decay} = 1.5 ± 1.0 s (17/10). (C) Camuiα^WT: τ_{fast} = 7.2 ± 1.0 s (59%) and τ_{slow} = 103 ± 31 s (41%) (25/13). Camuiα^T286A: τ_{decay} = 3.1 ± 1.0 s (15/8).

(D-F) Averaged fluorescence lifetime changes in the dendritic region as shown in (A-C), respectively. All data are shown in mean ± sem, and sem of time constants is obtained by bootstrapping.

5.2.2 Activation of Camuiα^{T286D} in response to high frequency stimulation

Similarly, at high frequency glutamate uncaging stimulation (7.9 Hz), activity of

Camuiα^{T286D} accumulated and τ_{decay} was obtained as 2.9 ± 0.6 s, which is similar to the

decay time measured at 0.49 Hz (Figure 5.2). This result indicate that CaMKIIα^{T286D}

activity can also be boosted by increasing the frequency of Ca^{2+} transients to rates that

allow for their integration by CaMKIIα^{T286D}, and this integration is likely mediated by the

higher binding fraction of CaM to CaMKIIα^{T286D}.
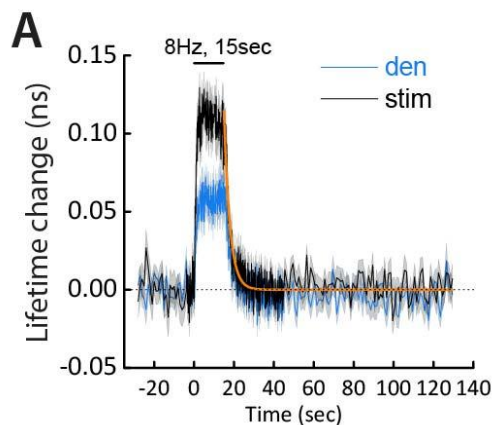
Figure 5.2: Camuiα^{T286D} activation in response to glutamate uncaging at 7.9 Hz
The decay time constant of Camuiα^{T286D} is τ = 2.9 ± 0.6 s (n = 34 spines/11 neurons). All data are shown in mean ± sem, and sem of time constants is obtained by bootstrapping.

5.2.3 Activation of Camuiα^{WT} in response to high frequency stimulation

Wild-type CaMKIIα activity also increased to a slightly higher level when high frequency stimulations were applied (Figure 3.1C, 5.1A-5.1C). τ_{decay} measured from different glutamate uncaging stimulations are: $\tau_{fast} = 6.9 \pm 0.5$ s (81%) and $\tau_{slow} = 127 \pm 84$ s (19%) (1.9 Hz for 30 pulses, Figure 5.1A), $\tau_{fast} = 7.8 \pm 0.9$ s (69%) and $\tau_{slow} = 192 \pm 132$ s (31%) (1.9 Hz for 120 pulses, Figure 5.1B), $\tau_{fast} = 7.2 \pm 1.0$ s (59%) and $\tau_{slow} = 103 \pm 31$ s (41%) (7.8 Hz for 120 pulses, Figure 5.1C). While the time constants were relatively constant, the slow component became much more pronounced at 7.8 Hz. Our results indicate that even in the absence of Thr286 phosphorylation, CaMKIIα^{T286A} activity can be boosted by increasing the frequency of Ca^{2+} transients to the rates that allow for their integration by CaMKIIα^{T286A}.

Chapter 6.   Association of CaMKIIα-CaM during spine plasticity

6.1 Introduction

Camuiα, a CaMKII FRET-based activity sensor, provides us the activity profile of CaMKII during the induction of spine plasticity. However, this conformation sensor of CaMKII lacks the information about the association between Ca^{2+}/CaM and CaMKII, which is also an integral part of CaMKII activation. In order to image CaMKII-CaM association, we developed a FRET-based sensor made of mEGFP-CaMKIIα and mCherry-CaM (Figure 6.1), and imaged their association with 2pFLIM. This CaM-CaMKII binding sensor was tested for its specificity and sensitivity (Figure 6.2).
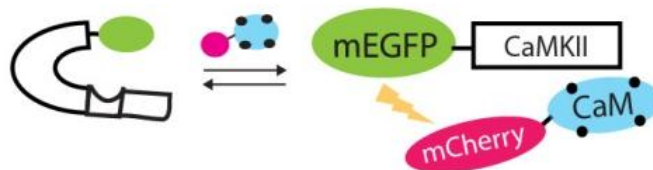
Figure 6.1: Sensor design of CaM/CaMKII binding
mEGFP and mCherry are fused to N-terminus of CaMKIIα and CaM, respectively.
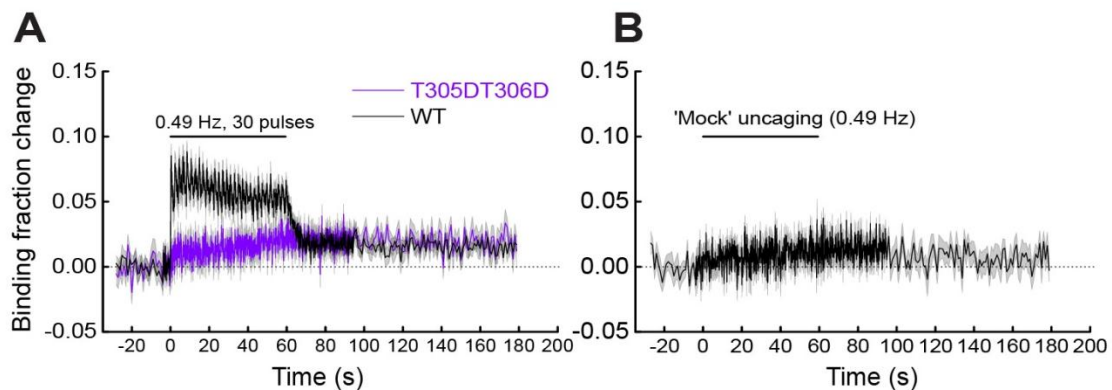
Figure 6.2: Specificity and sensitivity of CaMKII/CaM binding sensor
(A) To test the specificity of CaMKII/CaM binding sensor, we used CaMKII[T305DT306D] (mEGFP-tagged) as a FRET donor and measured the binding kinetics to mcherry-CaM during glutamate uncaging. Phospho-mimetic mutation to T305T306 precluded CaM binding; therefore, the slow increased component of the binding fraction change observed in CaMKII[T305DT306D] implied that it was a non-CaM/CaMKII dependent binding process (n = 34 spines/5 neurons).
(B) Binding fraction change measured under the "mock" uncaging stimulations (no MNI-glutamate in the bath solution). A limited binding fraction change of CaMKII/CaM binding was observed, indicating that the slow increased component in (A) is not originated from any possible photodamage processes (n = 18 spines/4 neurons). All data are shown in mean ± sem.

6.2 Results

6.2.1 CaMKIIα-CaM association during spine plasticity induction

We first measured CaMKII-CaM association during glutamate uncaging at 0.49 Hz. Unlike Camuiα activation, CaM-CaMKII binding appeared to be saturated by the first glutamate uncaging pulse. The subsequent stimulation pulses of glutamate uncaging did not result in a higher level of CaM-CaMKII binding (Figure 6.3). CaM dissociation time constant was obtained as 3.2 ± 0.7 s at 0.49 Hz glutamate uncaging. High frequency glutamate uncaging at 7.9 Hz resulted in a slightly slower dissociation time constant, $\tau = 6.2 \pm 1.2$ s (Figure 6.4).

In addition to the fast decay, we observed a signal decayed extremely slow (> 1 min) after sLTP induction (Figure 6.3E). This component appeared to be not related to binding of CaM to the CaM binding domain of CaMKII. A CaMKII mutant without binding capability (CaMKII[T305D, T306D]) also showed this slow component (Figure 6.2A).
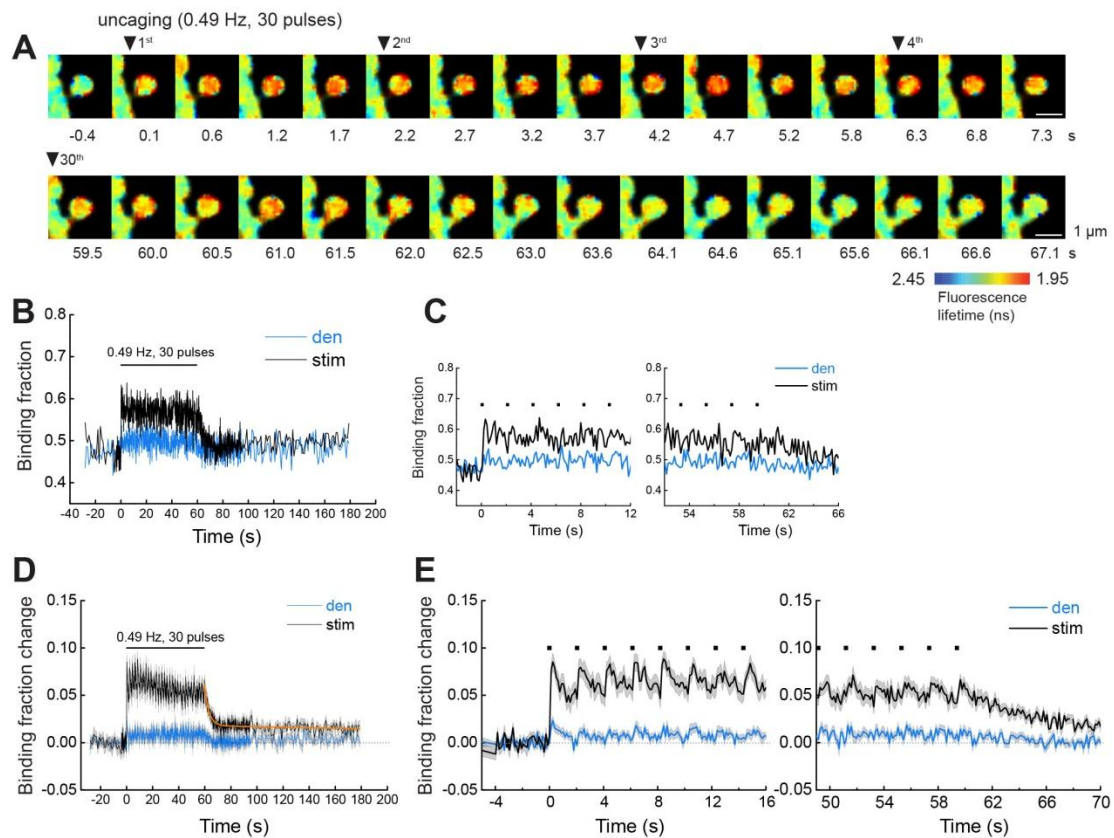
Figure 6.3: CaMKIIα-CaM association during glutamate uncaging
(A) Representative fluorescence lifetime images of CaMKII-CaM association during glutamate uncaging at 0.49 Hz. Warmer colors indicate higher binding fraction of CaM, corresponding to lower fluorescence lifetime of mEGFP-CaMKII.
(B) Time course of binding fraction change of CaMKII-CaM in (A) of the stimulated spine (black) and dendritic region (blue).
(C) Expanded view of the rising (left) and decay (right) phase of CaMKII-CaM association in (A). Black dots represent uncaging pulses.
(D) Averaged change in binding fraction of CaMKII-CaM (n = 27 spines/9 neurons). The orange curve indicates the decay of binding fraction change obtained by curve fitting of a double-exponential function: $F(t) = B_0 \cdot \left[P_{fast} \cdot e^{-t/\tau_{fast}} + P_{slow} \cdot e^{-t/\tau_{slow}}\right]$, where B_0 is the initial binding fraction change, τ_{fast} and τ_{slow} are the fast and slow decay time constants and P_{fast} and P_{slow} are the respective populations. The time constants are obtained as τ_{fast} = 3.2 ± 0.6 s (P_{fast} = 71%) and τ_{slow} = 572 ± 843 s (P_{slow} = 29%).
(E) Expanded view of the rising (left) and decay (right) phase of CaMKII-CaM association in (D). All data are shown in mean ± sem, and sem of time constants is obtained by bootstrapping.
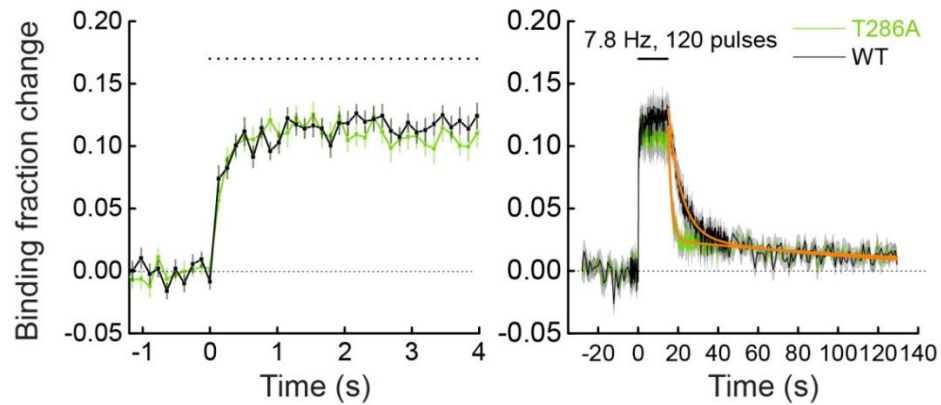
Figure 6.4: CaMKIIα-CaM association during high-frequency glutamate uncaging
Averaged change in binding fraction of CaMKII[WT]-CaM (black; n =24 spines/12 neurons) and CaMKII[T286A]-CaM association (green; n = 22 spines/11 neurons) in the stimulated spine during glutamate uncaging at 7.8 Hz. The orange curves on CaMKII[WT] and CaMKII[T286A] are obtained by curve fitting of a function: $F(t) = C \cdot e^{-t/\tau} + d_0$, where d_0 is a constant and represents the slow component. The decay time constants are obtained as τ = 6.2 ± 1.2 s for CaMKII[WT] and τ = 1.8 ± 0.2 s for CaMKII[T286A]. Left panel is expanded view of the right panel. All data are shown in mean ± sem, and sem of time constants is obtained by bootstrapping.

6.2.2 CaMKIIα-CaM association in response to a single glutamate uncaging pulse

To test whether the dissociation time is affected by the multiple pulses of Ca^{2+} elevations during sLTP induction, we measured CaMKII-CaM association in response to a single glutamate uncaging pulse (Figure 6.5).

The binding fraction of CaM-CaMKII association increased rapidly in the stimulated spine and decayed with a dissociation time constant of $\tau = 2.9 \pm 0.3$ s (Figure 6.5A). This time constant was similar to that obtained during sLTP induction (3.2 ± 0.6 s; Figure 6.3D), and similar to the decay time of phospho-mimetic CaMKIIα^{T286D} measured with Camuiα^{T286D} (3.0 ± 0.6 s; Figure 4.3B), which likely reflected CaM dissociation. This result demonstrated that the binding affinity of CaMKII towards CaM was not affected by the repetitive Ca^{2+} elevations during sLTP induction. It also implied that the Thr286 phosphorylation occurred rapidly in response to only a single pulse of glutamate uncaging.
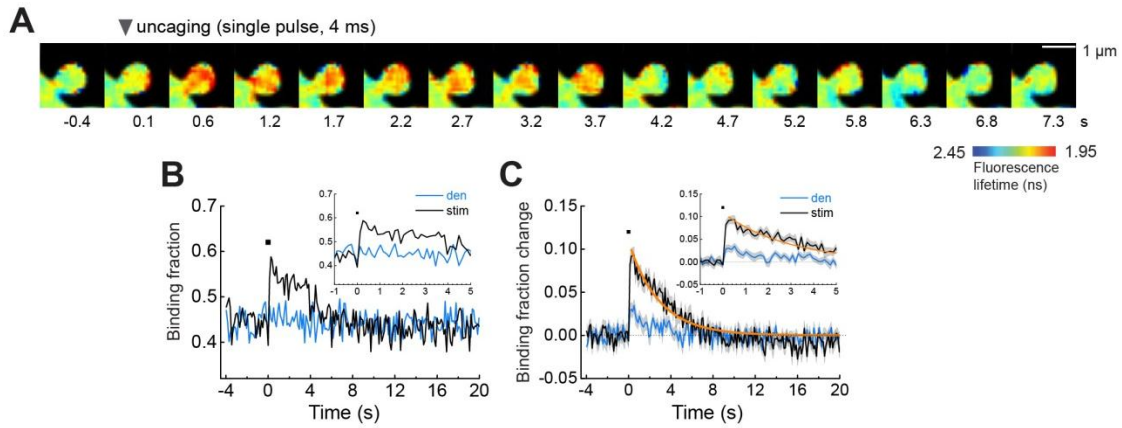
Figure 6.5: CaMKIIα-CaM association in response to a single glutamate uncaging pulse

(A) Representative fluorescence lifetime images of CaMKII-CaM association in response to a single glutamate uncaging pulse. Warmer colors indicate higher binding fraction of CaM, corresponding to lower fluorescence lifetime of mEGFP-CaMKII.

(B) Time course of binding fraction change of CaMKII-CaM in (A) of the stimulated spine (black) and dendritic region (blue).

(C) Averaged change in binding fraction of CaMKII-CaM (n = 28 spines/4 neurons). The orange curve indicates the decay of binding fraction change obtained by curve fitting of an exponential function: $F(t) = B_0 \cdot e^{-t/\tau}$, where B_0 is the initial binding fraction change, τ is the dissociation time constant. The time constant is obtained as $\tau = 2.9 \pm 0.3$ s. All data are shown in mean ± sem, and sem of time constants is obtained by bootstrapping.

6.2.3 CaMKIIα-CaM association at a near physiological temperature

The above experiments were performed at room temperature (25 ± 0.5°C). At a

near physiological temperature (34-35°C), CaM dissociated faster and we also observed

a slow component (τ_{fast} = 0.4 ± 0.5 s; Figure 6.6). From these results, the temperature

dependency of the dissociation kinetics in spines was determined to be Q_{10} = 7.3.
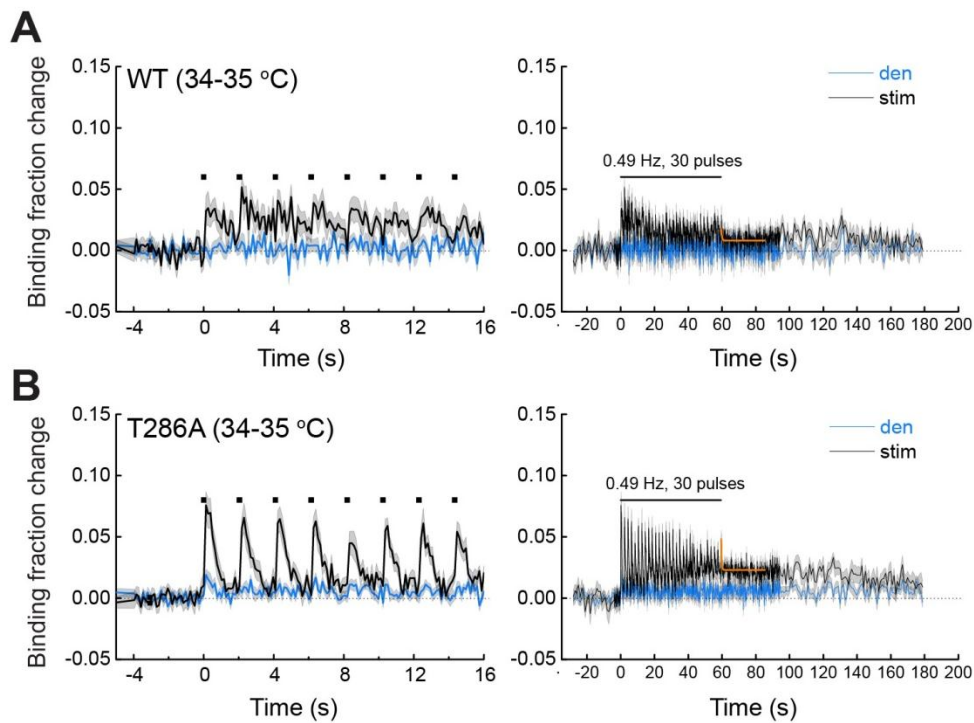
Figure 6.6: CaMKIIα-CaM association at a near physiological temperature (34-35 °C)
(A)(B) Averaged change in binding fraction of CaMKII[WT]-CaM (A; n =16 spines/5
neurons) and CaMKII[T286A]-CaM association (B; n = 19 spines/4 neurons) in the stimulated
spine (black) and dendritic region (blue) during sLTP induction at 0.49 Hz. The orange
curves on CaMKII[WT] and CaMKII[T286A] are obtained by curve fitting of a function:
$F(t) = C \cdot e^{-t/\tau} + d_0$, where d_0 is a constant and represents the slow component.
The decay time constants are obtained as τ = 0.4 ± 0.5 s for CaMKII[WT] (A) and τ = 0.3 ± 0.1
s for CaMKII[T286A] (B). Left panel in (A)(B) is expanded view of the right panel. All data
are shown in mean ± sem, and sem of time constants is obtained by bootstrapping.

6.2.4 The role of Thr286 phosphorylation in CaMKIIα-CaM association

6.2.4.1 Non-phosphorylatable mutant: CaMKIIα^{T286A}

Binding affinity of CaMKII to CaM is known to be regulated by Thr286

phosphorylation (Meyer et al., 1992). Thus, to examine the role of Thr286

phosphorylation, we first used mEGFP-CaMKIIα mutant in which the phosphorylation

site is mutated to alanine (mEGFP-CaMKIIα^{T286A}), which mimics non-phosphorylated

threonine. To eliminate the unwanted inter-subunit FRET between the mEGFP-

CaMKIIα^{T286A} and mCherry-CaM bound to the adjacent endogenous wild-type CaMKII,

we used hippocampal slices from *Camk2a*^{T286A} knock-in mice. Thus, in this scheme, all the

Thr286 in CaMKIIα subunits are mutated to Ala. We compared the activation of the

T286A mutant to that of mEGFP-CaMKII^{WT} in response to a single glutamate uncaging

pulse (Figure 6.7A). The binding fraction increased to the level similar to that of wild-

type and the dissociation was faster ($\tau = 1.2 \pm 0.1$s) (Figure 6.7A). The dissociation time

constant was comparable to the decay time of Camuiα^{T286A} ($\tau \sim 1.9$ s; Figure 4.2).

Next, we measured CaMKIIα^{T286A}-CaM association during sLTP induction

(glutamate uncaging at 0.49 Hz). In contrast to the persistent association of CaMKII^{WT}-

CaM, binding of CaM to CaMKIIα^{T286A} was transient, similar to activation of Camuiα^{T286A}

($\tau \sim 1.9$ s ; Figure 4.3A). The dissociation time constant was obtained as $\tau = 1.0 \pm 0.2$ s.
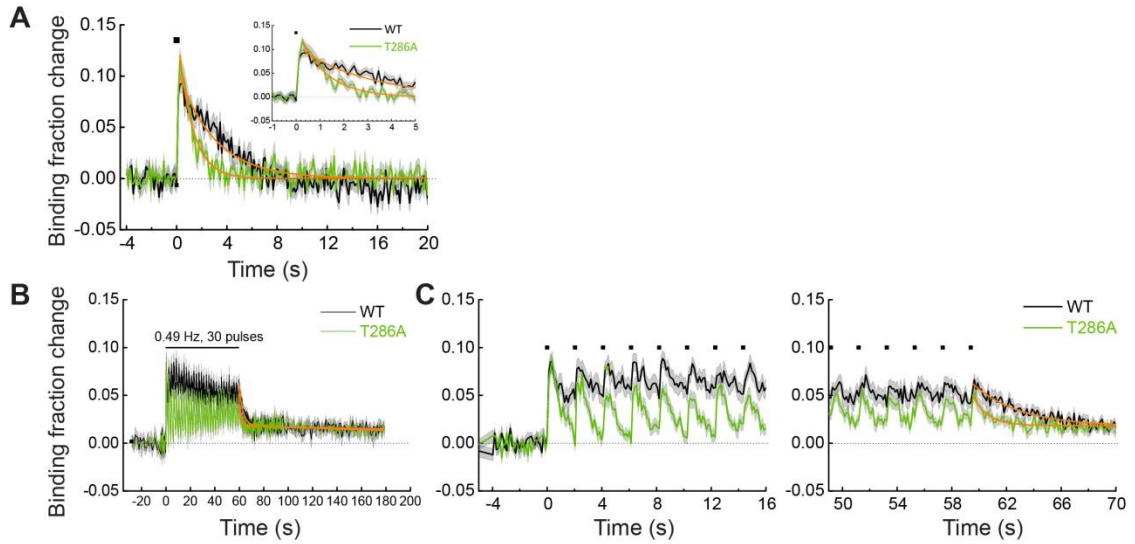
Figure 6.7: Association of CaMKIIα^{T286A}-CaM during glutamate uncaging
(A) Averaged change in binding fraction of CaMKIIα^{T286A}-CaM (green; n = 18 spines/ 4 neurons) in response to a single glutamate uncaging pulse (black square). The orange curves on CaMKIIα^{T286A} is obtained by curve fitting of an exponential function: $F(t) = C \cdot e^{-t/\tau}$. The dissociation time constant is obtained as $\tau = 1.2 \pm 0.1$ s. Inset is the expanded view. The data and fitted curve for CaMKII^{WT} are from (Figure 6.5) for the comparison.
(B) Averaged change in binding fraction of CaMKIIα^{T286A}-CaM (n = 24 spines/7 neurons) during glutamate uncaging at 0.49 Hz. The orange curve indicates the decay of binding fraction change obtained by curve fitting of a double-exponential function: $F(t) = B \cdot \left[P_{fast} \cdot e^{-t/\tau_{fast}} + P_{slow} \cdot e^{-t/\tau_{slow}} \right]$. The time constants are obtained as $\tau_{fast} = 1.0 \pm 0.2$ s (P_{fast} = 63%) and $\tau_{slow} = 356 \pm 221$ s (P_{slow} = 37%). The data and fitted curve for CaMKII^{WT} are from (Figure 6.3) for the comparison.
(C) Expanded view of the initial (left) and late (right) phase of CaMKIIα^{T286A}-CaM association in (B). All data are shown in mean ± sem, and sem of time constants is obtained by bootstrapping.

6.2.4.1 Phospho-mimetic mutant: CaMKIIα^{T286D}

To further investigate the role of Thr286 phosphorylation, we also imaged the association of CaMKII^{T286D}-CaM, which is a phospho-mimetic mutation. To minimize the unwanted inter-subunit FRET between the mEGFP-CaMKIIα^{T286D} and mCherry-CaM bound to the adjacent endogenous wild-type CaMKII, we used hippocampal slices from *Camk2a*$^{fl/fl}$ conditional knock-out mice. Hippocampal slices were transfected with Cre-recombinase, mEGFP-CaMKIIα^{T286D} and mCherry-CaM.

We imaged the association of CaMKIIα^{T286D}-CaM during glutamate uncaging at 0.49 Hz. Association of CaMKIIα^{T286D}-CaM showed a persistent binding during repetitive glutamate uncaging, similar to that of CaMKII^{WT}-CaM (Figure 6.8). The dissociation time constant was obtained as 1.9 ± 0.2 s (Figure 6.8), which is similar to that of CaMKII^{WT}($\tau \sim 3$ s; Figure 6.3D) and slower than that of CaMKIIα^{T286A} ($\tau \sim 1$ s; Figure 6.7B). This result suggested that CaM binding affinity is enhanced by the phosphorylation at Thr286.

The dissociation time constant is also similar to the decay of CaMKIIα^{T286D} activity ($\tau \sim 3$ s; Figure 4.3B), suggesting that the conformational change observed in Camuiα^{T286D} is mainly induced by the binding of Ca^{2+}/CaM.
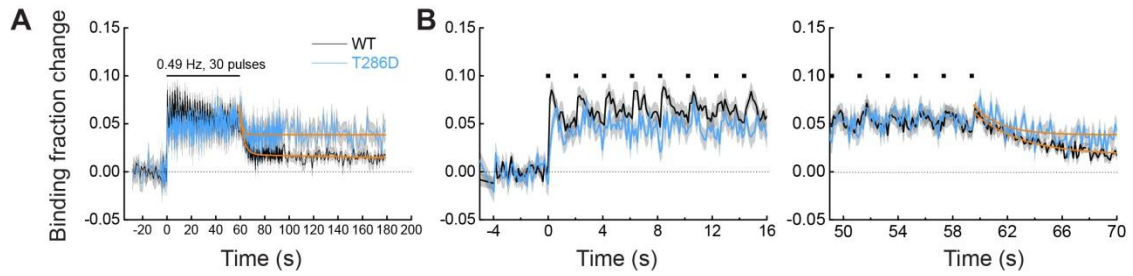
Figure 6.8: Association of CaMKIIα^{T286D}-CaM during glutamate uncaging

(A) Averaged change in binding fraction of CaMKIIα^{T286D}-CaM (n = 37 spines/12 neurons) during glutamate uncaging at 0.49 Hz. The orange curve indicates the decay of binding fraction change obtained by curve fitting of a function: $y = a \cdot e^{-bt} + y_0$. The time constants is obtained as $\tau_{\text{fast}} = 1.9 \pm 0.2$ s. The data and fitted curve for CaMKII$^{\text{WT}}$ are from (Figure 6.3) for the comparison.

(B) Expanded view of the initial (left) and late (right) phase of CaMKIIα^{T286D}-CaM association in (A). All data are shown in mean ± sem, and sem of time constants is obtained by bootstrapping.

6.3 Discussion

Activation of CaMKII is initiated by the binding of Ca^{2+}/CaM. To investigate the role of Thr286 phosphorylation in the initiation of CaMKII activation, here, we directly measured the association of CaMKIIα-CaM during the induction of spine plasticity.

Association of CaMKIIα-CaM showed a persistent binding during sLTP induction, which is different from the stepwise activation manner observed in Camuiα (Figure 3.1). The dissociation time constant is obtained as $\tau \sim 3$ s, faster than the decay of Camuiα ($\tau \sim 6$ s, Figure 3.1).

In the absence of Thr286 phosphorylation, association of CaMKIIα^{T286A}-CaM showed a transient binding during sLTP induction, which is similar to CaMKIIα^{T286A} activity (Figure 4.3A). The dissociation time constant is faster than that of CaMKIIα^{WT}, $\tau \sim 1$ s (~ 3 fold). These results demonstrated that phosphorylation at Thr286 enhanced the binding affinity of Ca^{2+}/CaM for ~ 3 fold under the dynamic Ca^{2+} transients during the induction of sLTP, and permits a persistent association of CaMKIIα-CaM. However, Ca^{2+} signals integration capability of CaMKIIα is mainly mediated by the autonomous activity of CaMKII (without the bound Ca^{2+}/CaM) (Figure 6.9). It also suggests that the decay of Camuiα^{WT} is mainly mediated by Thr286 dephosphorylation but not Ca^{2+}/CaM dissociation.

Pseudo-phosphorylation at Thr286 also showed a persistent association of CaMKIIα^{T286D}-CaM, and the dissociation time constant was obtained as $\tau \sim 2$ s. This

CaMKIIα^{T286D}-CaM association profile is similar to CaMKIIα^{T286D} activity during the

induction of sLTP (Figure 4.3). These results suggested that pseudo-phosphorylation at

Thr286 induces a ~ 3 fold, instead of a > 1000 fold (Meyer et al., 1992), increase in

Ca^{2+}/CaM binding affinity during sLTP induction. In addition, pseudo-phosphorylation

at Thr286 although retains partial CaMKII activity, it does not permanently recruit

Ca^{2+}/CaM during spine plasticity induction.
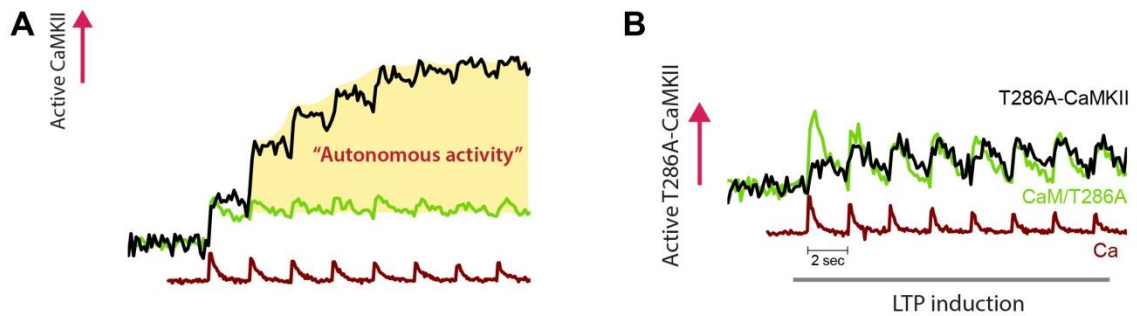
Figure 6.9: Schematic illustration of CaMKII activity during sLTP induction
Normalized Camuiα activation (black) and association of CaMKII-CaM (green) during
glutamate uncaging at 0.49 Hz (A: CaMKII^{WT}; B: CaMKII^{T286A}). Brown: Ca^{2+} elevations.
The yellow region in (A) denotes the activation mediated by CaMKII autonomous
activity.

Chapter 7.   The role of CaMKIIα Thr305/Thr306 inhibitory phosphorylation in CaMKII activation during spine plasticity

7.1 Introduction

Phosphorylation at Thr305 and Thr306 are known to inhibit the binding of CaM on CaMKII (Hanson and Schulman, 1992). Here, we asked how these inhibitory phosphorylation influences Ca^{2+}/CaM association and CaMKII activation during spine plasticity induction (Colbran, 1993; Hanson and Schulman, 1992).

7.2 Results

7.2.1 Association CaMKIIα^{T305A/T306A}-CaM during spine plasticity induction

To investigate the role of Thr305/Thr306 inhibitory phosphorylation during spine plasticity, we used the phospho-mimetic mutant CaMKII$\alpha^{T305DT306D}$ and measured its association with CaM during glutamate uncaging at 0.49 Hz (Figure 6.2A). As expected, inhibitory phosphorylation at Thr305/Thr306 precluded CaM binding. We did not observe any binding fraction change between mEGFP- CaMKII$\alpha^{T305DT306D}$ and mCherry-CaM.

Next, we used the non-phosphorylated mutant CaMKII$\alpha^{T305A/T306A}$ and measured its association with CaM in response to a single glutamate uncaging pulse. Compared to CaMKIIα^{WT}, binding fraction change of CaMKII$\alpha^{T305A/T306A}$ reached a level similar to that of CaMKIIα^{WT} but with a much slower decay, $\tau = 7.5 \pm 1.1$ S (Figure 7.1A). During the

repetitive glutamate uncaging at 0.49 Hz, the binding fraction change of

CaMKII$\alpha^{T305A/T306A}$ also reached a level similar to that of CaMKIIα^{WT}. The dissociation

time constant was obtained as $\tau = 9.3 \pm 1.8$ s (Figure 7.1B, 7.1C). Phosphorylation at

Thr305/Thr306 facilitated CaM dissociation and inhibited the rebinding of CaM. In

addition, these results showed that the enhanced CaM binding affinity of

CaMKII$\alpha^{T305A/T306A}$ did not result in a higher level of CaM binding during sLTP induction.

7.2.2 CaMKIIα$^{T305A/T306A}$ activity during spine plasticity induction

We also imaged Camui$\alpha^{T305A/T306A}$ activation during sLTP induction (Figure 7.2).

The activity of CaMKII$\alpha^{T305A/T306A}$ showed a stepwise activation similar to that of

CaMKIIα^{WT}, and reached a plateau similar to the level of CaMKIIα^{WT}. The decay was

obtained as $\tau_{fast} = 11.8 \pm 0.8$ s (72%) and $\tau_{slow} = 257 \pm 153$ s (28%). This result suggested that

in addition to CaM binding affinity, the decay of CaMKIIα activity is also regulated by

inhibitory phosphorylation at Thr305/Thr306. However, the plateau activity of CaMKIIα

seems to be insensitive of the phosphorylation state of Thr305/Thr306 during sLTP

induction.
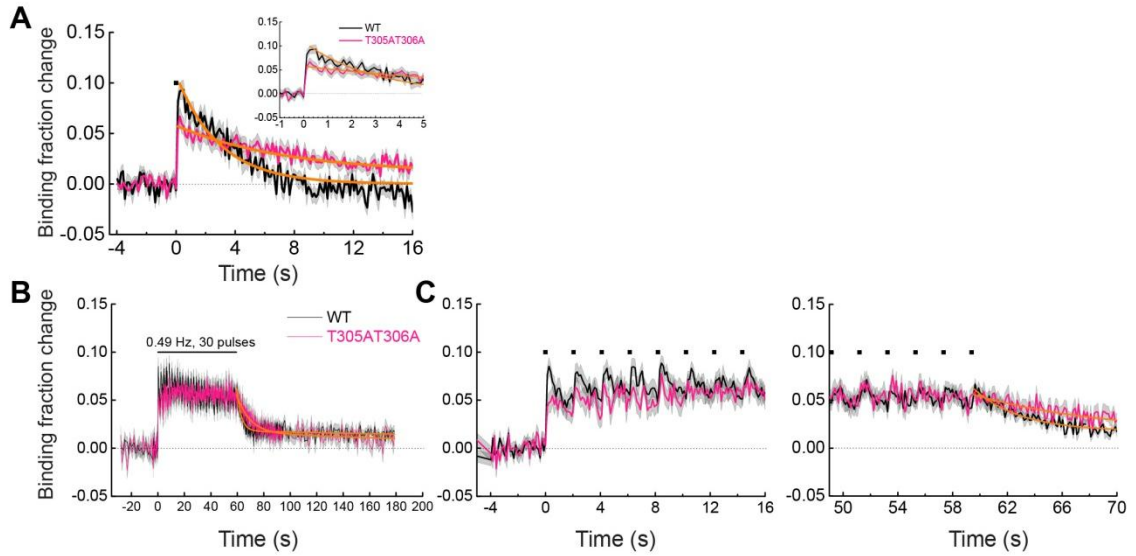
Figure 7.1: Association of CaMKIIα^T305A/T306A-CaM during sLTP

(A) Averaged change in binding fraction of CaMKIIα^T305A/T306A-CaM (magenta; n = 34 spines/ 6 neurons) in response to a single glutamate uncaging pulse (black square). The orange curves on CaMKIIα^T305A/T306A is obtained by curve fitting of an exponential function: $F(t) = C \cdot e^{-t/\tau}$. The dissociation time constant is obtained as τ = 7.5 ± 1.1 s. Inset is the expanded view. The data and fitted curve for CaMKII^WT are from (Figure 6.5) for the comparison.

(B) Averaged change in binding fraction of CaMKIIα^T305A/T306A-CaM (n = 27 spines/8 neurons) during glutamate uncaging at 0.49 Hz. The orange curve indicates the decay of binding fraction change obtained by curve fitting of a double-exponential function: $F(t) = B_0 \cdot \left[P_{fast} \cdot e^{-t/\tau_{fast}} + P_{slow} \cdot e^{-t/\tau_{slow}} \right]$. The time constants are obtained as τ_{fast} = 9.3 ± 1.8 s (P_{fast} = 71%) and τ_{slow} = 249 ± 229 s (P_{slow} = 29%). The data and fitted curve for CaMKII^WT are from (Figure 6.3) for the comparison.

(C) Expanded view of the initial (left) and late (right) phase of CaMKIIα^T305A/T306A-CaM association in (B). All data are shown in mean ± sem, and sem of time constants is obtained by bootstrapping.
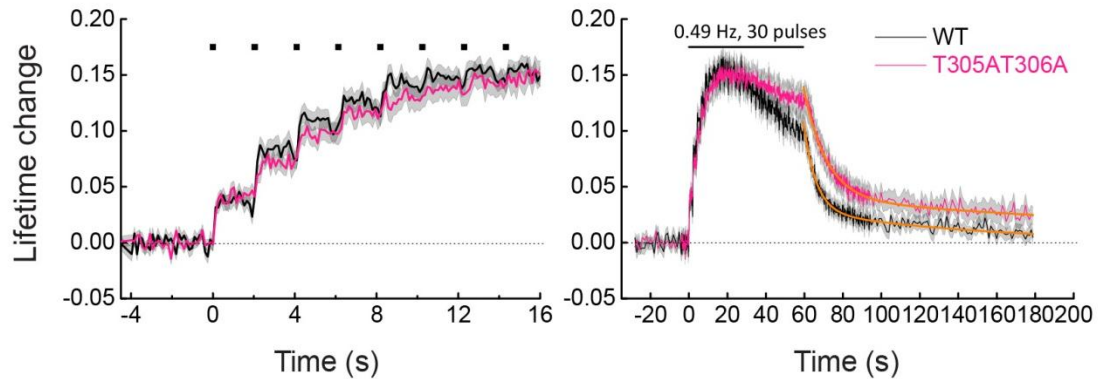
Figure 7.2: Camuiα^T305A/T306A activation during sLTP induction

Averaged change in fluorescence lifetime of Camuiα^T305A/T306A (magenta) and Camuiα^WT (black) in the stimulated spine during glutamate uncaging. The data and fitted curve for Camuiα^WT are from (Figure 3.1C) for the comparison. Left panel is expanded view of the right panel. The orange curve on Camuiα^T305A/T306A is obtained by curve fitting of a function: $F(t) = F_0 \cdot [P_{fast} \cdot e^{-t/\tau_{fast}} + P_{slow} \cdot e^{-t/\tau_{slow}}]$. The decay time constants are obtained as $\tau_{fast} = 11.8 \pm 0.9$ s (72%) and $\tau_{slow} = 255 \pm 153$ s (28%) (26 spines/5 neurons). All data are shown in mean ± sem, and sem of time constants is obtained by bootstrapping.

7.3 Discussion

Here, we measured the association of CaMKIIα[T305A/T306A] with CaM and

CaMKIIα[T305A/T306A] activity during glutamate uncaging at 0.49 Hz (Figure 7.1, 7.2).

Compared to CaMKIIα[WT], Ca^{2+}/CaM binding affinity is enhanced by ~ 3 fold (τ ~ 9 s)

when the non-phosphorylated mutant is used (Figure 7.1A). Despite this, association of

CaMKIIα[T305A/T306A]-CaM reaches a similar plateau as CaMKIIα[WT] (Figure 7.1B). These

results suggest that inhibitory phosphorylation at Thr306/Thr306 occurs during CaMKII

activation. Phosphorylation at Thr305/Thr306 facilitated Ca^{2+}/CaM dissociation and

inhibited rebinding of Ca^{2+}/CaM. In addition, our results suggest that the plateau of

CaMKIIα-CaM association is insensitive to the dissociation time constant. Instead, the

Ca^{2+} transients during glutamate uncaging might be an important factor since a higher

plateau was observed when high frequency glutamate uncaging was applied (Figure

6.4).

CaMKIIα[T305A/T306A] activity also exhibits a similar activation profile as CaMKIIα[WT]

(Figure 7.2). Activity of CaMKIIα[T305A/T306A] reaches a similar plateau, and has a similar

stepwise activation as that of CaMKIIα[WT]. Despite these, the decay time of

CaMKIIα[T305A/T306A] is ~ 2 fold slower, τ_{fast} ~ 12 s (72%) and τ_{slow} > 1 min (28%) (Figure 7.2).

The extended decay time of CaMKIIα[T305A/T306A] and the enhanced Ca^{2+}/CaM binding

affinity of CaMKIIα[T305A/T306A] (τ ~ 9 s) suggest that Camuiα activity is also regulated by

the binding affinity of Ca^{2+}/CaM. Our results also indicate that the plateau of CaMKIIα

activity is insensitive to phosphorylation at Thr305/Thr306.

Transgenic CaMKII$\alpha^{T305V/T306A}$ mice have been shown to have lower threshold for

hippocampal LTP (Elgersma et al., 2002). The extended decay time of CaMKII$\alpha^{T305A/T306A}$

activity (Figure 7.2) suggests that there might be a more flexible window in LTP

stimulation frequency required for LTP induction in transgenic CaMKII$\alpha^{T305V/T306A}$ mice.

Our results here provide a possible molecular mechanism for such finding.

Chapter 8. Spine plasticity in *Camk2a*^{T286A} knock-in mice is induced with increased stimulation frequency

8.1 Introduction

It is well known that phosphorylation at Thr286 is necessary for the induction of LTP, learning and memory (Giese et al., 1998). However, its requirement for sLTP remains unknown. Thus, we examined the role of Thr286 phosphorylation in sLTP using organotypic slices prepared from *Camk2a*^{T286A} knock-in mice. We measured structural plasticity in CA1 pyramidal neurons expressing mEGFP, and found that the sustained spine enlargement was greatly attenuated in the homozygous mice with the standard induction protocol (0.5 Hz, 30 pulses; $\Delta V_{sustained}$ = 16 ± 6% in *Camk2a*^{T286A} and $\Delta V_{sustained}$ = 89 ± 14% in litter-mate control) (Figure 8.1A, 8.1B, 8.1G). Although statistically not significant, heterozygous mice exhibited a trend towards partial impairments in sLTP ($\Delta V_{sustained}$ = 57 ± 11%) (Figure 8.1B, 8.1G).
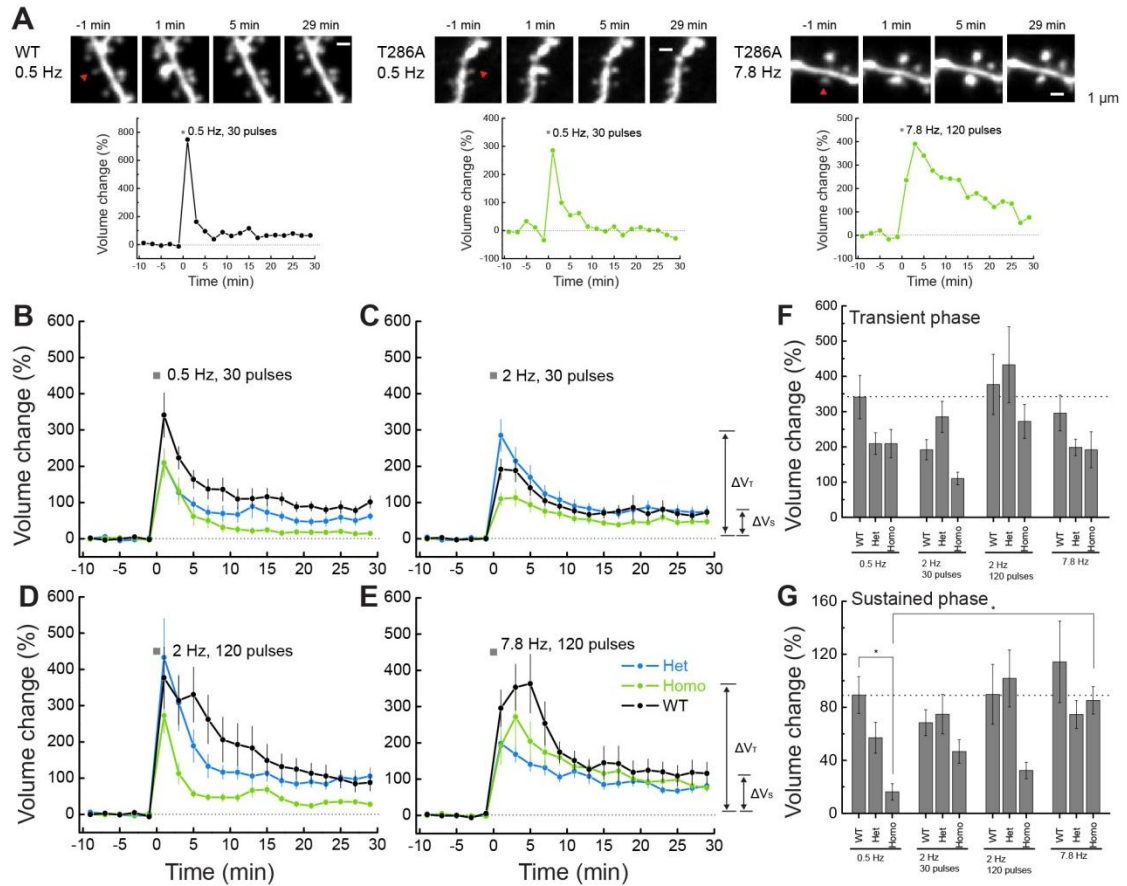
Figure 8.1: Structural plasticity induced by high frequency stimulation

(A) Fluorescence intensity images (mEGFP) of spine structural plasticity at different time points during sLTP. The arrowhead indicates the spot of two-photon glutamate uncaging. Scale bar, 1 μm.

(B-E) Structural LTP of neurons from *Camka*[T286A] wild-type (WT/WT), heterozygous (WT/T286A) or homozygous (T286A/T286A) mice induced by glutamate uncaging at 0.5 Hz for 30 pulses (B), 2 Hz for 30 pulses (C), 2 Hz for 120 pulses (D) or 7.8 Hz for 120 pulses (E). Number of samples (spines/neurons) are 22/22 for WT, 27/26 for Het, and 25/25 for Homo in (B); 17/16 for WT, 18/18 for Het, and 12/12 for Homo in (C); 15/15 for WT, 13/13 for Het, and 14/14 for Homo in (D), and 15/15 for Homo, 20/19 for Het, and 16/16 for Homo in (E).

(F-G) Quantifications of spine volume change during the transient phase (F; peak value recorded at 1 min) or the sustained phase (G; averaged over 25-30 min). Asterisks denote the statistical significance ($p < 0.05$; ANOVA followed by *post hoc* Bonferroni test). All data are shown in mean ± sem.

8.2 Results

8.2.1 sLTP is induced at high frequency glutamate uncaging in CA1 neurons from *Camk2a*[T286A] knock-in mice

If this impairment in spine structural plasticity is caused by the inability of

CaMKIIα[T286A] to integrate Ca^{2+} signals induced at this frequency, sLTP should be rescued

by increasing the frequency of glutamate uncaging. Indeed, when sLTP is induced by 2

Hz glutamate uncaging (for 30 or 120 pulses), the slightly impaired structural plasticity

in heterozygous *Camk2a*[T286A] mice was fully rescued ($\Delta V_{sustained}$ = 74.8 ± 14.9% for 2 Hz, 30

pulses and $\Delta V_{sustained}$ = 101.8 ± 21.4% for 2 Hz, 120 pulses; Figure 8.1C, 8.1D, 8.1G).

Furthermore, structural plasticity in homozygous C*amk2a*[T286] mice was fully rescued by

7.8 Hz glutamate uncaging (for 120 pulses) ($\Delta V_{sustained}$ = 85.2 ± 10.4%) (Figure 8.1E and

8.1G).

8.2.2 sLTP is impaired in CA1 neurons of *Camk2a*^{fl/fl} hippocampal slices induced at high frequency glutamate uncaging

To confirm that sLTP induced by high frequency glutamate uncaging

stimulations is CaMKII-dependent, we transfected slices prepared from conditional

knock-out mice of *Camk2a* (*Camk2a*^{fl/fl}) (Hinds et al., 2003) with tdTomato fused Cre

recombinase and mEGFP (or tdTomato and mEGFP as a control). We found that

neurons transfected with Cre recombinase showed impaired structural plasticity at all

frequencies (Figure 8.2), demonstrating that sLTP induced with high frequency

glutamate uncaging is still CaMKIIα-dependent. Furthermore, to exclude the possibility

that the rescue of sLTP is caused by altered Ca^{2+} dynamics in the mutant mice, we

measured Ca^{2+} elevations during sLTP induction (Figure 3.3). We found that Ca^{2+}

dynamics in $Camk2a^{T286A}$ was similar to that in WT, indicating that Ca^{2+} regulation is

normal in $Camk2a^{T286A}$ mice. Therefore, the rescue of sLTP induced by high frequency

glutamate uncaging is likely due to the high peak CaMKIIα^{T286A} activity in the

stimulated spines.
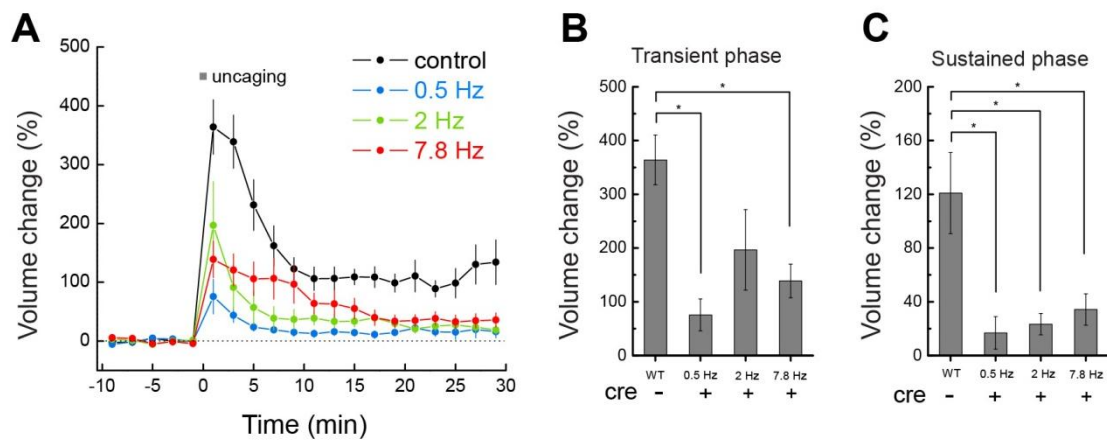
Figure 8.2: Structural LTP (sLTP) induced by high frequency glutamate uncaging in CaMKIIα conditional knock-out neurons
(A) sLTP induced at CA1 neurons from $Camk2a^{fl/fl}$ mice with exogeneous expression of Cre recombinase. WT group (black): no exogeneous expression of Cre recombinase, glutamate uncaging at 0.5 Hz for 30 pulses (n = 26 spines/13 neurons). Blue: glutamate uncaging at 0.5 Hz for 30 pulses (n =15 spines/13 neurons). Green: glutamate uncaging at 2 Hz for 120 pulses (n =12 spines/11 neurons). Red: glutamate uncaging at 7.8 Hz for 120 pulses (n =17 spines/12 neurons).
(B-C) Quantification of spine volume change during transient phase (B; peak value recorded at 1 min) and sustained phase (C; averaged over 25-30 min). Spine volume change induced by glutamate uncaging in $Camk2a^{fl/fl}$ CA1 neurons was significantly impaired at all frequencies compared to the spine volume change induced by 0.5 Hz glutamate uncaging in the control group (black). Asterisks denote statistical significance ($p < 0.05$; ANOVA followed by *post hoc* Bonferroni test). All data are shown in mean ± sem.

8.2.3 Functional plasticity is induced at high frequency electrical stimulation in CA1 neurons from *Camk2a*[T286A] knock-in mice

Lastly, we studied whether the impaired functional plasticity in *Camk2a*[T286A] mice

could be rescued by high frequency stimulation. To test this, we prepared acute

hippocampal slices from *Camk2a*[T286A] mice or liter-mate control mice (4-5 weeks). We

performed whole cell patch clamp recordings of CA1 pyramidal neurons and measured

EPSCs in response to stimulation of the Schaffer collateral pathway. LTP was induced by

pairing low frequency stimulation (2 Hz for 15 s) with depolarization of the neuron to 0

mV. Assuming a ~20% release probability (Branco and Staras, 2009), 2 Hz synaptic

stimulation corresponds to ~0.5 Hz uncaging, our standard sLTP protocol. While robust

LTP was induced in wild-type neurons by this protocol (ΔEPSC = 96 ± 16 %; averaged

over 40-63 min), *Camk2a*[T286A] neurons showed impaired LTP (ΔEPSC = 18 ± 10 %) (Figure

8.3), in agreement with previous studies (Giese et al., 1998). However, when we applied

high frequency stimulation (40 Hz, 15 s; corresponding to ~8 Hz glutamate uncaging),

LTP in *Camk2a*[T286A] mice (ΔEPSC = 76 ± 20 %) was induced (Figure 8.3).
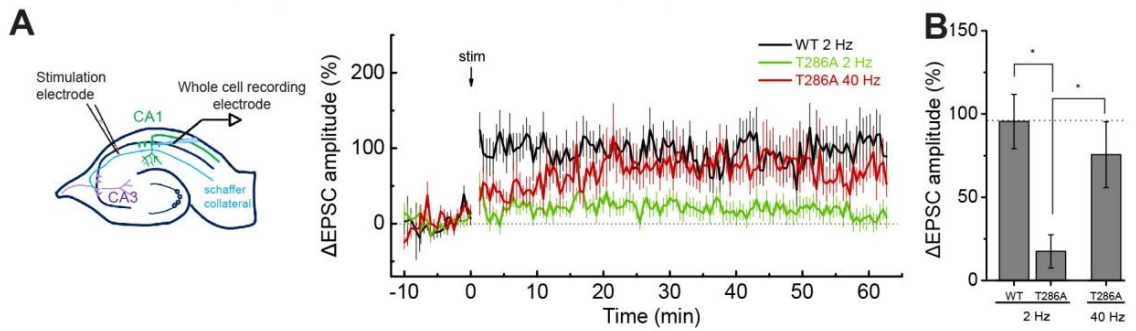
Figure 8.3: Structural plasticity induced by high frequency stimulation

(A) Whole-cell recording of LTP induced at the Schaffer collateral in CA1 neurons from *Camk2a*[T286A] and litter-mate control mice. LTP is induced by electrical stimulations at 2 Hz or 40 Hz for 15 s with depolarization to 0 mV. Number of neurons is 19 for WT, 20 for T286A (2 Hz) and 27 for T286A (40 Hz).

(B) Quantification of EPSC potentiation averaged over 40-63 min. Asterisks denote the statistical significance ($p < 0.05$; ANOVA followed by *post hoc* Bonferroni test). All data are shown in mean ± sem.

8.3 Discussion

Our results demonstrate that the impaired structural and functional plasticity in CA1 neurons of *Camk2a*[T286A] mice can be rescued by high frequency stimulation, which boosts the impaired activation of CaMKII[T286A]. These results suggest phosphorylation at Thr286 significantly broadens the frequency domain over which CaMKII can integrate Ca^{2+} signals, and permits CaMKII to integrate Ca^{2+} signals at a physiological relevant frequency to induce synaptic plasticity.

Chapter 9.   A proposed kinetic model of CaMKII activation during spine plasticity induction

9.1 Introduction

Based on the kinetic parameters we obtained from Camuiα activation and from association of CaMKIIα-CaM and its mutant variants during the induction of spine plasticity, we proposed the following kinetic model of CaMKII activation which has two different states of Thr286-phophorylated CaMKII (without bound CaM, the "autonomous" state of CaMKII). We constructed a set of rate equations (elementary reaction) to describe CaMKII biochemical reactions based on our proposed model (Table 2). We used the law of mass action to obtain non-linear ordinary differential equations (ODEs) and to solve the concentration of each species (see detail in Chapter 2.10).

9.2 Proposed kinetics model

$$K + CaM \underset{k_4}{\overset{k_3}{\rightleftharpoons}} \left[KCaM \underset{k_6}{\overset{k_5}{\rightleftharpoons}} PCaM \right] \underset{k_8}{\overset{k_7}{\rightleftharpoons}} CaM + P \overset{k_{11}}{\longrightarrow} K$$

with P connected to P_2 via $k_{10} \big\Downarrow k_9$ and $P_2 \overset{k_{12}}{\nearrow} K$

Scheme 1: CaMKII activation model

Scheme 1 is the proposed model. Where K is CaMKII, CaM is the active form of calmodulin with one or two bound Ca^{2+} (see detail in the following discussion), P and P_2 are the proposed two different states of Thr286-phosphorylated CaMKII with inhibitory phosphorylation at Thr305 or/and Thr306. Thus, reaction 8 is assumed to be slow and

not preferable. Figure 9.1 is the simulated results. The associated rate constants and rate

equations are listed in Table 1 and 2, respectively. The simulated CaMKII activation

showed a stepwise activation and reached to its plateau within ~ 10 s, which is similar to

Camuiα activation measured during glutamate uncaging at 0.49 Hz. Association of

CaMKII-CaM also reached to its plateau at the first few stimulations. The decay times of

CaMKII activity were obtained as $\tau_{fast} = 6.4\ s$ (76%) and $\tau_{slow} = 58.4\ s$ (24%).

Dissociation time of CaM was obtained as $\tau = 3.2\ s$. These time constants were similar

to that obtained from Camuiα and CaMKIIα-CaM association during spine plasticity

induction. We will discuss the effect of each rate constant on CaMKII activation in the

following sections.
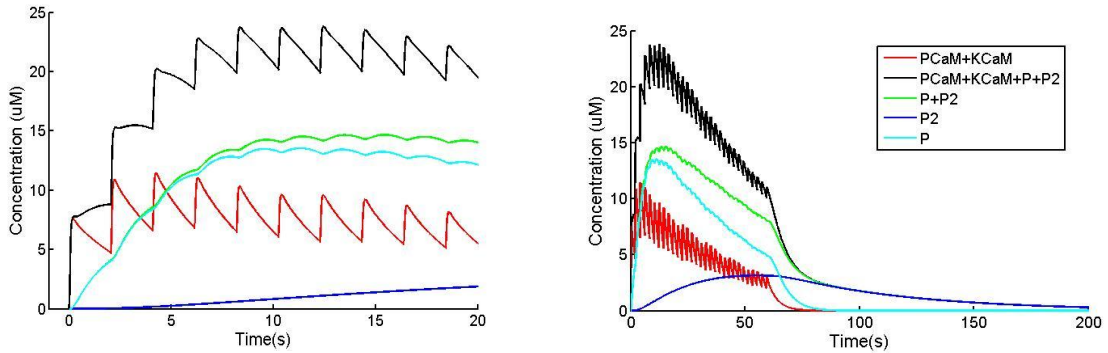
Figure 9.1: Simulated CaMKII activation based on scheme 1
Black: concentration of total active CaMKII. Red: concentration of CaM bound to
CaMKII and to Thr286-phosphorylated CaMKII. Green: concentration of Thr286-
phosphorylated CaMKII (P and P_2 form). Light blue: concentration of P form of CaMKII.
Blue: concentration of P_2 form of CaMKII. The decay time of CaMKII activity (black) was
obtained by curve fitting of a double exponential function: $Y(t) = Y_0 \cdot \left[P_{fast} \cdot e^{-t/\tau_{fast}} + P_{slow} \cdot e^{-t/\tau_{slow}} \right]$ and decay times were obtained as $\tau_{fast} = 6.4\ s$ (76%) and $\tau_{slow} = 58.4\ s$ (24%). Dissociation time of CaM (red) was obtained by curve fitting of and
exponential function: $Y(t) = Y_0 \cdot e^{-t/\tau}$ and dissociation time was obtained as $\tau = 3.2\ s$.
Left panel is the expanded view of the right panel.

Ca²⁺ transients modelling

To simplify the simulation, the influx of NMDA-receptor mediated Ca²⁺ during repetitive glutamate uncaging is modelling as:

$$[Ca]_i = [Ca]_0 e^{-d(i-1)/\tau_2}$$

$$[Ca]_t = [Ca]_i e^{-[t-d(i-1)]/\tau_1}$$

Where i = number of uncaging pulses (integers, 1 to 30),

$d = 1/uncaging\ frequency, \tau_1 = 0.05\ s$ (Ca²⁺ clearance time constant) (Lee et al., 2009),

$\tau_2 = 30.0\ s$ (reflects glutamate uncaging evoked NMDA-receptor desensitization) (Lee et al., 2009). Figure 9.2 shows the modelling result of Ca²⁺ transients.
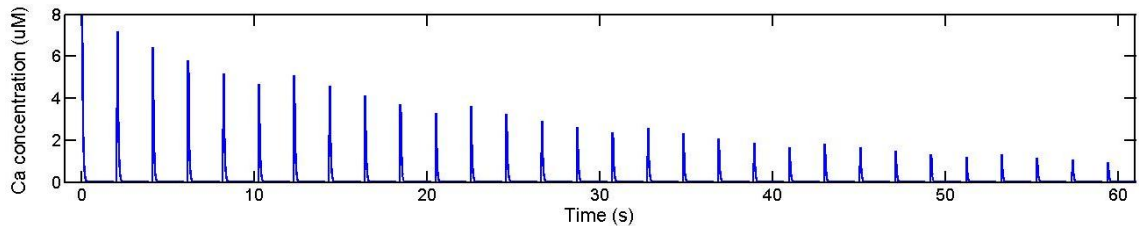
Figure 9.2: Ca²⁺ transients modelling
Modelling Ca²⁺ transients during glutamate uncaging at 0.49 Hz and [Ca]₀ is set as 8 µM.

Effect of Ca²⁺ transients

Ca²⁺ transients can be measured by Ca²⁺ sensitive dye during glutamate uncaging (Grienberger and Konnerth, 2012). Elevation of Ca²⁺ concentration is estimated to be ~ 1-10 µM (Lee et al., 2009; Sabatini et al., 2002). To determine the effect of [Ca]₀ on the proposed model, we simulated our model based on the following [Ca]₀: 0.1, 1, 8, 20, 50 µM (Figure 9.3). Increases in [Ca]₀ elevates CaMKII activity, but the trend of the activation profile seems to remain unaffected.
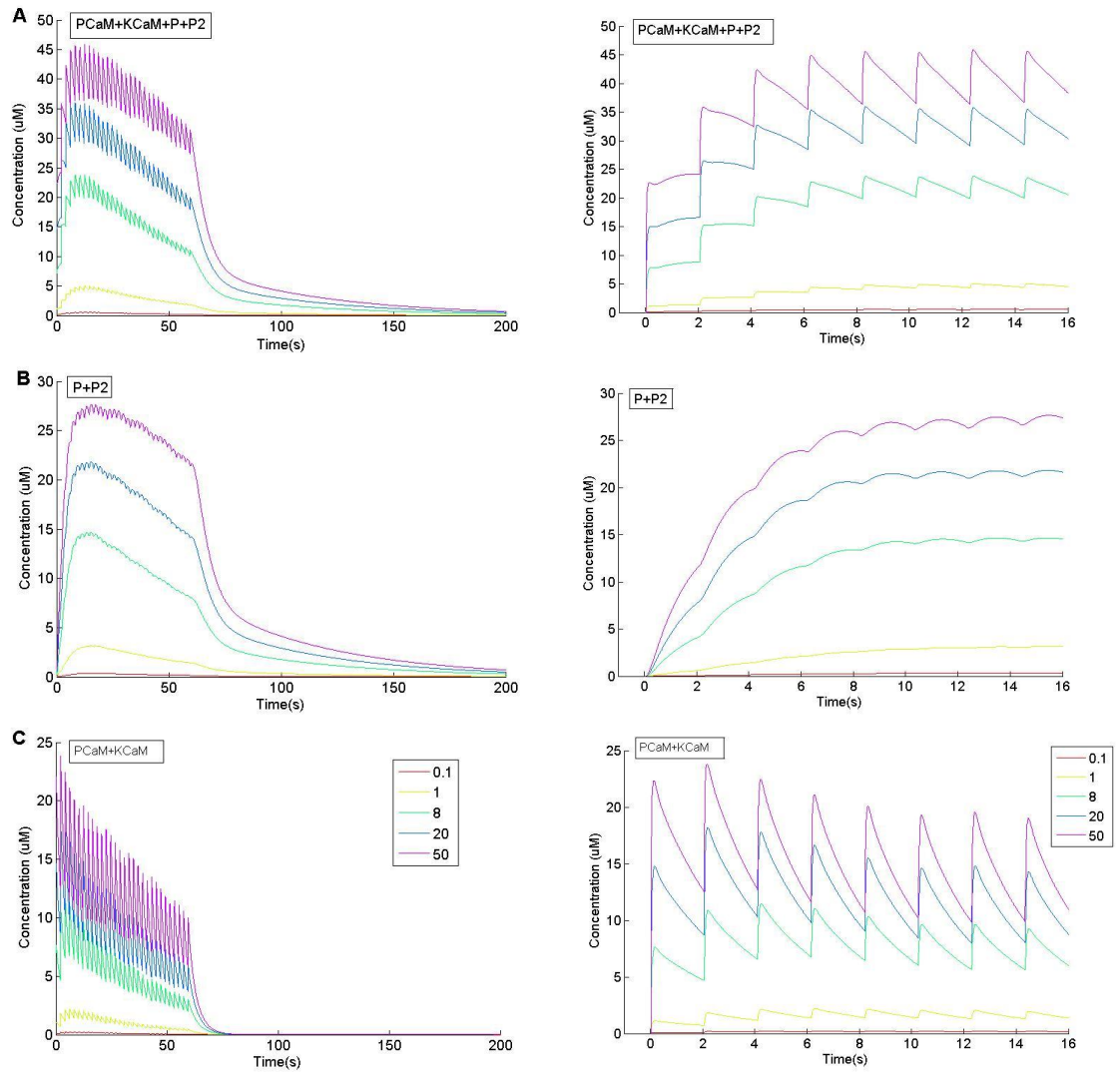
Figure 9.3: Effect of Ca²⁺ transients on CaMKII activation
(A-C) Right panels are expanded view of left panels.
(A) Effect of $[Ca]_0$ on total CaMKII activity.
(B) Effect of $[Ca]_0$ on Thr286-phosphorylated CaMKII activity.
(C) Effect of $[Ca]_0$ on CaMKII-CaM association.

Effect of Calmodulin concentration

There are four Ca^{2+} binding sites on calmodulin (two on N-lobe and two on C-lobe CaM, respectively). Dissociation of N-lobe Ca^{2+} is much faster than C-lobe Ca^{2+} (~100 fold). It's been showed that Ca_2CaM (C-lobe) is the major calmodulin species during Ca^{2+} transients, and the binding of Ca^{2+} on each lobe is cooperative (Pepke et al., 2010). Therefore, to simplify our model, we assumed that active calmodulin (CaM) only requires binding of one Ca^{2+}, and Ca^{2+} dissociation follows the slow phase of the dissociation step (Equation 1) (Martin et al., 1985).

Equation 1:

$$Ca^{2+} + CaM_d \underset{k_2}{\overset{k_1}{\rightleftharpoons}} CaM$$
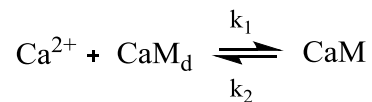
where CaM_d is the inactive form of calmodulin without any bound Ca^{2+}, and CaM is the active form. To determine the effect of $[CaM_d]_0$ on the proposed model, we simulated our model based on the following $[CaM_d]_0$: 10, 30, 50, 70, 100, 200 μM, where $[CaM_d]_0$ to $[CaMKII]_0$ (70 μM) ratio is: 0.14, 0.43, 0.71, 1, 1.43, 2.86, respectively (Figure 9.4). Increases in $[CaM_d]_0$ elevates total CaMKII activity. When CaM is a limiting factor to CaMKII (i.e. $[CaM_d]_0$ / $[CaMKII]_0$ < 1), the stepwise activation of CaMKII is clearly observed (Figure 9.4A). The integration behavior is faded with increases in $[CaM_d]_0$ / $[CaMKII]_0$. The activation pattern of CaMKII-CaM association is also affected by the increases in $[CaM_d]_0$. When $[CaM_d]_0$ is 200 μM, the first two stimulations causes the highest concentration of CaMKII-CaM association. This is different from the simulated

104

results of other conditions where the association caused by the first stimulation is

slightly less than that caused by the following stimulations (Figure 9.4C).
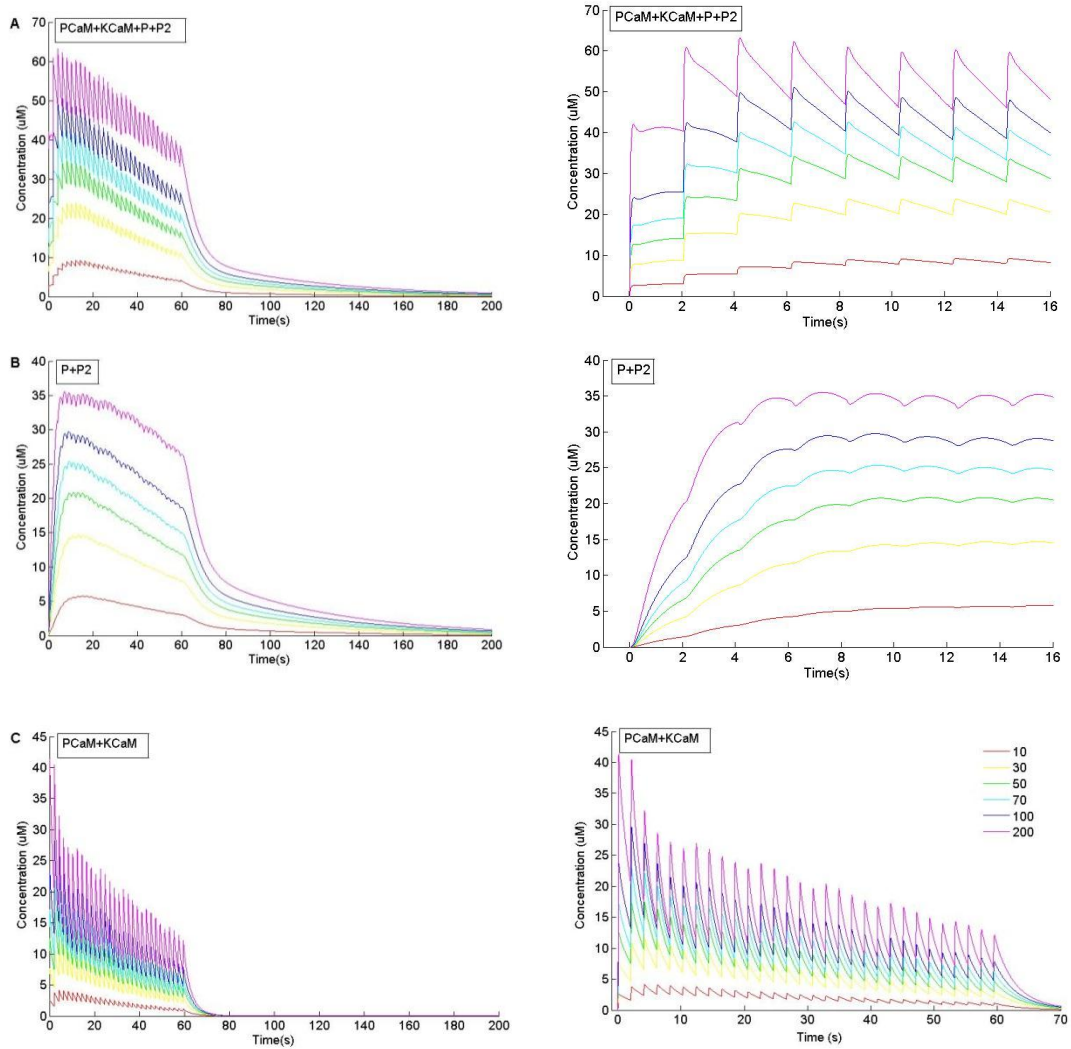
Figure 9.4: Effect of CaM concentration on CaMKII activation
(A-C) Right panels are expanded view of left panels.
(A) Effect of $[CaM_d]_0$ on total CaMKII activity.
(B) Effect of $[CaM_d]_0$ on Thr286-phosphorylated CaMKII activity.
(C) Effect of $[CaM_d]_0$ on CaMKII-CaM association.

Effect of Thr286 phosphorylation rate

To determine the effect of Thr286 phosphorylation rate on CaMKII activation, we simulated our model based on the following k_{cat} (k_5 in Scheme 1): 2, 6.3, 12, 20, 50, 100 s^{-1} (Figure 9.5). Increases in k_{cat} elevates CaMKII activity, but in a milder manner. CaMKII activity remains at a similar level when k_{cat} increases from 50 to 100 s^{-1} (Figure 9.5A). This result suggests that once k_{cat} passes its threshold value (~ 50 s^{-1}), increases in Thr286 phosphorylation rate might only have minimal effects on CaMKII activation. In addition, when Thr286 phosphorylation is slow (k_{cat} = 2 s^{-1}), the stepwise activation of CaMKII reveals a double-exponential like decay between each stimulations (Figure 9.5A). These two decay components possibly reflect the dissociation of CaM from KCaM and PCaM, respectively. At a faster phosphorylation rate, increases of Thr286-phosphorylated CaMKII (Figure 9.5B) balance the decreases of CaMKII-CaM association (Figure 9.5C). Therefore, a stepwise activation of CaMKII is observed and the two decay components vanish between each stimulations.
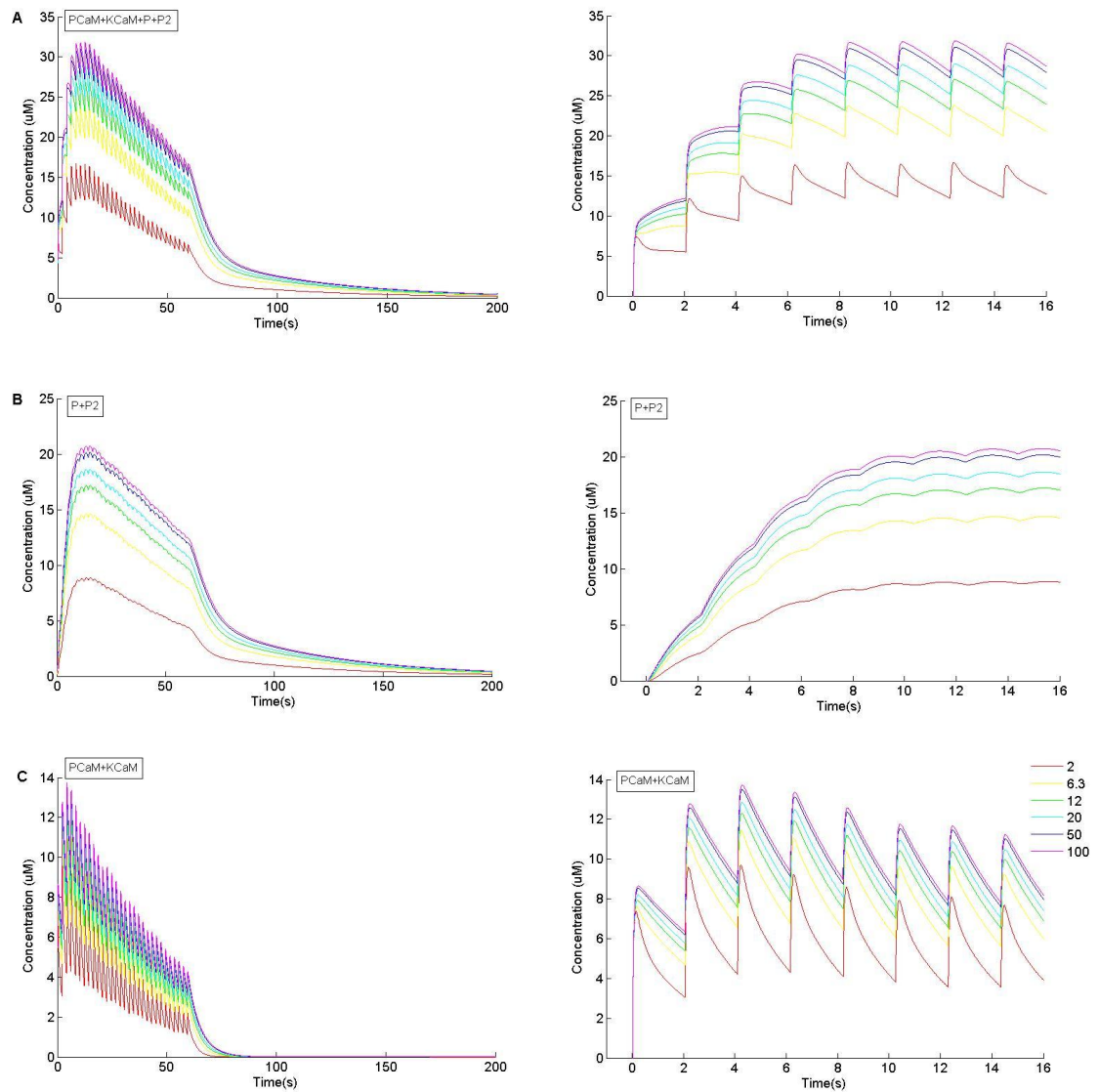
Figure 9.5: Effect of Thr286 phosphorylation rate on CaMKII activation
(A-C) Right panels are expanded view of left panels.
(A) Effect of Thr286 phosphorylation rate on total CaMKII activity.
(B) Effect of Thr286 phosphorylation rate on Thr286-phosphorylated CaMKII activity.
(C) Effect of Thr286 phosphorylation rate on CaMKII-CaM association.

Effect of Thr305/Thr306 inhibitory phosphorylation

In scheme 1, we assumed that P and P_2 form of CaMKII are the two different states of Thr286-phosphorylated CaMKII with inhibitory phosphorylation at Thr305 or/and Thr306 (Reaction 7, Scheme 1).

$$\text{PCaM} \underset{k_8}{\overset{k_7}{\rightleftharpoons}} \text{CaM} + \text{P}$$

T305/T306 phosphorylation
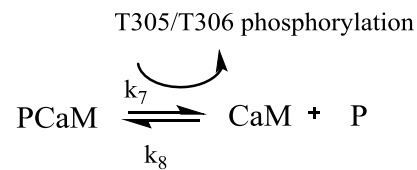
Thr286 and Thr305/Thr306 dephosphorylation can be carried out by PP1 (PSD fraction) and PP2A (cytosolic fraction) (Blitzer et al., 1998; Colbran, 2004; Ishida et al., 1998; Lisman et al., 2012; Michalski, 2013). Here, we assumed that phosphatases have no selection towards its substrates (Thr286 or Thr305/Thr306); therefore, the dephosphorylation rate for Thr286 and for Thr305/Thr306 should be similar. Reaction 11 and Reaction 12 in Scheme 1 are the dephosphorylation reactions of residues Thr286 and Thr305/Thr306.

To validate our assumption, we performed the simulation of CaMKII[T305A/T306A] activation based on the adjusted rate constants. In this scenario, the rate constant of CaM binding to CaMKII (k_3) and to Thr286-phosphorylated CaMKII (k_8) should be the same since there should be no selection between these two forms. Dissociation of CaM from CaMKII[T305A/T306A] was measured to be ~ 2.5 fold slower (Figure 7.1). Thus, we refined k_7 from 0.5 to 0.2 s^{-1}. We used the adjusted k_7 and k_8 to perform the simulated CaMKII[T305A/T306A] activation (Figure 9.6).

Our simulated result (Figure 9.6) showed that compared to CaMKII[WT] (Figure

9.1), the total CaMKII[T305A/T306A] activity was not affected by the enhanced binding affinity

of CaM. Instead, CaMKII-CaM association was enhanced ([KCaM]+[PCaM]) and the

activity of Thr286-phosphorylated CaMKII decreased ([P]+[P₂]). The decay time of

CaMKII[T305A/T306A] activity was obtained as $\tau_{fast} = 11.5\ s$ (81%) and

$\tau_{slow} = 64.0\ s$ (19%). The dissociation time of CaM was obtained as $\tau = 9.5\ s$. These

time constants were similar to that obtained from Camuiα[T305A/T306A] (Figure 7.2) and

CaMKII[T305A/T306A] –CaM association (Figure 7.1B) during glutamate uncaging at 0.49 Hz.
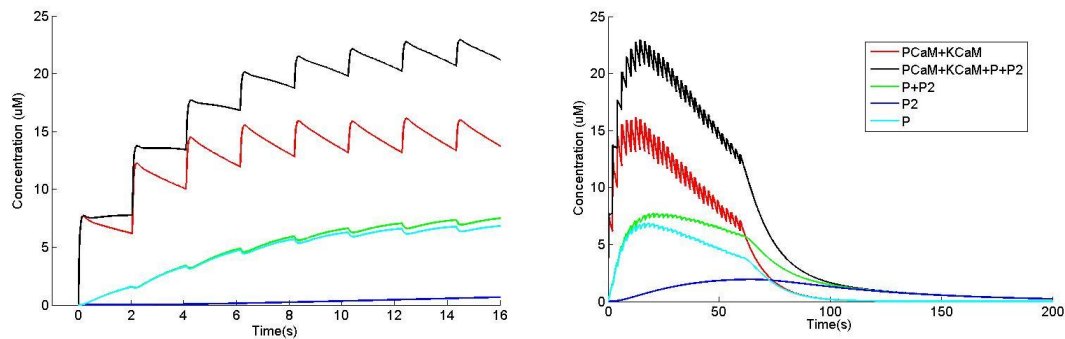
Figure 9.6: Simulated CaMKII[T305A/T306A] activation based on scheme 1
Black: concentration of total active CaMKII. Red: concentration of CaM bound to
CaMKII and to Thr286-phosphorylated CaMKII. Green: concentration of Thr286-
phosphorylated CaMKII (P and P₂ form). Light blue: concentration of P form of CaMKII.
Blue: concentration of P₂ form of CaMKII. The decay time of CaMKII[T305A/T306A] activity
(black) was obtained by curve fitting of a double exponential function: $Y(t) = Y_0 \cdot$
$\left[P_{fast} \cdot e^{-t/\tau_{fast}} + P_{slow} \cdot e^{-t/\tau_{slow}}\right]$ and decay times were obtained as
$\tau_{fast} = 11.5\ s$ (81%)and $\tau_{slow} = 64.0\ s$ (19%). Dissociation time of CaM (red) was
obtained by curve fitting of and exponential function: $Y(t) = Y_0 \cdot e^{-t/\tau}$ and dissociation
time was obtained as $\tau = 9.5\ s$. Left panel is the expanded view of the right panel.

9.3 Discussion

The proposed CaMKII activation model goes well with our measured kinetics (Scheme 1). Our model indicates that there might be another 'trapped' state of Thr286-phosphorylated CaMKII which has a longer lifetime (~ 60 s) but with a minor fraction (~ 30%). The two different states of Thr286-phosphorylated CaMKII might be originated from two different compartments of CaMKII (such as PSD and the cytosolic fraction) which have different phosphatase accessibility. It could also originate from two different types of phosphatases which have different k_{cat} (such as PP1 and PP2A). Further experiments are required to disentangle these two different states.

Most of the rate constants are adapted from the previous literature and our measurements, and are further refined during the simulation (Table 1).

Chapter 10.   General discussion and future directions

10.1 General discussion

Here, I investigated the role of CaMKII in signal processing during synaptic plasticity. To measure the precise kinetics of CaMKII activation, we improved the temporal resolution of two-photon fluorescence lifetime imaging (128 ms/frame) to measure the activation kinetics of CaMKII in response to Ca^{2+} transients during structural plasticity induction. This higher temporal resolution imaging revealed a stepwise activation of CaMKII following each repetitive Ca^{2+} elevations, indicating that CaMKII is a leaky integrator of Ca^{2+} signals (Figure 3.1, 5.1A-5.1C). The integration time of CaMKII (6-8 s) also defines the frequency of stimulation required for inducing plasticity (Matsuzaki et al., 2004).

Our observations clarify the critical function of Thr286 phosphorylation for plasticity: it permits CaMKII to integrate Ca^{2+} signals at a physiologically relevant frequency. The decay time of the non-phosphorylated mutant CaMKII[T286A] and phospho-mimetic mutant CaMKII[T286D] was ~3- and ~2-fold faster than that of wild-type CaMKII, respectively. The faster decay time of the mutants substantially compromised the integration capability of CaMKII for the same frequency of stimulation. This suggests that active Thr286 phosphorylation is required for an optimum integration of Ca^{2+} signals (Figure 3.5, 4.5). Although the basal activity of CaMKII[T286D] was elevated, it was further activated by the binding of Ca^{2+}/calmodulin. The fast decay of CaMKII[T286D]

111

activity, perhaps due to the dissociation of Ca^{2+}/ calmodulin, suggests that

dephosphorylation of Thr286 plays some role in the optimum decay time (6 – 8 s) of

CaMKII (but see (Otmakhov et al., 2015)).

I also found that spine plasticity can be induced in *Camk2a*[T286A] knock-in mice by

using high frequency stimulation (Figure 8.1). Our results indicate that the high peak

CaMKII[T286A] activity, even achieved without Thr286 phosphorylation, is able to relay Ca^{2+}

signals to downstream molecules such as RhoA and Cdc42 whose activity have been

shown to last > 30 min in supporting spine plasticity (Murakoshi et al., 2011; Nishiyama

and Yasuda, 2015). While prolonged Thr286 phosphorylation may occur during LTP

(Lengyel et al., 2004), it appears not to be necessary for the maintenance of structural

plasticity and LTP. Instead, my findings demonstrate that phosphorylation at Thr286 is

critical for the optimum integration of Ca^{2+} signals which is required for synaptic

plasticity induction.

10.2 Future directions

CaMKII in LTD

The above findings indicate that the role of Thr286 phosphorylation is for the

efficient integration of Ca^{2+} signaling during repetitive stimulation of LTP induction.

This delicate measurement provides quantitative evidence for the importance of CaMKII

Thr286 phosphorylation during LTP. This result also provides a molecular basis for

CaMKIIα function as a frequency decoder that resides in postsynaptic dendritic spines.

Long-term depression (LTD) at single dendritic spines is induced by the weak and the low frequency stimulation (~0.1 Hz, 0.3 mM Ca^{2+}) (Oh et al., 2013). Several pharmacological studies have demonstrated the involvement of CaMKII in LTD (Coultrap et al., 2014; Pi et al., 2010). However, since the time interval between the repetitive stimulation is relatively long (~10 s) and the [Ca^{2+}] transients is supposedly low, it is highly possible that CaMKIIα is not fully activated during LTP induction. To confirm the involvement of CaMKIIα in LTD, we will have to directly probe camuiα activation during LTD induction and use genetic methods to support the finding.

Does trapped state of Thr286-phosphorylated CaMKII exist?

The proposed CaMKII kinetics scheme indicates that there might be two different states of Thr286-phosphorylated CaMKII. The two different states might be due to different protein phosphatase activity or different accessibility to protein phosphatase. Both protein phosphatase 1 (PP1) and protein phosphatase 2A (PP2A) have been shown to be possible candidates (Blitzer et al., 1998; Colbran, 2004; Ishida et al., 1998; Lisman et al., 2012). However, the lack of specificity of the inhibitors and difficulties in knocking-out or knocking-down protein phosphatase might make this distinction challenging to solve.

Is CaMKII/NMDAR complex critical in supporting LTP?

CaMKII/NMDAR complex has been an attractive model in supporting LTP (Lisman and Raghavachari, 2015; Lisman and Zhabotinsky, 2001; Sanhueza and Lisman,

2013). Evidence, however, relies exclusively on *in vitro* binding assays and experiments.

Quantitatively, on average, individual spines contain only ~5 copies of NMDARs, while

the highly abundant CaMKII has >1000 molecules (Otmakhov and Lisman, 2012).

Therefore, presumably, only a tiny fraction of CaMKII is bound to NMDARs. Mutational

analysis which impairs binding of CaMKII (I205K) towards NMDARs indirectly

demonstrated the importance of this interaction. However, mutant CaMKII I205K might

have impaired affinity towards CaM as predicted in the crystal structure (Chao et al.,

2010). Direct imaging of CaMKII/NMDAR complex will improve our understanding of

the molecular basis of this hypothesis, although it will be challenging to directly image

the interaction between CaMKII and NMDARs with the existing tools.

CaMKIIβ in LTP

I have mainly focused on the role of CaMKIIα isoform in LTP. CaMKIIβ, on the

other hand, constitutes about ¼ of CaMKII and forms heteromers with CaMKIIα in

hippocampal CA1 neurons (Erondu and Kennedy, 1985; Otmakhov and Lisman, 2012).

Studies have been shown that the kinase activity of CaMKIIβ is dispensable in LTP but

its role in the association to actin filaments is necessary to target CaMKIIα to the PSD

during LTP (Borgesius et al., 2011; Shen et al., 1998). Overall, CaMKIIα and CaMKIIβ

share high sequence homology and the main difference lies in the linker region (links the

regulatory segment and the association domain). The length of the linker has been

proposed to be a possible regulator in the frequency decoding behavior of CaMKII

(Chao et al., 2011). To address the role of CaMKIIβ in sLTP, we will have to directly probe CaMKIIβ activation (via 'camuiβ') with the combination of other genetic and pharmacological methods.

Possible advancements of techniques

The direct protein activity imaging technique (FRET-FLIM) I used here relies on the overexpression of the interested protein with a sustainable quantity compared to the endogenous protein. For the phospho-mimetic CaMKII, camuiα^{T286D}, I was experiencing low expression level in CA1 neurons, accumulation of the construct in the cell body, and the transfected neuron were prone to unhealthy condition. Although this issue was solved by suppressing the basal neuronal activity by bath application of high Mg^{2+} (10 mM in total tissue medium), this impedes the possibility of imaging other "constitutively active" form of interested proteins. It would be helpful if we can "caged" the active form of protein by a universal method and release the cage right before our experiments by optogenetics or pharmacological methods (Dagliyan et al., 2013; Molino and Wang, 2014; Yi et al., 2014). In addition, it would also be helpful if we can label the endogenous proteins with fluorophores to perform FRET-FLIM measurements. The direct labeling of the endogenous proteins can eliminate the unwanted overexpression effect and preserve the physiological condition (Sander and Joung, 2014). However, this might be labor-intensive and may not be easily applied.

115

References

Abel, T., Nguyen, P.V., Barad, M., Deuel, T.A., Kandel, E.R., and Bourtchouladze, R. (1997). Genetic demonstration of a role for PKA in the late phase of LTP and in hippocampus-based long-term memory. Cell *88*, 615-626.

Ahmed, R., Zha, X.M., Green, S.H., and Dailey, M.E. (2006). Synaptic activity and F-actin coordinately regulate CaMKIIalpha localization to dendritic postsynaptic sites in developing hippocampal slices. Mol Cell Neurosci *31*, 37-51.

Anderson, M.E., Braun, A.P., Wu, Y., Lu, T., Wu, Y., Schulman, H., and Sung, R.J. (1998). KN-93, an inhibitor of multifunctional Ca++/calmodulin-dependent protein kinase, decreases early afterdepolarizations in rabbit heart. J Pharmacol Exp Ther *287*, 996-1006.

Banke, T.G., Bowie, D., Lee, H., Huganir, R.L., Schousboe, A., and Traynelis, S.F. (2000). Control of GluR1 AMPA receptor function by cAMP-dependent protein kinase. J Neurosci *20*, 89-102.

Barria, A., Derkach, V., and Soderling, T. (1997a). Identification of the Ca2+/calmodulin-dependent protein kinase II regulatory phosphorylation site in the alpha-amino-3-hydroxyl-5-methyl-4-isoxazole-propionate-type glutamate receptor. J Biol Chem *272*, 32727-32730.

Barria, A., and Malinow, R. (2005). NMDA receptor subunit composition controls synaptic plasticity by regulating binding to CaMKII. Neuron *48*, 289-301.

Barria, A., Muller, D., Derkach, V., Griffith, L.C., and Soderling, T.R. (1997b). Regulatory phosphorylation of AMPA-type glutamate receptors by CaM-KII during long-term potentiation. Science *276*, 2042-2045.

Bats, C., Groc, L., and Choquet, D. (2007). The interaction between Stargazin and PSD-95 regulates AMPA receptor surface trafficking. Neuron *53*, 719-734.

Bayer, K.U., De Koninck, P., Leonard, A.S., Hell, J.W., and Schulman, H. (2001). Interaction with the NMDA receptor locks CaMKII in an active conformation. Nature *411*, 801-805.

Bayer, K.U., De Koninck, P., and Schulman, H. (2002). Alternative splicing modulates the frequency-dependent response of CaMKII to Ca(2+) oscillations. EMBO J *21*, 3590-3597.

Bayer, K.U., LeBel, E., McDonald, G.L., O'Leary, H., Schulman, H., and De Koninck, P. (2006). Transition from reversible to persistent binding of CaMKII to postsynaptic sites and NR2B. J Neurosci *26*, 1164-1174.

Bear, M.F., and Malenka, R.C. (1994). Synaptic plasticity: LTP and LTD. Curr Opin Neurobiol *4*, 389-399.

Benson, D.L., Isackson, P.J., Gall, C.M., and Jones, E.G. (1992). Contrasting patterns in the localization of glutamic acid decarboxylase and Ca2+/calmodulin protein kinase gene expression in the rat central nervous system. Neuroscience *46*, 825-849.

Berridge, M.J. (1997). The AM and FM of calcium signalling. Nature *386*, 759-760.

Bliss, T.V., and Lomo, T. (1973). Long-lasting potentiation of synaptic transmission in the dentate area of the anaesthetized rabbit following stimulation of the perforant path. J Physiol *232*, 331-356.

Blitzer, R.D., Connor, J.H., Brown, G.P., Wong, T., Shenolikar, S., Iyengar, R., and Landau, E.M. (1998). Gating of CaMKII by cAMP-regulated protein phosphatase activity during LTP. Science *280*, 1940-1942.

Blitzer, R.D., Wong, T., Nouranifar, R., Iyengar, R., and Landau, E.M. (1995). Postsynaptic cAMP pathway gates early LTP in hippocampal CA1 region. Neuron *15*, 1403-1414.

Boehm, J., Kang, M.G., Johnson, R.C., Esteban, J., Huganir, R.L., and Malinow, R. (2006). Synaptic incorporation of AMPA receptors during LTP is controlled by a PKC phosphorylation site on GluR1. Neuron *51*, 213-225.

Borgesius, N.Z., van Woerden, G.M., Buitendijk, G.H., Keijzer, N., Jaarsma, D., Hoogenraad, C.C., and Elgersma, Y. (2011). betaCaMKII plays a nonenzymatic role in hippocampal synaptic plasticity and learning by targeting alphaCaMKII to synapses. J Neurosci *31*, 10141-10148.

Bortolotto, Z.A., and Collingridge, G.L. (1998). Involvement of calcium/calmodulin-dependent protein kinases in the setting of a molecular switch involved in hippocampal LTP. Neuropharmacology *37*, 535-544.

Branco, T., and Staras, K. (2009). The probability of neurotransmitter release: variability and feedback control at single synapses. Nat Rev Neurosci *10*, 373-383.

Brown, G.P., Blitzer, R.D., Connor, J.H., Wong, T., Shenolikar, S., Iyengar, R., and Landau, E.M. (2000). Long-term potentiation induced by theta frequency stimulation is regulated by a protein phosphatase-1-operated gate. J Neurosci *20*, 7880-7887.

Buard, I., Coultrap, S.J., Freund, R.K., Lee, Y.S., Dell'Acqua, M.L., Silva, A.J., and Bayer, K.U. (2010). CaMKII "autonomy" is required for initiating but not for maintaining neuronal long-term information storage. J Neurosci *30*, 8214-8220.

Burgin, K.E., Waxham, M.N., Rickling, S., Westgate, S.A., Mobley, W.C., and Kelly, P.T. (1990). In situ hybridization histochemistry of Ca2+/calmodulin-dependent protein kinase in developing rat brain. J Neurosci *10*, 1788-1798.

Chao, L.H., Pellicena, P., Deindl, S., Barclay, L.A., Schulman, H., and Kuriyan, J. (2010). Intersubunit capture of regulatory segments is a component of cooperative CaMKII activation. Nat Struct Mol Biol *17*, 264-272.

Chao, L.H., Stratton, M.M., Lee, I.H., Rosenberg, O.S., Levitz, J., Mandell, D.J., Kortemme, T., Groves, J.T., Schulman, H., and Kuriyan, J. (2011). A mechanism for tunable autoinhibition in the structure of a human Ca2+/calmodulin- dependent kinase II holoenzyme. Cell *146*, 732-745.

Cho, Y.H., Giese, K.P., Tanila, H., Silva, A.J., and Eichenbaum, H. (1998). Abnormal hippocampal spatial representations in alphaCaMKIIT286A and CREBalphaDelta- mice. Science *279*, 867-869.

Colbran, R.J. (1993). Inactivation of Ca2+/calmodulin-dependent protein kinase II by basal autophosphorylation. J Biol Chem *268*, 7163-7170.

Colbran, R.J. (2004). Protein phosphatases and calcium/calmodulin-dependent protein kinase II-dependent synaptic plasticity. J Neurosci *24*, 8404-8409.

Coultrap, S.J., Freund, R.K., O'Leary, H., Sanderson, J.L., Roche, K.W., Dell'Acqua, M.L., and Bayer, K.U. (2014). Autonomous CaMKII mediates both LTP and LTD using a mechanism for differential substrate site selection. Cell Rep *6*, 431-437.

Coussens, C.M., and Teyler, T.J. (1996). Protein kinase and phosphatase activity regulate the form of synaptic plasticity expressed. Synapse *24*, 97-103.

Dagliyan, O., Shirvanyants, D., Karginov, A.V., Ding, F., Fee, L., Chandrasekaran, S.N., Freisinger, C.M., Smolen, G.A., Huttenlocher, A., Hahn, K.M., *et al.* (2013). Rational design of a ligand-controlled protein conformational switch. Proc Natl Acad Sci U S A *110*, 6800-6804.

De Koninck, P., and Schulman, H. (1998). Sensitivity of CaM kinase II to the frequency of Ca2+ oscillations. Science *279*, 227-230.

Derkach, V., Barria, A., and Soderling, T.R. (1999). Ca2+/calmodulin-kinase II enhances channel conductance of alpha-amino-3-hydroxy-5-methyl-4-isoxazolepropionate type glutamate receptors. Proc Natl Acad Sci U S A *96*, 3269-3274.

Dudek, S.M., and Bear, M.F. (1992). Homosynaptic long-term depression in area CA1 of hippocampus and effects of N-methyl-D-aspartate receptor blockade. Proc Natl Acad Sci U S A *89*, 4363-4367.

Dupont, G., Houart, G., and De Koninck, P. (2003). Sensitivity of CaM kinase II to the frequency of Ca2+ oscillations: a simple model. Cell Calcium *34*, 485-497.

Elgersma, Y., Fedorov, N.B., Ikonen, S., Choi, E.S., Elgersma, M., Carvalho, O.M., Giese, K.P., and Silva, A.J. (2002). Inhibitory autophosphorylation of CaMKII controls PSD association, plasticity, and learning. Neuron *36*, 493-505.

Emptage, N., Bliss, T.V., and Fine, A. (1999). Single synaptic events evoke NMDA receptor-mediated release of calcium from internal stores in hippocampal dendritic spines. Neuron *22*, 115-124.

Erondu, N.E., and Kennedy, M.B. (1985). Regional distribution of type II Ca2+/calmodulin-dependent protein kinase in rat brain. J Neurosci *5*, 3270-3277.

Foster, K.A., McLaughlin, N., Edbauer, D., Phillips, M., Bolton, A., Constantine-Paton, M., and Sheng, M. (2010). Distinct roles of NR2A and NR2B cytoplasmic tails in long-term potentiation. J Neurosci *30*, 2676-2685.

Fujii, H., Inoue, M., Okuno, H., Sano, Y., Takemoto-Kimura, S., Kitamura, K., Kano, M., and Bito, H. (2013). Nonlinear decoding and asymmetric representation of neuronal input information by CaMKIIalpha and calcineurin. Cell Rep *3*, 978-987.

Giese, K.P., Fedorov, N.B., Filipkowski, R.K., and Silva, A.J. (1998). Autophosphorylation at Thr286 of the alpha calcium-calmodulin kinase II in LTP and learning. Science *279*, 870-873.

Grienberger, C., and Konnerth, A. (2012). Imaging calcium in neurons. Neuron *73*, 862-885.

Hanson, P.I., Kapiloff, M.S., Lou, L.L., Rosenfeld, M.G., and Schulman, H. (1989). Expression of a multifunctional Ca2+/calmodulin-dependent protein kinase and mutational analysis of its autoregulation. Neuron *3*, 59-70.

Hanson, P.I., Meyer, T., Stryer, L., and Schulman, H. (1994). Dual role of calmodulin in autophosphorylation of multifunctional CaM kinase may underlie decoding of calcium signals. Neuron *12*, 943-956.

Hanson, P.I., and Schulman, H. (1992). Inhibitory autophosphorylation of multifunctional Ca2+/calmodulin-dependent protein kinase analyzed by site-directed mutagenesis. J Biol Chem *267*, 17216-17224.

Harris, K.M., and Kater, S.B. (1994). Dendritic spines: cellular specializations imparting both stability and flexibility to synaptic function. Annu Rev Neurosci *17*, 341-371.

Harvey, C.D., Yasuda, R., Zhong, H., and Svoboda, K. (2008). The spread of Ras activity triggered by activation of a single dendritic spine. Science *321*, 136-140.

Hayama, T., Noguchi, J., Watanabe, S., Takahashi, N., Hayashi-Takagi, A., Ellis-Davies, G.C., Matsuzaki, M., and Kasai, H. (2013). GABA promotes the competitive selection of dendritic spines by controlling local Ca2+ signaling. Nat Neurosci *16*, 1409-1416.

Hayashi-Takagi, A., Yagishita, S., Nakamura, M., Shirai, F., Wu, Y.I., Loshbaugh, A.L., Kuhlman, B., Hahn, K.M., and Kasai, H. (2015). Labelling and optical erasure of synaptic memory traces in the motor cortex. Nature *525*, 333-338.

Hayashi, Y., Shi, S.H., Esteban, J.A., Piccini, A., Poncer, J.C., and Malinow, R. (2000). Driving AMPA receptors into synapses by LTP and CaMKII: requirement for GluR1 and PDZ domain interaction. Science *287*, 2262-2267.

Hidaka, H., and Yokokura, H. (1996). Molecular and cellular pharmacology of a calcium/calmodulin-dependent protein kinase II (CaM kinase II) inhibitor, KN-62, and proposal of CaM kinase phosphorylation cascades. Adv Pharmacol *36*, 193-219.

Higley, M.J., and Sabatini, B.L. (2012). Calcium signaling in dendritic spines. Cold Spring Harb Perspect Biol *4*, a005686.

Hinds, H.L., Goussakov, I., Nakazawa, K., Tonegawa, S., and Bolshakov, V.Y. (2003). Essential function of alpha-calcium/calmodulin-dependent protein kinase II in neurotransmitter release at a glutamatergic central synapse. Proc Natl Acad Sci U S A *100*, 4275-4280.

Holmes, W.R. (1990). Is the function of dendritic spines to concentrate calcium? Brain Res *519*, 338-342.

Hudmon, A., Lebel, E., Roy, H., Sik, A., Schulman, H., Waxham, M.N., and De Koninck, P. (2005a). A mechanism for Ca2+/calmodulin-dependent protein kinase II clustering at synaptic and nonsynaptic sites based on self-association. J Neurosci *25*, 6971-6983.

Hudmon, A., and Schulman, H. (2002). Structure-function of the multifunctional Ca2+/calmodulin-dependent protein kinase II. Biochem J *364*, 593-611.

Hudmon, A., Schulman, H., Kim, J., Maltez, J.M., Tsien, R.W., and Pitt, G.S. (2005b). CaMKII tethers to L-type Ca2+ channels, establishing a local and dedicated integrator of Ca2+ signals for facilitation. J Cell Biol *171*, 537-547.

Ingebritsen, T.S., and Cohen, P. (1983). Protein phosphatases: properties and role in cellular regulation. Science *221*, 331-338.

Ishida, A., and Fujisawa, H. (1995). Stabilization of calmodulin-dependent protein kinase II through the autoinhibitory domain. J Biol Chem *270*, 2163-2170.

Ishida, A., Kameshita, I., and Fujisawa, H. (1998). A novel protein phosphatase that dephosphorylates and regulates Ca2+/calmodulin-dependent protein kinase II. J Biol Chem *273*, 1904-1910.

Ji, Y., Li, B., Reed, T.D., Lorenz, J.N., Kaetzel, M.A., and Dedman, J.R. (2003). Targeted inhibition of Ca2+/calmodulin-dependent protein kinase II in cardiac longitudinal sarcoplasmic reticulum results in decreased phospholamban phosphorylation at threonine 17. J Biol Chem *278*, 25063-25071.

Jiang, X., Lautermilch, N.J., Watari, H., Westenbroek, R.E., Scheuer, T., and Catterall, W.A. (2008). Modulation of CaV2.1 channels by Ca2+/calmodulin-dependent protein kinase II bound to the C-terminal domain. Proc Natl Acad Sci U S A *105*, 341-346.

Kakiuchi, S., Yasuda, S., Yamazaki, R., Teshima, Y., Kanda, K., Kakiuchi, R., and Sobue, K. (1982). Quantitative determinations of calmodulin in the supernatant and particulate fractions of mammalian tissues. J Biochem *92*, 1041-1048.

Katsuki, H., Izumi, Y., and Zorumski, C.F. (1997). Noradrenergic regulation of synaptic plasticity in the hippocampal CA1 region. J Neurophysiol *77*, 3013-3020.

Kennedy, M.B., Beale, H.C., Carlisle, H.J., and Washburn, L.R. (2005). Integration of biochemical signalling in spines. Nat Rev Neurosci *6*, 423-434.

121

Kennedy, M.J., Davison, I.G., Robinson, C.G., and Ehlers, M.D. (2010). Syntaxin-4 defines a domain for activity-dependent exocytosis in dendritic spines. Cell *141*, 524-535.

Koch, C., and Zador, A. (1993). The function of dendritic spines: devices subserving biochemical rather than electrical compartmentalization. J Neurosci *13*, 413-422.

Koester, H.J., and Sakmann, B. (1998). Calcium dynamics in single spines during coincident pre- and postsynaptic activity depend on relative timing of back-propagating action potentials and subthreshold excitatory postsynaptic potentials. Proc Natl Acad Sci U S A *95*, 9596-9601.

Kolodziej, S.J., Hudmon, A., Waxham, M.N., and Stoops, J.K. (2000). Three-dimensional reconstructions of calcium/calmodulin-dependent (CaM) kinase IIalpha and truncated CaM kinase IIalpha reveal a unique organization for its structural core and functional domains. J Biol Chem *275*, 14354-14359.

Kovalchuk, Y., Eilers, J., Lisman, J., and Konnerth, A. (2000). NMDA receptor-mediated subthreshold Ca(2+) signals in spines of hippocampal neurons. J Neurosci *20*, 1791-1799.

Krapivinsky, G., Medina, I., Krapivinsky, L., Gapon, S., and Clapham, D.E. (2004). SynGAP-MUPP1-CaMKII synaptic complexes regulate p38 MAP kinase activity and NMDA receptor-dependent synaptic AMPA receptor potentiation. Neuron *43*, 563-574.

Kristensen, A.S., Jenkins, M.A., Banke, T.G., Schousboe, A., Makino, Y., Johnson, R.C., Huganir, R., and Traynelis, S.F. (2011). Mechanism of Ca2+/calmodulin-dependent kinase II regulation of AMPA receptor gating. Nat Neurosci *14*, 727-735.

Kwon, H.B., and Sabatini, B.L. (2011). Glutamate induces de novo growth of functional spines in developing cortex. Nature *474*, 100-104.

Lee, H.K., Barbarosie, M., Kameyama, K., Bear, M.F., and Huganir, R.L. (2000). Regulation of distinct AMPA receptor phosphorylation sites during bidirectional synaptic plasticity. Nature *405*, 955-959.

Lee, H.K., Takamiya, K., He, K., Song, L., and Huganir, R.L. (2010). Specific roles of AMPA receptor subunit GluR1 (GluA1) phosphorylation sites in regulating synaptic plasticity in the CA1 region of hippocampus. J Neurophysiol *103*, 479-489.

Lee, S.J., Escobedo-Lozoya, Y., Szatmari, E.M., and Yasuda, R. (2009). Activation of CaMKII in single dendritic spines during long-term potentiation. Nature *458*, 299-304.

Lee, S.J., and Yasuda, R. (2009). Spatiotemporal Regulation of Signaling in and out of Dendritic Spines: CaMKII and Ras. Open Neurosci J *3*, 117-127.

Lengyel, I., Voss, K., Cammarota, M., Bradshaw, K., Brent, V., Murphy, K.P., Giese, K.P., Rostas, J.A., and Bliss, T.V. (2004). Autonomous activity of CaMKII is only transiently increased following the induction of long-term potentiation in the rat hippocampus. Eur J Neurosci *20*, 3063-3072.

Leonard, A.S., Lim, I.A., Hemsworth, D.E., Horne, M.C., and Hell, J.W. (1999). Calcium/calmodulin-dependent protein kinase II is associated with the N-methyl-D-aspartate receptor. Proc Natl Acad Sci U S A *96*, 3239-3244.

Lisman, J., and Raghavachari, S. (2015). Biochemical principles underlying the stable maintenance of LTP by the CaMKII/NMDAR complex. Brain Res *1621*, 51-61.

Lisman, J., Schulman, H., and Cline, H. (2002). The molecular basis of CaMKII function in synaptic and behavioural memory. Nat Rev Neurosci *3*, 175-190.

Lisman, J., Yasuda, R., and Raghavachari, S. (2012). Mechanisms of CaMKII action in long-term potentiation. Nat Rev Neurosci *13*, 169-182.

Lisman, J.E., and Zhabotinsky, A.M. (2001). A model of synaptic memory: a CaMKII/PP1 switch that potentiates transmission by organizing an AMPA receptor anchoring assembly. Neuron *31*, 191-201.

Liu, X.Y., Mao, L.M., Zhang, G.C., Papasian, C.J., Fibuch, E.E., Lan, H.X., Zhou, H.F., Xu, M., and Wang, J.Q. (2009). Activity-dependent modulation of limbic dopamine D3 receptors by CaMKII. Neuron *61*, 425-438.

Lledo, P.M., Zhang, X., Sudhof, T.C., Malenka, R.C., and Nicoll, R.A. (1998). Postsynaptic membrane fusion and long-term potentiation. Science *279*, 399-403.

Lomo, T. (1971). Patterns of activation in a monosynaptic cortical pathway: the perforant path input to the dentate area of the hippocampal formation. Exp Brain Res *12*, 18-45.

Lucic, V., Greif, G.J., and Kennedy, M.B. (2008). Detailed state model of CaMKII activation and autophosphorylation. Eur Biophys J *38*, 83-98.

Luthi, A., Wikstrom, M.A., Palmer, M.J., Matthews, P., Benke, T.A., Isaac, J.T., and Collingridge, G.L. (2004). Bi-directional modulation of AMPA receptor unitary conductance by synaptic activity. BMC Neurosci *5*, 44.

Majewska, A., Brown, E., Ross, J., and Yuste, R. (2000). Mechanisms of calcium decay kinetics in hippocampal spines: role of spine calcium pumps and calcium diffusion through the spine neck in biochemical compartmentalization. J Neurosci *20*, 1722-1734.

Makino, H., and Malinow, R. (2009). AMPA receptor incorporation into synapses during LTP: the role of lateral movement and exocytosis. Neuron *64*, 381-390.

Malenka, R.C. (2003). The long-term potential of LTP. Nat Rev Neurosci *4*, 923-926.

Malenka, R.C., Kauer, J.A., Perkel, D.J., Mauk, M.D., Kelly, P.T., Nicoll, R.A., and Waxham, M.N. (1989). An essential role for postsynaptic calmodulin and protein kinase activity in long-term potentiation. Nature *340*, 554-557.

Malenka, R.C., and Nicoll, R.A. (1993). NMDA-receptor-dependent synaptic plasticity: multiple forms and mechanisms. Trends Neurosci *16*, 521-527.

Malinow, R., Schulman, H., and Tsien, R.W. (1989). Inhibition of postsynaptic PKC or CaMKII blocks induction but not expression of LTP. Science *245*, 862-866.

Martin, S.R., Andersson Teleman, A., Bayley, P.M., Drakenberg, T., and Forsen, S. (1985). Kinetics of calcium dissociation from calmodulin and its tryptic fragments. A stopped-flow fluorescence study using Quin 2 reveals a two-domain structure. Eur J Biochem *151*, 543-550.

Matsuzaki, M., Ellis-Davies, G.C., Nemoto, T., Miyashita, Y., Iino, M., and Kasai, H. (2001). Dendritic spine geometry is critical for AMPA receptor expression in hippocampal CA1 pyramidal neurons. Nat Neurosci *4*, 1086-1092.

Matsuzaki, M., Honkura, N., Ellis-Davies, G.C., and Kasai, H. (2004). Structural basis of long-term potentiation in single dendritic spines. Nature *429*, 761-766.

Matsuzaki, M., and Kasai, H. (2011). Two-photon uncaging microscopy. Cold Spring Harb Protoc *2011*, pdb.prot5620.

Mayford, M., Bach, M.E., Huang, Y.Y., Wang, L., Hawkins, R.D., and Kandel, E.R. (1996). Control of memory formation through regulated expression of a CaMKII transgene. Science *274*, 1678-1683.

Meyer, T., Hanson, P.I., Stryer, L., and Schulman, H. (1992). Calmodulin trapping by calcium-calmodulin-dependent protein kinase. Science *256*, 1199-1202.

Michalski, P.J. (2013). The delicate bistability of CaMKII. Biophys J *105*, 794-806.

Miller, S.G., and Kennedy, M.B. (1986). Regulation of brain type II Ca2+/calmodulin-dependent protein kinase by autophosphorylation: a Ca2+-triggered molecular switch. Cell *44*, 861-870.

Molino, N.M., and Wang, S.W. (2014). Caged protein nanoparticles for drug delivery. Curr Opin Biotechnol *28*, 75-82.

Morris, E.P., and Torok, K. (2001). Oligomeric structure of alpha-calmodulin-dependent protein kinase II. J Mol Biol *308*, 1-8.

Morris, R.G., Anderson, E., Lynch, G.S., and Baudry, M. (1986). Selective impairment of learning and blockade of long-term potentiation by an N-methyl-D-aspartate receptor antagonist, AP5. Nature *319*, 774-776.

Morris, R.G., Garrud, P., Rawlins, J.N., and O'Keefe, J. (1982). Place navigation impaired in rats with hippocampal lesions. Nature *297*, 681-683.

Mulkey, R.M., Endo, S., Shenolikar, S., and Malenka, R.C. (1994). Involvement of a calcineurin/inhibitor-1 phosphatase cascade in hippocampal long-term depression. Nature *369*, 486-488.

Murakoshi, H., Lee, S.J., and Yasuda, R. (2008). Highly sensitive and quantitative FRET-FLIM imaging in single dendritic spines using improved non-radiative YFP. Brain Cell Biol *36*, 31-42.

Murakoshi, H., Wang, H., and Yasuda, R. (2011). Local, persistent activation of Rho GTPases during plasticity of single dendritic spines. Nature *472*, 100-104.

Nikandrova, Y.A., Jiao, Y., Baucum, A.J., Tavalin, S.J., and Colbran, R.J. (2010). Ca2+/calmodulin-dependent protein kinase II binds to and phosphorylates a specific SAP97 splice variant to disrupt association with AKAP79/150 and modulate alpha-amino-3-hydroxy-5-methyl-4-isoxazolepropionic acid-type glutamate receptor (AMPAR) activity. J Biol Chem *285*, 923-934.

Nishiyama, J., and Yasuda, R. (2015). Biochemical Computation for Spine Structural Plasticity. Neuron *87*, 63-75.

Noguchi, J., Matsuzaki, M., Ellis-Davies, G.C., and Kasai, H. (2005). Spine-neck geometry determines NMDA receptor-dependent Ca2+ signaling in dendrites. Neuron *46*, 609-622.

O'Keefe, J., and Dostrovsky, J. (1971). The hippocampus as a spatial map. Preliminary evidence from unit activity in the freely-moving rat. Brain Res *34*, 171-175.

Oh, W.C., Hill, T.C., and Zito, K. (2013). Synapse-specific and size-dependent mechanisms of spine structural plasticity accompanying synaptic weakening. Proc Natl Acad Sci U S A *110*, E305-312.

Oh, W.C., Parajuli, L.K., and Zito, K. (2015). Heterosynaptic structural plasticity on local dendritic segments of hippocampal CA1 neurons. Cell Rep *10*, 162-169.

Opazo, P., and Choquet, D. (2011). A three-step model for the synaptic recruitment of AMPA receptors. Mol Cell Neurosci *46*, 1-8.

Opazo, P., Labrecque, S., Tigaret, C.M., Frouin, A., Wiseman, P.W., De Koninck, P., and Choquet, D. (2010). CaMKII triggers the diffusional trapping of surface AMPARs through phosphorylation of stargazin. Neuron *67*, 239-252.

Otmakhov, N., Griffith, L.C., and Lisman, J.E. (1997). Postsynaptic inhibitors of calcium/calmodulin-dependent protein kinase type II block induction but not maintenance of pairing-induced long-term potentiation. J Neurosci *17*, 5357-5365.

Otmakhov, N., and Lisman, J. (2012). Measuring CaMKII concentration in dendritic spines. J Neurosci Methods *203*, 106-114.

Otmakhov, N., Regmi, S., and Lisman, J.E. (2015). Fast Decay of CaMKII FRET Sensor Signal in Spines after LTP Induction Is Not Due to Its Dephosphorylation. PLoS One *10*, e0130457.

Otmakhov, N., Tao-Cheng, J.H., Carpenter, S., Asrican, B., Dosemeci, A., Reese, T.S., and Lisman, J. (2004). Persistent accumulation of calcium/calmodulin-dependent protein kinase II in dendritic spines after induction of NMDA receptor-dependent chemical long-term potentiation. J Neurosci *24*, 9324-9331.

Otmakhova, N.A., Otmakhov, N., Mortenson, L.H., and Lisman, J.E. (2000). Inhibition of the cAMP pathway decreases early long-term potentiation at CA1 hippocampal synapses. J Neurosci *20*, 4446-4451.

Park, M., Penick, E.C., Edwards, J.G., Kauer, J.A., and Ehlers, M.D. (2004). Recycling endosomes supply AMPA receptors for LTP. Science *305*, 1972-1975.

Patterson, M., and Yasuda, R. (2011). Signalling pathways underlying structural plasticity of dendritic spines. Br J Pharmacol *163*, 1626-1638.

Patterson, M.A., Szatmari, E.M., and Yasuda, R. (2010). AMPA receptors are exocytosed in stimulated spines and adjacent dendrites in a Ras-ERK-dependent manner during long-term potentiation. Proc Natl Acad Sci U S A *107*, 15951-15956.

Pepke, S., Kinzer-Ursem, T., Mihalas, S., and Kennedy, M.B. (2010). A dynamic model of interactions of Ca2+, calmodulin, and catalytic subunits of Ca2+/calmodulin-dependent protein kinase II. PLoS Comput Biol *6*, e1000675.

Petersen, J.D., Chen, X., Vinade, L., Dosemeci, A., Lisman, J.E., and Reese, T.S. (2003). Distribution of postsynaptic density (PSD)-95 and Ca2+/calmodulin-dependent protein kinase II at the PSD. J Neurosci *23*, 11270-11278.

Pi, H.J., Otmakhov, N., Lemelin, D., De Koninck, P., and Lisman, J. (2010). Autonomous CaMKII can promote either long-term potentiation or long-term depression, depending on the state of T305/T306 phosphorylation. J Neurosci *30*, 8704-8709.

Poncer, J.C., Esteban, J.A., and Malinow, R. (2002). Multiple mechanisms for the potentiation of AMPA receptor-mediated transmission by alpha-Ca2+/calmodulin-dependent protein kinase II. J Neurosci *22*, 4406-4411.

Rellos, P., Pike, A.C., Niesen, F.H., Salah, E., Lee, W.H., von Delft, F., and Knapp, S. (2010). Structure of the CaMKIIdelta/calmodulin complex reveals the molecular mechanism of CaMKII kinase activation. PLoS Biol *8*, e1000426.

Rezazadeh, S., Claydon, T.W., and Fedida, D. (2006). KN-93 (2-[N-(2-hydroxyethyl)]-N-(4-methoxybenzenesulfonyl)]amino-N-(4-chlorocinnamyl)-N -methylbenzylamine), a calcium/calmodulin-dependent protein kinase II inhibitor, is a direct extracellular blocker of voltage-gated potassium channels. J Pharmacol Exp Ther *317*, 292-299.

Robison, A.J., Bartlett, R.K., Bass, M.A., and Colbran, R.J. (2005). Differential modulation of Ca2+/calmodulin-dependent protein kinase II activity by regulated interactions with N-methyl-D-aspartate receptor NR2B subunits and alpha-actinin. J Biol Chem *280*, 39316-39323.

Roche, K.W., O'Brien, R.J., Mammen, A.L., Bernhardt, J., and Huganir, R.L. (1996). Characterization of multiple phosphorylation sites on the AMPA receptor GluR1 subunit. Neuron *16*, 1179-1188.

Rongo, C., and Kaplan, J.M. (1999). CaMKII regulates the density of central glutamatergic synapses in vivo. Nature *402*, 195-199.

Rosenberg, O.S., Deindl, S., Sung, R.J., Nairn, A.C., and Kuriyan, J. (2005). Structure of the autoinhibited kinase domain of CaMKII and SAXS analysis of the holoenzyme. Cell *123*, 849-860.

Rotenberg, A., Mayford, M., Hawkins, R.D., Kandel, E.R., and Muller, R.U. (1996). Mice expressing activated CaMKII lack low frequency LTP and do not form stable place cells in the CA1 region of the hippocampus. Cell *87*, 1351-1361.

Rusakov, D.A., Stewart, M.G., and Korogod, S.M. (1996). Branching of active dendritic spines as a mechanism for controlling synaptic efficacy. Neuroscience *75*, 315-323.

Sabatini, B.L., Oertner, T.G., and Svoboda, K. (2002). The life cycle of Ca(2+) ions in dendritic spines. Neuron *33*, 439-452.

Sabatini, B.L., and Svoboda, K. (2000). Analysis of calcium channels in single spines using optical fluctuation analysis. Nature *408*, 589-593.

Sander, J.D., and Joung, J.K. (2014). CRISPR-Cas systems for editing, regulating and targeting genomes. Nat Biotechnol *32*, 347-355.

Sanhueza, M., and Lisman, J. (2013). The CaMKII/NMDAR complex as a molecular memory. Mol Brain *6*, 10.

Schnell, E., Sizemore, M., Karimzadegan, S., Chen, L., Bredt, D.S., and Nicoll, R.A. (2002). Direct interactions between PSD-95 and stargazin control synaptic AMPA receptor number. Proc Natl Acad Sci U S A *99*, 13902-13907.

Shen, K., and Meyer, T. (1999). Dynamic control of CaMKII translocation and localization in hippocampal neurons by NMDA receptor stimulation. Science *284*, 162-166.

Shen, K., Teruel, M.N., Subramanian, K., and Meyer, T. (1998). CaMKIIbeta functions as an F-actin targeting module that localizes CaMKIIalpha/beta heterooligomers to dendritic spines. Neuron *21*, 593-606.

Shi, S.H., Hayashi, Y., Petralia, R.S., Zaman, S.H., Wenthold, R.J., Svoboda, K., and Malinow, R. (1999). Rapid spine delivery and redistribution of AMPA receptors after synaptic NMDA receptor activation. Science *284*, 1811-1816.

Sik, A., Hajos, N., Gulacsi, A., Mody, I., and Freund, T.F. (1998). The absence of a major Ca2+ signaling pathway in GABAergic neurons of the hippocampus. Proc Natl Acad Sci U S A *95*, 3245-3250.

Silva, A.J., Paylor, R., Wehner, J.M., and Tonegawa, S. (1992a). Impaired spatial learning in alpha-calcium-calmodulin kinase II mutant mice. Science *257*, 206-211.

Silva, A.J., Stevens, C.F., Tonegawa, S., and Wang, Y. (1992b). Deficient hippocampal long-term potentiation in alpha-calcium-calmodulin kinase II mutant mice. Science *257*, 201-206.

Singla, S.I., Hudmon, A., Goldberg, J.M., Smith, J.L., and Schulman, H. (2001). Molecular characterization of calmodulin trapping by calcium/calmodulin-dependent protein kinase II. J Biol Chem *276*, 29353-29360.

Smedler, E., and Uhlen, P. (2014). Frequency decoding of calcium oscillations. Biochim Biophys Acta *1840*, 964-969.

Sobczyk, A., and Svoboda, K. (2007). Activity-dependent plasticity of the NMDA-receptor fractional Ca2+ current. Neuron *53*, 17-24.

Stefan, M.I., Edelstein, S.J., and Le Novere, N. (2008). An allosteric model of calmodulin explains differential activation of PP2B and CaMKII. Proc Natl Acad Sci U S A *105*, 10768-10773.

Svoboda, K., Tank, D.W., and Denk, W. (1996). Direct measurement of coupling between dendritic spines and shafts. Science *272*, 716-719.

Svoboda, K., and Yasuda, R. (2006). Principles of two-photon excitation microscopy and its applications to neuroscience. Neuron *50*, 823-839.

Takao, K., Okamoto, K., Nakagawa, T., Neve, R.L., Nagai, T., Miyawaki, A., Hashikawa, T., Kobayashi, S., and Hayashi, Y. (2005). Visualization of synaptic Ca2+ /calmodulin-dependent protein kinase II activity in living neurons. J Neurosci *25*, 3107-3112.

Takeuchi, Y., Fukunaga, K., and Miyamoto, E. (2002). Activation of nuclear Ca(2+)/calmodulin-dependent protein kinase II and brain-derived neurotrophic factor gene expression by stimulation of dopamine D2 receptor in transfected NG108-15 cells. J Neurochem *82*, 316-328.

Thomas, M.J., Moody, T.D., Makhinson, M., and O'Dell, T.J. (1996). Activity-dependent beta-adrenergic modulation of low frequency stimulation induced LTP in the hippocampal CA1 region. Neuron *17*, 475-482.

Tzortzopoulos, A., Best, S.L., Kalamida, D., and Torok, K. (2004). Ca2+/calmodulin-dependent activation and inactivation mechanisms of alphaCaMKII and phospho-Thr286-alphaCaMKII. Biochemistry *43*, 6270-6280.

Ullah, M., Schmidt, H., Cho, K.H., and Wolkenhauer, O. (2006). Deterministic modelling and stochastic simulation of biochemical pathways using MATLAB. Systems Biology, IEE Proceedings *153*, 53-60.

Vest, R.S., Davies, K.D., O'Leary, H., Port, J.D., and Bayer, K.U. (2007). Dual mechanism of a natural CaMKII inhibitor. Mol Biol Cell *18*, 5024-5033.

Walikonis, R.S., Oguni, A., Khorosheva, E.M., Jeng, C.J., Asuncion, F.J., and Kennedy, M.B. (2001). Densin-180 forms a ternary complex with the (alpha)-subunit of Ca2+/calmodulin-dependent protein kinase II and (alpha)-actinin. J Neurosci *21*, 423-433.

Walkup, W.G.t., Washburn, L., Sweredoski, M.J., Carlisle, H.J., Graham, R.L., Hess, S., and Kennedy, M.B. (2015). Phosphorylation of synaptic GTPase-activating protein (synGAP) by Ca2+/calmodulin-dependent protein kinase II (CaMKII) and cyclin-dependent kinase 5 (CDK5) alters the ratio of its GAP activity toward Ras and Rap GTPases. J Biol Chem *290*, 4908-4927.

Wang, Z., Edwards, J.G., Riley, N., Provance, D.W., Jr., Karcher, R., Li, X.D., Davison, I.G., Ikebe, M., Mercer, J.A., Kauer, J.A., *et al.* (2008). Myosin Vb mobilizes recycling endosomes and AMPA receptors for postsynaptic plasticity. Cell *135*, 535-548.

Woodgett, J.R., Cohen, P., Yamauchi, T., and Fujisawa, H. (1984). Comparison of calmodulin-dependent glycogen synthase kinase from skeletal muscle and calmodulin-dependent protein kinase-II from brain. FEBS Lett *170*, 49-54.

Yagishita, S., Hayashi-Takagi, A., Ellis-Davies, G.C., Urakubo, H., Ishii, S., and Kasai, H. (2014). A critical time window for dopamine actions on the structural plasticity of dendritic spines. Science *345*, 1616-1620.

Yamagata, Y., Kobayashi, S., Umeda, T., Inoue, A., Sakagami, H., Fukaya, M., Watanabe, M., Hatanaka, N., Totsuka, M., Yagi, T., *et al.* (2009). Kinase-dead knock-in mouse reveals an essential role of kinase activity of Ca2+/calmodulin-dependent protein kinase IIalpha in dendritic spine enlargement, long-term potentiation, and learning. J Neurosci *29*, 7607-7618.

Yang, Y., Tao-Cheng, J.H., Bayer, K.U., Reese, T.S., and Dosemeci, A. (2013). Camkii-mediated phosphorylation regulates distributions of Syngap-alpha1 and -alpha2 at the postsynaptic density. PLoS One *8*, e71795.

Yang, Y., Wang, X.B., Frerking, M., and Zhou, Q. (2008). Spine expansion and stabilization associated with long-term potentiation. J Neurosci *28*, 5740-5751.

Yasuda, R. (2006). Imaging spatiotemporal dynamics of neuronal signaling using fluorescence resonance energy transfer and fluorescence lifetime imaging microscopy. Curr Opin Neurobiol *16*, 551-561.

Yasuda, R. (2012). Imaging intracellular signaling using two-photon fluorescent lifetime imaging microscopy. Cold Spring Harb Protoc *2012*, 1121-1128.

Yasuda, R., and Murakoshi, H. (2011). The mechanisms underlying the spatial spreading of signaling activity. Curr Opin Neurobiol *21*, 313-321.

Yi, J.J., Wang, H., Vilela, M., Danuser, G., and Hahn, K.M. (2014). Manipulation of endogenous kinase activity in living cells using photoswitchable inhibitory peptides. ACS Synth Biol *3*, 788-795.

Zhai, S., Ark, E.D., Parra-Bueno, P., and Yasuda, R. (2013). Long-distance integration of nuclear ERK signaling triggered by activation of a few dendritic spines. Science *342*, 1107-1111.

Zhou, Q., Homma, K.J., and Poo, M.M. (2004). Shrinkage of dendritic spines associated with long-term depression of hippocampal synapses. Neuron *44*, 749-757.

Zhou, Y., Takahashi, E., Li, W., Halt, A., Wiltgen, B., Ehninger, D., Li, G.D., Hell, J.W., Kennedy, M.B., and Silva, A.J. (2007). Interactions between the NR2B receptor and CaMKII modulate synaptic plasticity and spatial learning. J Neurosci *27*, 13843-13853.

Zhu, J.J., Qin, Y., Zhao, M., Van Aelst, L., and Malinow, R. (2002). Ras and Rap control AMPA receptor trafficking during synaptic plasticity. Cell *110*, 443-455.

Zucker, R.S. (1999). Calcium- and activity-dependent synaptic plasticity. Curr Opin Neurobiol *9*, 305-313.

Biography

Jui-Yun Chang

Birthplace

Taipei, Taiwan   July 2, 1987

Education

Ph.D in Biochemistry

Duke University, Durham, NC, U.S.A.   Sep 2010 – Sep 2016

B.S in Chemistry (with Distinction)

National Taiwan University, Taipei, Taiwan   Sep 2005 – June 2009

Publications

- **Chang, J.Y.**, Parra-Bueno, P., Yasuda, R. (2016) CaMKII integrates calcium signals to induce spine plasticity via Thr286 phosphorylation. (Submitted)
- **Chang, J.Y.** and Li, H.W. (2010) Intersubunit regulation between nuclease and helicase domains of RecBCD enzyme. Biophysical Society Annual Meeting (Poster)

Honors and Awards

Duke University Graduate School Fellowship   2010-2016

Dean of College of Science Award, National Taiwan University   June 2009

Undergraduate Research Scholarship, National Science Council, Taiwan   2008-2009